Numerical Simulation of Hydraulic Fracturing Water Effects on Shale Gas Permeability Alteration

- Authors
- Authors and affiliations

- Vena. F. Eveline
- I. Yucel Akkutlu
- George J. Moridis
-
  - o
-
  - o
-
  - o

1. 1.
2. 2.

Article
First Online: 10 December 2016

Abstract

Hydraulic fracturing has been recognized as the necessary well completion technique to achieve economic production from shale gas formation. However, following the fracturing, fluid–wall interactions can form a damaged zone nearby the fracture characterized by strong capillarity and osmosis effects. Here, we present a new reservoir multi-phase flow model which includes these mechanisms to predict formation damage in the aftermath of the fracturing during shut-in and production periods. In the model, the shale matrix is treated as a multi-scale porosity medium including interconnected organic, inorganic slit-shaped, and clay porosity fields. Prior to the fracturing, the matrix holds gas in the organic and the inorganic slit-shaped pores, water with dissolved salt in the inorganic slit-shaped pores and the clay pores. During and after fracturing, imbibition causes water invasion into the matrix, and then, the injected water–clay interaction may lead to clay-swelling pressure development due to osmosis. The swelling pressure gives additional stress to slit-shaped pores and cause permeability reduction in the inorganic matrix. We develop a simulator describing a system of three pores, two phases (aqueous and gaseous phases), and three components (H_2O,$CH_4$$H_2O$,$CH_4$, and salt), including osmosis and clay-swelling effect on the permeability. The simulation of

aqueous-phase transport through clay shows that high swelling pressure can occur in clays as function of salt type, salt concentration difference, and clay-membrane efficiency. The new model is used to demonstrate the damage zone characteristics. The simulation of two-phase flow through the shale formation shows that, although fracturing is a rapid process, fluid–wall interactions continue to occur after the fracturing due to imbibition mechanism, which allows water to penetrate into the inorganic pore network and displace the gas in-place near the fracture. This water invasion leads to osmosis effect in the formation, which cause clay swelling and the subsequent permeability reduction. Continuing shale–water interactions during the production period can expand the damage zone further.

Keywords

Numerical simulation Osmosis Formation damage Clay swelling Hydraulic fracturing

List of Symbols

A_{nm}Anm
: Surface are between element n and m (m^2m2)

C_{μ}Cμ
: Sorbed-gas concentration in kerogen grain volume (mol/m^3mol/m3)

$D_{H_2O_{o,A}};D_{CH_4o,A};D_{Salto,A}$Do,AH2O;Do,ACH4;Do,ASalt
: Free-diffusion coefficient of H_2OH2O, CH_4CH4 and salt in the aqueous phase (m^2/sm2/s)

$\mathbf{F}_{H_2OA};\mathbf{F}_{SaltA}$FAH2O;FASalt
: Total mass flux of H_2OH2O and salt in aqueous-phase flow (kg/sm^2kg/sm2)

$\mathbf{F}_{H_2OA|||_{adv}};\mathbf{F}_{H_2OG|||_{adv}}$FAH2O|adv;FGH2O|adv
: Advective mass flux of H_2OH2O in aqueous- and gas-phase flow (kg/sm^2kg/sm2)

$\mathbf{F}_{CH_4A|||_{adv}};\mathbf{F}_{CH_4G|||_{adv}}$FACH4|adv;FGCH4|adv
: Advective mass flux of CH_4CH4 in aqueous- and gas-phase flow (kg/sm^2kg/sm2)

$\mathbf{F}_{SaltA|||_{adv}}$FASalt|adv
: Advective mass flux of salt in aqueous-phase flow (kg/sm^2kg/sm2)

$\mathbf{F}_{H_2OA|||_{dif}};\mathbf{F}_{H_2OG|||_{dif}}$FAH2O|dif;FGH2O|dif
: Diffusion mass flux of H_2OH2O in aqueous- and gas-phase flow (kg/sm^2kg/sm2)

$\mathbf{F}_{CH_4A|||_{dif}};\mathbf{F}_{CH_4G|||_{dif}}$FACH4|dif;FGCH4|dif
: Diffusion mass flux of CH_4CH4 in aqueous- and gas-phase flow (kg/sm^2kg/sm2)

$\mathbf{F}_{SaltA|||dif}$FASalt|dif
: Diffusion mass flux of salt in aqueous-phase flow (kg/sm^2kg/sm2)

k_IkI
: Slit-shaped pore permeability (m^2m2)

$k_m$km
: Permeability of porous medium acting as semi-permeable membrane (m^2m2)

k_0k0
: Slit-shaped pore permeability at zero effective stress (m^2m2)

ℓ_{IC}ℓIC
: Shape factor ($1/m^2$1/m2)

m
: Coefficient in Gangi's permeability model (-)

M_κMκ
: Mass accumulation of component κκ

M_sMs
: Salt molar mass (kg/mol)

M_{CH_4}MCH4
: Molecular weight of CH_4CH4 (kg/mol)

P
: Slit-shaped pore pressure (Psi; Pa)

P_A;P_GPA;PG
: Aqueous- and gas-phase pressure (Psi; Pa)

$P_{A,I}$PA,I
: Inorganic slit-shaped pore pressure (Psi; Pa)

$P_{A,C}$PA,C
: Clay-pore pressure (Psi; Pa)

P_{conf}Pconf
: Confining pressure (Psi; Pa)

P_1P1
: Effective stress when the slit-shaped pores are close completely (Psi; Pa)

P_LPL
: Langmuir pressure (Psi; Pa)

q_κqκ
: Source/sink of component κκ (kg/sm^3kg/sm3)

q_{H_2O};q_{Salt};q_{CH_4}qH2O;qSalt;qCH4
: Source/sink of component H_2OH2O, salt and CH_4CH4 (kg/sm^3kg/sm3)

R

Gas constant, equal to 8.3145 (J/mol K) or 0.082 (atm l/mol K)

$R_{\kappa,k+1n}R_{n\kappa,k+1}$

Residuals of component *K* at time k+1, in element n

$S_A;S_GSA;SG$

Aqueous- and gas-phase saturation

t

Time

T

Temperature (∘C; K∘C; K)

$\bar{V}\bar{V}$

Partial molar volume of solvent (liters per mol)

x_sxs

Salt mass fraction

$x_{H_2OA};x_{SaltA};x_{CH_4A}xAH2O;xASalt;xACH4$

Mass fraction of component H_2OH2O, salt and CH_4CH4 in aqueous-phase flow

$x_{H_2OG};x_{SaltG};x_{CH_4G}xGH2O;xGSalt;xGCH4$

Mass fraction of component H_2OH2O, salt and CH_4CH4 in gas-phase flow

$x_{SaltA,I};x_{H_2OA,I}xA,ISalt;xA,IH2O$

Salt and H_2OH2O mass fraction in inorganic pore

$x_{SaltA,C};x_{H_2OA,C}xA,CSalt;xA,CH2O$

Salt and H_2OH2O mass fraction in clay pore

V_nVn

Volume of element n (m_2m2)

$V_{sL}VsL$

Langmuir volume, sorbed-gas volume per total grain mass ($m_3/kgm3/kg$)

$w_{H_2OA,IC};w_{CH_4A,IC};w_{SaltA,IC}wA,ICH2O;wA,ICCH4;wA,ICSalt$

Mass-exchange of H_2OH2O, CH_4CH4 and salt between slit-shaped and clay-pore mass ($kgm_{-3}s_{-1}kgm-3s-1$)

Greek Letters

$\alpha\alpha$

Effective stress coefficient (-)

$\varepsilon_{ks}\varepsilon ks$

Total organic content, organic grain volume per total grain volume (-)

$\kappa\kappa$

Component

μ_A and $\mu_G\mu A$ and μG

$\mu_A;\mu_G$
: Viscosity of aqueous- and gas-phase (Pa s)

π
: Osmotic pressure (Pa)

$\rho_A;\rho_G$
: Aqueous- and gas-phase density (kg/m3)

ρ_f
: Fluid density (kg/m3)

ρ_{grain}
: Grain density (kg/m3)

$\rho_{sc,gas}$
: Gas density in standard condition (kg/m3)

σ
: Clay-membrane efficiency (-)

$\tau_A;\tau_G$
: Tortuosity of the aqueous- and gas-phase (-)

v
: Dissociation coefficient (-)

ϕ
: Porosity of porous medium (fraction)

ϕ_C
: Clay porosity (fraction)

ϕ_I
: Inorganic slit-shaped pore porosity (fraction)

ϕ_k
: Organic (kerogen) porosity (fraction)

1 Introduction

1.1 Background

Due to tight nature of shale formations, shale gas wells require stimulation, such as hydraulic fracturing, in order to produce economically. One of the fracturing methods frequently applied to shale is slickwater fracturing. During the treatment, a water-based fluid is injected in large volumes in order to overcome the parting pressure of the formation and fracture and to transport proppants into the created fractures effectively. Field experience has shown that not all of the injected water flows back when the production stage begins, however. For example, the recovery of the flowback water varied between 10–30% of the injected volume during the first few months of production in Haynesville shale wells (Fan et al. 2010). A large portion of the injected water is left behind in the created fracture system (Fan et al. 2010; Sharma and Agrawal 2013). In addition, it is argued that the recovery of the flowback water is low because a portion of the injected

water could invade into the formation and left behind during the production. Experimental works have shown imbibition of water into the shale matrix (Pagels et al. 2013; Bertoncello et al. 2014; Bostrom et al. 2014).

Water invasion into the formation could take place during the fracturing and, perhaps to an even larger extent, after the fracturing, during the well shut-in and production stages. The invading water is expected to damage the formation due to two major effects: water-blocking effect and clay-swelling effect.

1.1.1 Water-Blocking Effect

Water that fills the fractures will imbibe into the shale matrix due to water-wet properties of the inorganic clayey matrix. Invading water locally displaces the gas in the matrix and creates a multi-phase flow environment near the fracture. Unfavorable saturation conditions during the production can influence the gas flow and, consequently, hinder the gas well performance. This phenomenon, known as water-blocking or phase-trapping, is one of the most severe damage mechanisms in low-permeability gas reservoirs with sub-irreducible water saturation (Bennion et al. 1994; Bennion and Thomas 2005).

Previously, simulation study in tight gas reservoirs showed water-blocking can significantly reduce gas production due to capillarity-driven permeability damage in the invaded zone (Holditch 1979). A recent experiment of water imbibition into shale showed that the imbibing-water remains trapped in the pore network and decreases permeability to gas (Bertoncello et al. 2014). A simulation and history-matching study by Bertoncello et al. (2014) showed that water invasion during fracturing was responsible for reduction in gas production. Other experimental works showed that permeability damage due to imbibition and water blockage could be a time-dependent process for some shales and could be a permanent damage for other shales. Transient behavior of water-blocking have been studied independently by researchers (Kamath and Laroche 2003; Bertoncello et al. 2014; Bostrom et al. 2014).

Bertoncello et al. (2014) studied water-blocking in shale gas reservoir due to water imbibition mechanism using simulation. In their description of the formation, two types of pores coexist in the shale reservoir: large pores in oil-wet organic matrix and small pores in water-wet inorganic matrix. Accordingly, during hydraulic fracturing, high-pressure water leaks off into the shale matrix, invading the large oil-wet pores first, displacing the oil and subsequently being trapped. The trapped water will naturally imbibe into the small, water-wet pores and decrease the water saturation along the fracture face and in the oil-wet pore network. They conducted a simulation-based history-matching study to observe the effect of water invasion. As a baseline

case, a scenario was considered with no water invasion. Due to the absence of water invasion, the bottomhole pressure remained high even during early production when the production rate was the largest, which confirmed the water invasion during fracturing was responsible for the reduced gas production. In other cases including the water invasion effect indicated that immediate well cleanup following stimulation could improve well deliverability. When the well is flowed back immediately, invasion into the matrix was limited; hence, more of the fracturing fluid was recovered at the surface. Other cases with different depth of water invasion were also considered and showed that deeper invasion will cause lower gas production rate especially in early production time. In the case when early cleanup is infeasible for operational reasons, significant water-blocking may occur. According to their analysis, remediation of this water-blocking can be done by shutting in the well long enough to allow imbibition of water from the large oil-wet pores to the small water-wet pores. This could decrease water saturation in the matrix near the fracture face and free the oil-wet pores. During the shut-in, water imbibition removes the water from the main flow paths into small pores and allows easier access for the free gas flow. More water imbibes into small matrix pores, the less water recovery these wells experience.

Other simulation works studied imbibition by rapid suck-in of the fracturing water into the water-wet pores in the shale matrix and dissipation of the water saturation beyond the zone of primary invasion. This process cleans up injected water in fractures and cause enhancement in gas production rate after the shut-in period (Cheng 2012; Fakcharoenphol et al. 2013; Almulhim et al., 2014).

1.1.2 Clay-Swelling Effect

Invading water interactions with clays in the shale formation lead to development of swelling-related in situ stress development. Swelling in clay minerals and in shale has been observed for decades. Chenevert (1970) conducted water adsorption experiments using shale samples containing clay minerals (illite, kaolinite, montmorillonite, and chlorite). When the samples were exposed to fresh water, volumetric expansion of the samples was observed indicating that the samples swelled. Shale samples rich in montmorillonite showed larger expansion than the other shale samples. The observed expansion was anisotropic such that the expansion in the direction perpendicular to the shale bedding planes were larger than those in the direction parallel to the bedding plane. When shale samples were confined, large hydrational stresses were developed within the samples as a function of the duration of adsorption.

Formation damage occurs when the reservoir rock contains highly reactive minerals such as clays known to be sensitive to fresh water. Shale is a

sedimentary rock rich in clays. Experimental works involving shale–water interactions have previously showed permeability impairment when shale is brought in contact with water (Chenevert 1970; Bostrom et al. 2014). Severe formation damage takes place due to clay swelling when the clay content of the shale is high (Aksu et al. 2015).

Osmosis has been suggested as the possible transport mechanism for the swelling pressure development inside shale (Marine and Fritz 1981; Fritz and Marine 1983). The swelling of clays is due to an imbalance between the chemical potentials of the contacted fresh water and the water in clay pores.

1.2 Objectives and Approaches

Low water recovery after hydraulic fracturing operation in some shale gas wells indicates that water stays in subsurface, in the wellbore, in the fractures, and in the adjacent shale matrix. There will be continuing interaction between the injected water and the shale matrix that can induce damage over extended times.

In this paper, using theoretical modeling and numerical simulation, we are interested in understanding the mechanisms of imbibition and osmosis (and their interplay) developing in a multi-scale pore network representative of resource shale formations, quantifying their impact on permeability impairment due to continuing shale–water interaction in shale gas well hydraulic fractures. The motivation of this work is that if we have a better understanding of hydraulic fracturing fluid damage, we can conduct well stimulation operations in a manner that can avoid the damage and, hence, lead to a significantly improved well performance.

We thus present a new modeling approach to numerically measure the impact of hydraulic fracturing fluid in shale formations in the presence of both imbibition and osmosis effects. During the application of the model, it is assumed that water cannot be removed from the fractures completely; hence, water–shale interaction occurs at the fracture surfaces continuously. This is different from previous work, for example, experimental works that observed the time dependence of permeability due to water imbibition in shale samples by Bostrom et al. (2014). In their experimental work, after water imbibition period, which shows reduction in permeability, water was removed and permeability was continuously monitored during a certain period in the absence of water. In addition, we considered in our simulations elongated shut-in times to study large-time behavior of the water invasion and the formation damage. Finally, due to number of page limitation, the flow-back stage simulation and analysis are left out and will be discussed in a subsequent manuscript in near future.

In the first part of this paper, a new theoretical shale petrophysical model is proposed with three distinct (multi-scale) porosity fields in the matrix. We show the hydraulic connectivity among the porosity fields and consider modeling imbibition and osmosis in this multi-scale pore structure. Osmosis occurs in shale due to clays acting as a semi-permeable membrane and leads to clay swelling and reduction in shale permeability. In the second part, the adapted osmosis model will be introduced and discussed. A significant level of improvement in theoretical description of osmosis has been experienced during the last decade based on non-equilibrium thermodynamic arguments. Then, a mathematical model and its numerical solution of aqueous-phase transport in clay including osmosis will be presented and the model will be validated using a previously conducted laboratory experiment. Next, results of a set of forward simulations will be presented to investigate single aqueous-phase transport in clay assuming a block of clay transected by a fracture filled with relatively dilute water. In the third part, mathematical formulation and numerical solution of two-phase flow in shale gas with clay-swelling effect will be presented. Then, a set of numerical simulations are conducted to show the impact of salt type, salt concentration difference, clay-membrane efficiency, and initial water saturation to permeability alteration in the shale formation near the hydraulic fracture. These simulations are performed considering initial and boundary condition representative of the post-hydraulic fracturing operation when the aqueous-phase fills the created hydraulic fracture and when there is continuing water–matrix interactions at the fracture wall. Finally, we discuss impact of hydraulic fracturing fluid damage to shale gas well performance.

2 Petrophysical Model of Shale

Shale is a sedimentary rock that is composed of extremely fine-grained particles, typically less than 4 microns in diameter, but may contain variable amounts of silt-sized particles, up to 62.5 microns with wide variation of composition including clay, quartz, feldspar, carbonates, and organic matter (Passey et al. 2010). In this paper, we will focus our discussion to clay minerals in shale, specifically imbibition and osmosis processes observed and to the associated permeability damage. Shale may contain varied types and amount of clay minerals. Common clay minerals found in shale are kaolinite, smectite (typically montmorillonite), illite, and chlorite.

Clay in general is a layered silicate mineral. It has basic silicate structure unit consisting of silica tetrahedron and alumina octahedron which are combined in different proportions (typically, 1:1 or 2:1) to form sheet structures that have large amount of unbalanced electric charges. The varieties of clay minerals are made by different combination of basic sheet

structures with different forms of bonding between the combined sheets (Asef and Farrokhrouz 2013).

Four different types of water can be found in shale associated with the clays: intercrystalline water, osmotic water, bound water, and free water, where porosity is defined as sum of free water, osmotic water, and to a lesser extent intercrystalline water (Asef and Farrokhrouz 2013). Intercrystalline water is present in association with cations to neutralize negative charges in clay particle; osmotic water is an adsorbed surface layer associated with negative clay charges; bound water is structurally hydrogen and hydroxyl groups within clay molecule itself; and free water is in the pore space between clay grains. Here, our focus is mostly on the osmotic water or interlayer water present between clay sheets which can cause swelling pressure.

Multi-scale, multi-porosity nature of shale matrix that is going to be adopted in this work is an extension of another petrophysical model that has recently been described by Wasaki and Akkutlu (2015). Accordingly, resource shale contains organic round pores and slit-shaped pores. Round-shaped organic pores are generated by thermal maturation and during conversion of kerogen into hydrocarbon fluids, while slit-shaped pores are a result of cracking caused by fluid pressures in excess of hydrostatic.

Unlike the Wasaki and Akkutlu (2015) approach, however, the shale matrix in this study holds additionally the so-called clay pores, see Fig. 1. Organic pores are pores inside organic materials. These pores may contain natural gas in adsorbed and free-states. Slit-shaped pores which have a geometry of a narrow channel or a micro-crack are pores that are located in the inorganic matrix. These pores have hydraulic connection to or transected the organic pores. The length dimension of these slit-shaped pores are varied and may range from one to tens micrometer. These pores could also be considered as the micro- and nano-scale cracks developed parallel to the bedding planes. The slit-shaped pores mostly has water-wet wettability and may contain water and gas. Clay pores, on the other hand, are the voids in between interlayer clay sheets.

Swelling pressure or hydration pressure can be described as a lumped physico-chemical forces acting primarily in the clay fabric which includes the van der Waals attraction, the electrostatic Born repulsion, and short-range repulsive–attractive forces generated from hydration/solvation of clay surfaces and the ions inside the interlayer clay pores (van Oort 2003). In a shale system containing clays and other silt-sized minerals, besides the physico-chemical forces described before, other forces can be categorized as the mechanical forces which include *in situ* vertical and horizontal stresses, pore pressure, and stress acting at intergranular contact points.

As described in detail in the next section, osmosis is the possible mechanism to generate swelling pressure inside clay pores. Here, we will discuss mechanism of formation damage in altered zone which is due to reduction in slit-shaped pore permeability caused by clay-swelling pressure. Altered zone is the shale matrix zone adjacent to hydraulic fracture which experience changes in reservoir properties due to hydraulic fracturing water imbibed into shale matrix.

The slit-shaped pores permeability is stress dependent and described by Gangi's permeability model (Gangi 1978; Wasaki and Akkutlu 2015) as follows:

$$k_I = k_0\{1-(P_{conf}-\alpha P P_1)^m\}^3 \quad (1)$$

Here, k_I is the slit-shaped pore permeability (m^2); $k_0 (m^2)$; $P_{conf} (m^2)$; α is the effective stress coefficient; P_1 is the effective stress when the slit-shaped pores are close completely (i.e., when $k_I = 0$); and m is a coefficient related with the surface roughness of the slit-shaped pores.
In Eq. (1), permeability is function of effective stress $(P_{conf}-\alpha P)$ that increasing effective stress will cause reduction in permeability value. Swelling pressure inside clay pores give additional stress to slit-shaped pores, which account for increasing confining pressure, thus reduce slit-shaped pore permeability.

Open image in new window

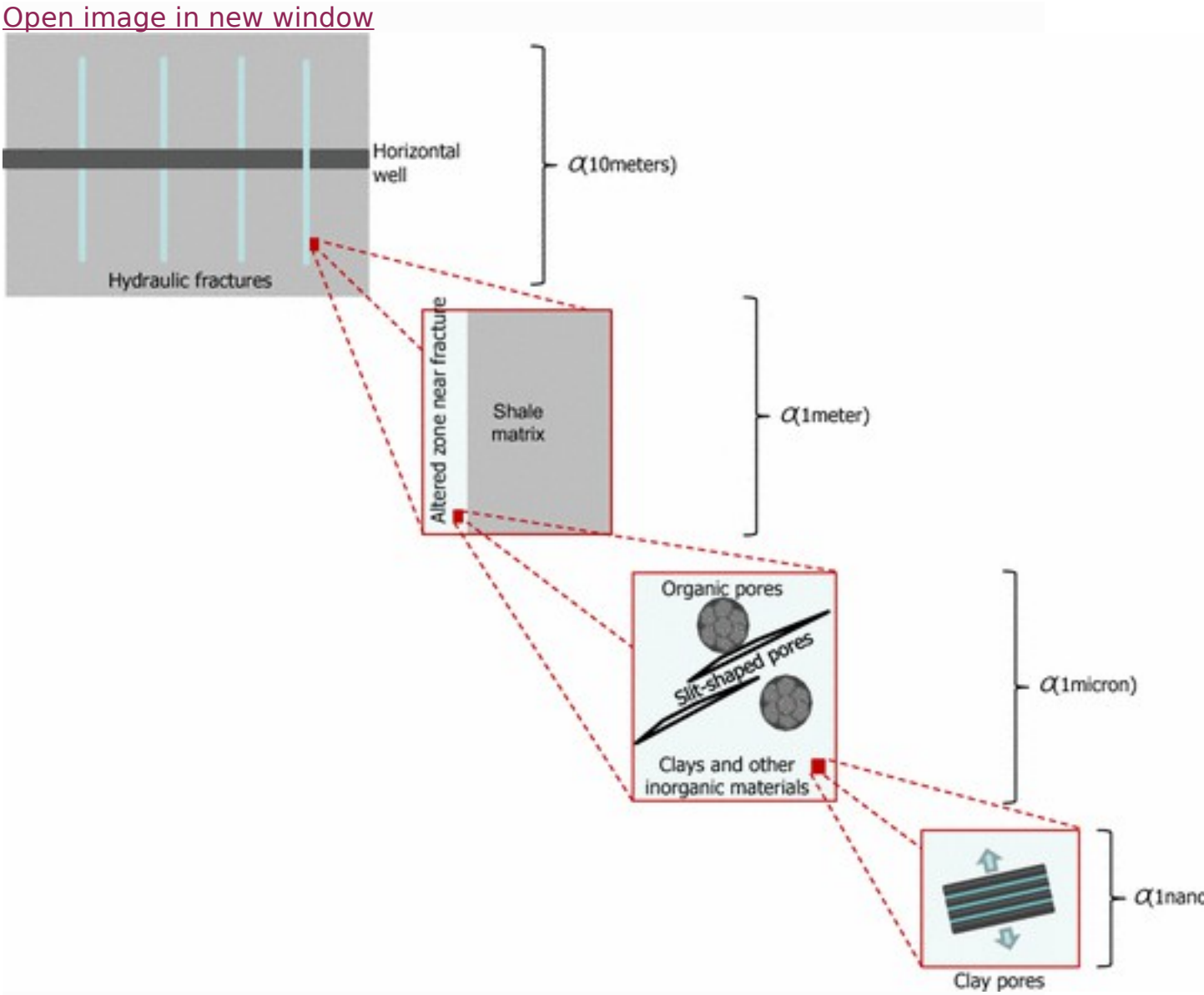

Fig. 1
Conceptual petrophysical model of shale matrix with altered zone due to hydraulic fracturing. *Blue arrows* represent the swelling-related stress caused by water invasion into clay interlayer pores (Eveline et al. 2016)

Open image in new window

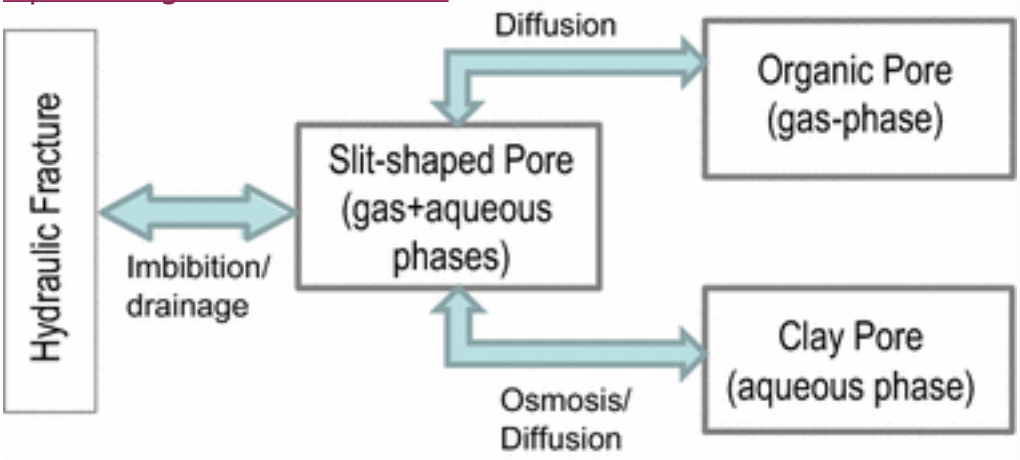

Fig. 2
Flow path between hydraulic fractures, slit-shaped pore, organic pore and clay pore

Figure 1 shows the proposed multiscale of pore structure within shale matrix and interaction paths between water and shale matrix due to hydraulic fracturing operation. Shale matrix contains three types of pores with different scales, as mentioned before, are organic, slit-shaped, and clay pores. Figure 2 shows the connection between hydraulic fracture and these pores. After hydraulic fracturing operation, there are hydraulic fracturing fluid containing water remained in the created hydraulic fractures. This water will interact with shale matrix and create an altered zone where permeability impairment may occur due to this interaction. This permeability impairment known also as formation damage can be caused by several mechanisms and one of them is caused by build up of pressure inside clay pores which dynamically change with time. This build-up of pressure inside clay pores which caused by osmotic mechanism can give additional stress and can reduce slit-shaped pore permeability which is stress-dependent characteristically.

3 Aqueous-phase Transport in Clay Including Osmosis

Before we continue developing a model that describe shale matrix as in the conceptual petrophysical model in Sect. 2, first here, we will discuss the development of mathematical model and simulator involving flow and transport of single aqueous phase in single clay pore which include osmosis as a transport mechanism through clay pore. The purpose of this step is to validate the osmosis model in clay before using it in modeling shale with three pores.

3.1 Osmosis Model

Osmosis could be considered as a molecular diffusion in the presence of a membrane. More specifically, it is a transport mechanism which occurs when a semi-permeable membrane separates two aqueous solutions of different chemical potential due to different salt concentration. Clay minerals can act as semi-permeable membrane because of the negative charges on clay particle surfaces (Marine and Fritz 1981). The negative charges attract cations in solution to adsorb onto clay surface and form a diffuse layer adjacent to the adsorb layer to create double layer. This double layer tends to prevent passage of charged ions through the semi-permeable membrane and only allow uncharged molecules such as water to pass. When the clay membrane is facing aqueous solution having different salt concentration from solution inside the clay, osmosis will occur such that uncharged water molecules flow from the lower salinity solution into the clay. If the more saline solution is contained within a confined clay membrane such as the clays in the subsurface formations, the water being transported into the confined clay will further increase the hydrostatic pressure inside the clay. The osmotic transport will continue until water activity in both solutions eventually becomes equal.

At equilibrium, for an ideal membrane, the increase in the hydrostatic pressure $(\Delta p)(\Delta p)$ is equal to osmotic pressure $(\pi)(\pi)$, which is defined as follows (Marine and Fritz (1981))

$$\pi = RTV^{-} \ln \text{activity of low salinity water} \text{activity of high-salinity water} \pi = RTV^{-} \ln \text{activity of low salinity water} \text{activity of high-salinity water} \quad (2)$$

Here, the activity of water is a unitless number, in which magnitude is dependent on salt concentration, pressure, and temperature. Water from the low-salinity solution will flow through membrane to the high-salinity solution side, to increase the activity of that solution by increasing hydrostatic pressure of that side. Activity of the water on the high-salinity side increases with the increase in hydrostatic pressure. The flow will continue until the activity of both solutions becomes equal.

Flux of mass and energy across a membrane can be driven by pressure, temperature, chemical, and electrical potential gradients (Marine and Fritz 1981; van Oort et al. 1996; Bader and Kooi 2005). In this paper, theoretical description of osmosis follows chemical osmosis model developed by Bader and Kooi (2005) which assumes the two driving forces of the mass flux are the hydraulic pressure and the chemical potential gradients. The model has been derived for an aqueous phase with single solute species. The osmotic pressure is approximated as follows:

$$\pi = vRT\rho^{f} M^{s} \nabla x^{s} \pi = vRT\rho^{f} M^{s} \nabla x^{s} \quad (3)$$

Here, $x_s$xs is the salt mass fraction; M_sMs is the salt molar mass (kg/mol) (kg/mol), and *v* is dissociation coefficient for the salt dissociating into *v* ions, which, for example, $v=2$v=2 for $MgSO_4$MgSO4, NaCl and KCl. Salt concentration is the main factor affecting osmotic pressure. However, for different salt types, equal salt concentration is not resulting equal osmotic pressure because different salt types have different molar mass and dissociation coefficient. For salts with equal dissociation coefficient, here $v=2$v=2 for example, the salts which have higher molar mass such as $MgSO_4$MgSO4than salts such as NaCl and KCl yield lower osmotic pressure.

Open image in new window

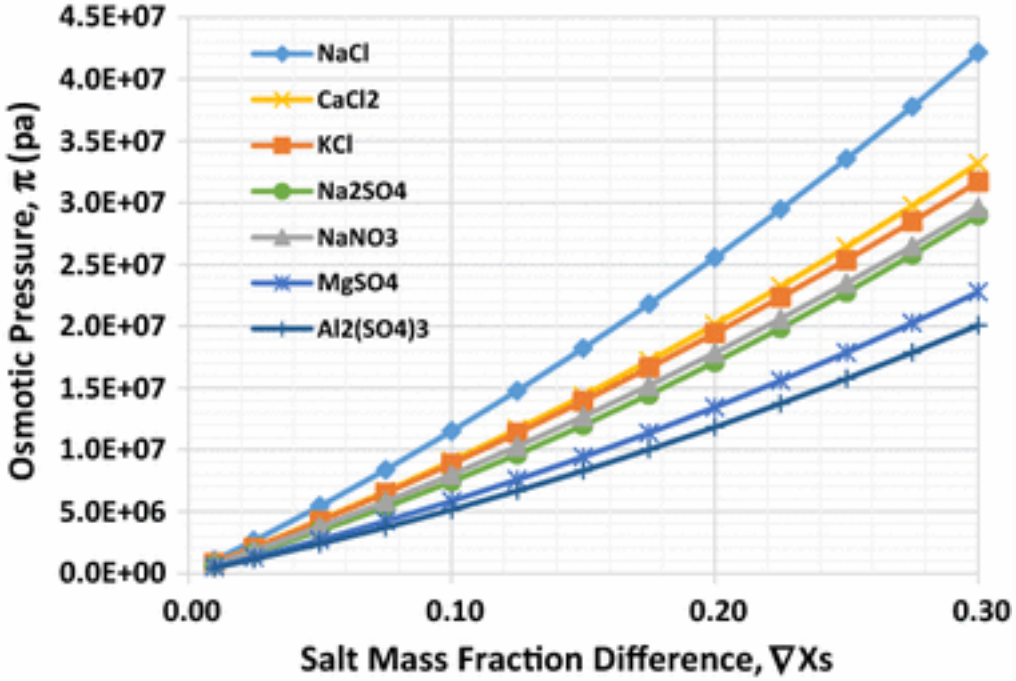

Fig. 3

Osmotic pressure for different salts and varying salt concentration difference are given at an initial pressure of 1.0E+7 Pa and temperature of $100\circ C$100∘C

Consider a container holding two aqueous solutions with different salt concentration separated by a semi-permeable membrane initially has pressure of 1.0E+7 Pa and temperature of $100\circ C$100∘C. The associated pressure increase (osmotic pressure) in the side of the semi-permeable membrane containing higher salt concentration can be calculated using Eq. (3). Then, the estimated changes in pressure due to osmosis are shown in Fig. 3 for different types of salts and different salt concentration values.

3.2 Mathematical Model and Numerical Solution

In this part, we describe a mathematical formulation and simulator which is developed to predict single aqueous-phase transport in clay involving

osmosis. Recently, a similar model has been presented in Eveline et al. (2016). The simulator is an expansion of TAMU-FTsim, which is a variant of the TOUGH+simulator (Moridis 2014; Moridis and Freeman 2014).

This particular simulator describes a system of single pore and two phases/two components. The two phases are aqueous phase and gas phase, and the two components are H_2OH2O and salt. Component H_2OH2O exists in both phases, while component salt is dissolved in the aqueous phase which is described as salt mass fraction of the aqueous phase. In the mathematical model below, only the aqueous phase is described, as we intend to simulate only single aqueous phase through clay.

Mathematical Model

The mass balance equations solved can be written in the following general form (Pruess et al. 1999):

$$ddt\int_{V_n} M_\kappa dV_n = \int_{\Gamma_n} \mathbf{F}_{\kappa\kappa}\cdot\mathbf{n}d\Gamma_n + \int_{V_n} q_\kappa dV_n ddt\int_{V_n} M_\kappa dV_n = \int_{\Gamma_n} F_{\kappa\kappa}\cdot n d\Gamma_n + \int_{V_n} q_\kappa dV_n \quad (4)$$

By applying Gauss' divergence theorem, Eq. (4) can be converted into the following partial differential equation (Pruess et al. 1999):

$$dM_\kappa dt = -div\mathbf{F}_{\kappa\kappa} + q_\kappa dM_\kappa dt = -divF_{\kappa\kappa} + q_\kappa \quad (5)$$

In the Eqs. (4) and (5), V_nVn is a volume element n; $M_\kappa n$; M_κ is mass accumulation of component $\kappa\kappa$; $\mathbf{F}_\kappa F_\kappa$is flux of component $\kappa\kappa$; and $q_\kappa q_\kappa$ is the source/sink of component $\kappa\kappa$.
In the form of Eq. (5), the H_2OH2O and salt mass balance equation in single aqueous-phase flow are as follows:

$$\partial\partial t(x^{H_2OA}\rho_A\phi) + \nabla.\mathbf{F}^{H_2OA} = q^{H_2O}\partial\partial t(xAH2O\rho A\phi) + \nabla.FAH2O = qH2O \quad (6)$$

$$\partial\partial t(x^{SaltA}\rho_A\phi) + \nabla.\mathbf{F}^{SaltA} = q^{Salt}\partial\partial t(xASalt\rho A\phi) + \nabla.FASalt = qSalt \quad (7)$$

The total mass flux equation of H_2OH2O and salt is defined below that the total mass flux of each component is a summation of advective and diffusive mass flux including osmosis which here defined following a mathematical model in Bader and Kooi, 2005.

$$\mathbf{F}^{H_2OA} = x^{H_2OA}\rho_A\{-k_m\mu_A\nabla(P_A) + \lambda\rho_A\nabla(x^{SaltA})\} FAH2O = xAH2O\rho A\{-km\mu A\nabla(PA) + \lambda\rho A\nabla(xASalt)\} \quad (8)$$

$$\mathbf{F}^{SaltA} = (1-\sigma)\rho_A x^{SaltA}\{-k_m\mu_A\nabla(P_A) + \lambda\rho_A\nabla(x^{SaltA})\} - (1-\sigma)\rho_A\phi\tau_A D^{Salto,A}\nabla(x^{SaltA}) FASalt = (1-\sigma)\rho A xASalt\{-km\mu A\nabla(PA) + \lambda\rho A\nabla(xASalt)\} - (1-\sigma)\rho A\phi\tau A Do,ASalt\nabla(xASalt)$$

(9)

where

$$\lambda=\sigma k^m \mu^A M^s v R T \lambda=\sigma k m \mu A M s v R T$$

(10)

Here, the transport of salt is a function of membrane efficiency (σ) (σ) where $\sigma=1\sigma=1$ for ideal membrane, $\sigma=0\sigma=0$ for non-reflective membrane, and $0<\sigma<10<\sigma<1$ for leaky/non-ideal membrane (Marine and Fritz 1981; van Oort et al. 1996; Bader and Kooi 2005).

Numerical Solution

The simulator developed in this part includes three thermophysical states which are single aqueous phase, single gas phase, and two-phases, aqueous and gas phases. However, as we intend to simulate only single aqueous phase through clay, here we focus to the thermophysical state of single aqueous phase.

In the thermophysical state of single aqueous phase, we choose primary variables that can uniquely described the system which involving osmosis. The primary variables are pressure, salt molar fraction and temperature. The salt fraction in the aqueous phase specifically will change the density of the aqueous phase.

The mass balance equations are discretized in space using the integral finite difference method, and time is discretized as a first-order finite difference. All the unknown thermodynamic parameters in the flux and source/sink terms are evaluated at the new time level or in fully implicit manner. The mass balance equations become residual equations, a set of coupled nonlinear algebraic equations as follows:

$$R_{\kappa,k+1n}=M_{\kappa,k+1n}-M_{\kappa,kn}-\Delta t V_n[\sum_m A_{nm}\mathbf{F}_{\kappa,k+1nm}+V_n q_{\kappa,k+1n}]=0 R n\kappa,k+1= Mn\kappa,k+1-Mn\kappa,k-\Delta t Vn[\sum mAnmFnm\kappa,k+1+Vnqn\kappa,k+1]=0$$

(11)

Here, k and k+1 are the current time and the new time level, respectively; $R_{\kappa,k+1n}Rn\kappa,k+1$ is the residuals of component $\kappa\kappa$ at time k+1, in element n; Δtn; Δt is the time step; V_nVn is element volume; $A_{nm}Anm$ is the flow surface between elements n and m. The unknowns are the $n_{element}\times n_{equation}nelement\times nequation$ independent primary variables $(X_i;i=1,\ldots,n_{element}\times n_{equation})(Xi;i=1,\ldots,nelement\times nequation)$ where $n_{element}nelement$ is the number of elements and $n_{equation}nequation$ is the number of equations for each element. The number of equations corresponds to the number of the primary variables.

Equation (11) is solved numerically using the Newton/Raphson iteration method. We introduce an iteration index *p* and expand the residuals in Eq. (11) at iteration step $p+1p+1$ in a Taylor series as follows:

$$R_{n\kappa,k+1}(X_{i,p+1}) = R_{n\kappa,k+1}(X_{i,p}) + \sum_i \partial R_{n\kappa,k+1}\partial X_i \Big|\Big|_p (X_{i,p+1} - X_{i,p}) + \cdots = 0 R_{n\kappa,k+1}(X_{i,p+1}) = R_{n\kappa,k+1}(X_{i,p}) + \sum_i \partial R_{n\kappa,k+1}\partial X_i \Big|_p (X_{i,p+1} - X_{i,p}) + \cdots = 0 \quad (12)$$

We get Jacobian matrix equations by retaining only the first derivative of Eq. (12) and rearranging terms to yield:

$$-\sum_i \partial R_{\kappa,k+1n}\partial X_i \Big|\Big|\Big|_p (X_{i,p+1} - X_{i,p}) = R_{n\kappa,k+1}(X_{i,p}) - \sum_i \partial R_{n\kappa,k+1}\partial X_i \Big| p(X_{i,p+1} - X_{i,p}) = R_{n\kappa,k+1}(X_{i,p}) \quad (13)$$

The Jacobian matrix, $\sum_i \partial R_{\kappa,k+1n}\partial X_i \sum_i \partial R_{n\kappa,k+1}\partial X_i$, is constructed by differentiating the set of residual equations in terms of primary variables $(X_i)(X_i)$. The dimension of the Jacobian matrix is $(n_{element} \times n_{equation}) \times (n_{element} \times n_{equation})$ $(nelement \times nequation) \times (nelement \times nequation)$. Solution of Eq. (13) proceeds in an iterative manner until the residuals $(R_{\kappa,k+1n})(R_{n\kappa,k+1})$ are reduced below a preset convergence tolerance that describes an acceptable (and very low) mass and/or energy balance error.

3.3 Validation of the Simulation Model using Osmosis Experiment

To validate the mathematical model and numerical solution of aqueous-phase flow through clay involving osmosis described in Sect. 3.2, we simulate previous osmosis experiment in clay sample (Keijzer 2000; Bader and Kooi 2005). The simulation parameters are shown in Table 1. We matched pressure increase due to osmosis (Fig. 4), as measured on a clay sample, thus providing evidence to validate the mathematical model of single aqueous-phase flow in clay including osmosis in the transport equations.

Figure 4 shows delta pressure (refer to the initial pressure) inside a clay sample in which ends are connected to two separate reservoirs with different salt concentration. The clay sample itself contains high salt concentration, equal to that in one of the reservoirs. Initially, pressure in the whole arrangement (clay and the two reservoirs) is equal. As the experiment is started, there is water influx from low salt reservoir into clay due to osmosis and pressure inside clay is increasing immediately. However, with time, pressure inside clay turn to decreasing behavior. This is because of two reason: First, as pressure in clay is increasing, there is reverse influx from clay into the low salt reservoir driven by pressure; second, the clay-membrane efficiency is not 100%; therefore, salt dissolved in the aqueous

phase can flow in and out which makes the initial high salt concentration in clay is even lower than initial value and lowering water influx due to osmosis.

Table 1

Parameters used in the chemical osmosis experiment (Keijzer 2000; Bader and Kooi 2005)

Parameter	Value	Unit
Rock and Fluid Properties		
Initial Pressure	5.00E+05	Pa
Initial Temperature	25	∘C∘C
Porosity	0.56	
Permeability	1.20E−09	m2m2
Salt diffusion coefficient	2.60E−13	m2/sm2/s
Membrane efficiency (σ)(σ)	0.0165	
Salt concentration in low salt reservoir	0.01	mol/L NaCl
Salt concentration in high salt reservoir	0.1	mol/L NaCl

Open image in new window

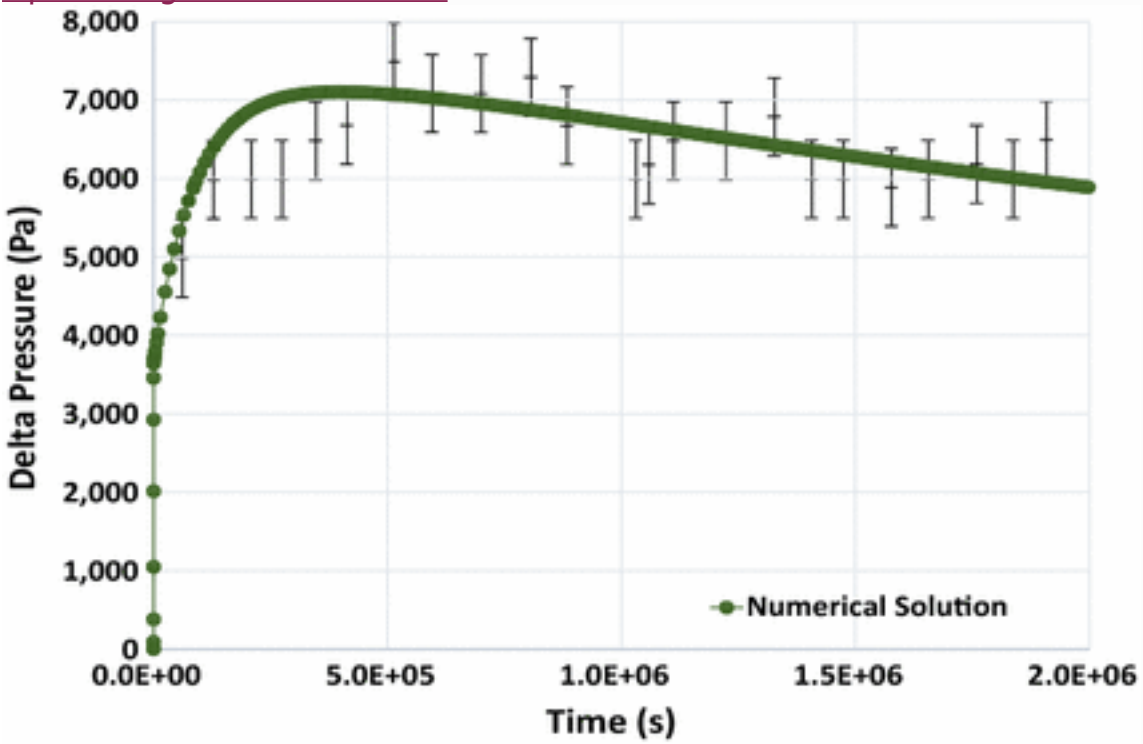

Fig. 4
Comparison between numerical simulation of single aqueous-phase flow in clay results and experimental data (Keijzer 2000; Bader and Kooi 2005) adopted from Eveline et al. (2016)

3.4 Simulation of Aqueous-phase Flow in Clay including Osmosis

Next, in order to understand behavior of the osmosis-related pressure increase (i.e., swelling pressure), we used the validated model in a series of forward simulations varying salt concentration differences. In these studies, we estimated the distribution of pressure across the clay. We also conducted simulations using different membrane efficiency. The simulations were one-dimensional (1D) of a system with dimensions of 5x100x10 m, which was divided into 500 equal-sized elements in the x-direction. The initial pressure was 2.07E+7 Pa and the temperature was 50◦C50◦C. The clay had an initial permeability of 218 nD and porosity of 10%. The first gridblock (corresponding to the fracture element) had a constant pressure of 2.07E+7 Pa, a temperature of 50◦C50◦C, and a NaCl salinity with a mass fraction of 0.01. Initially, the other elements of the system were fully saturated with H2OH2O with a NaCl mass fraction 0.05. Figure 5shows the simulation results after 90 days.

Open image in new window

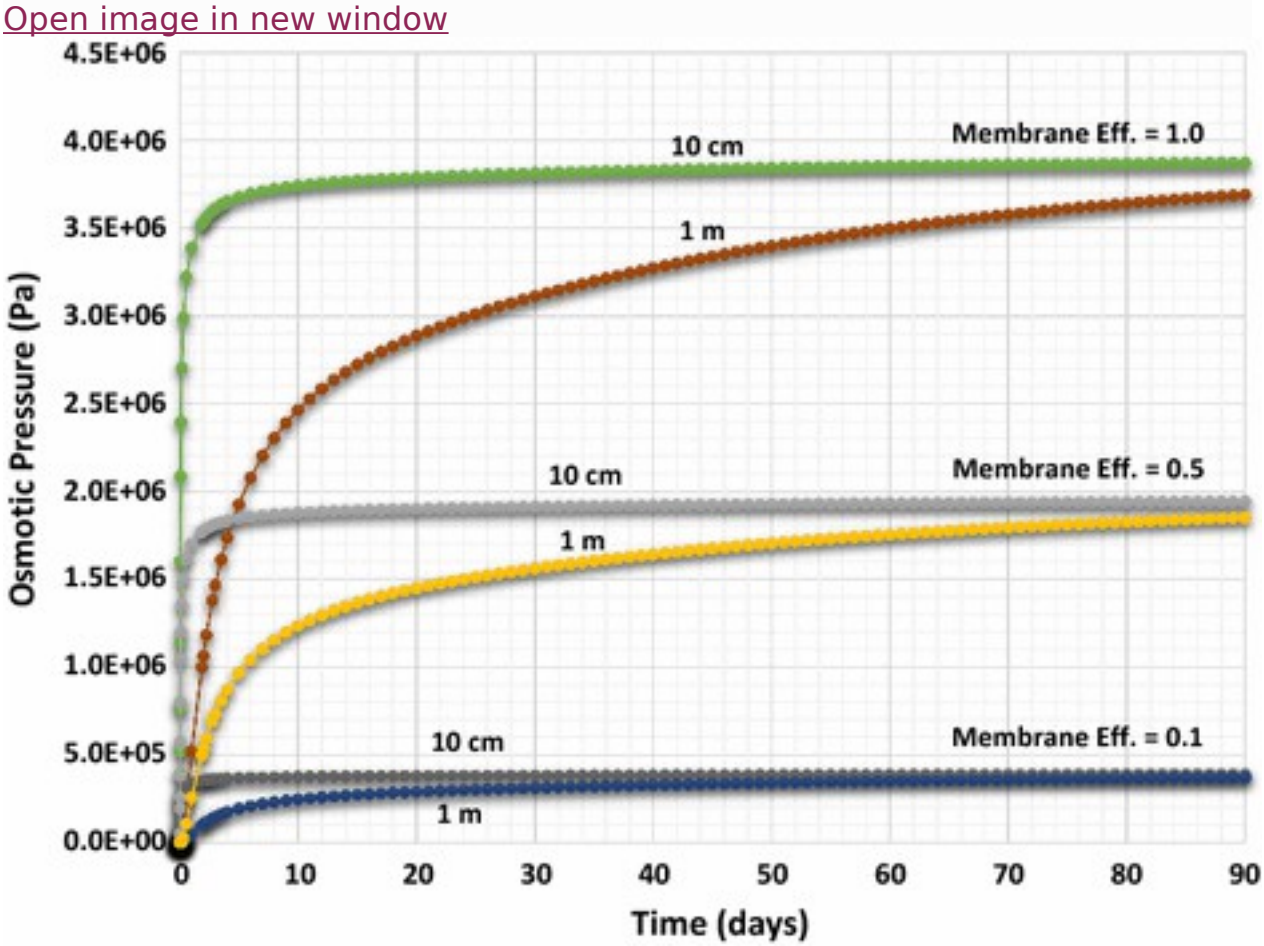

Fig. 5
Pressure evolution up to 90 days within a distance of 10 and 100 cm from a constant pressure element at the left boundary with varying membrane efficiency: 10, 50 and 100%

For a membrane efficiency of 10%, the results show that the salt concentration difference raised the pressure in the clay pores about 4.0E+5 Pa in less than two day within a distance of 10 cm from the fracture. At 55 day, the distance over which the pressure rose by 4.0E+5 Pa extended to 1 m, respectively. This pressure increase is due to the large contrast in salt concentration between the two adjacent elements. However, due to limited membrane efficiency, some of the salt ions can freely move across the element boundaries. Consequently, the observed pressure increase cannot reach the ideal osmotic pressure value and stays somewhat low. Initially, it is the chemical potential gradient that drives the water flux from the element with low salt concentration toward the adjacent element with high concentration. As the pressure increases, the hydraulic gradient begins to control the flux and drive water away from the fracture element.

In the case of membrane efficiency of 50%, the pressure increase predicted by the simulation is much higher. The existing contrast in salt concentration raises the pressure now to about 1.7E+6 Pa in less than 2 day within a distance of 10 cm from the fracture boundary, and to 1 m at about 55 day, respectively. As in to previous case, the limited membrane efficiency can cause some of the salt ions to move freely across the element boundaries, thus preventing the pressure increase to reach the value of the ideal osmotic pressure.

Using a membrane efficiency of 100% (ideal membrane), the pressure increase now reaches the ideal osmotic pressure value of about 3.8E+6 Pa which is comparable to the osmotic pressure calculated using Eq. (3). The salt concentration difference raises the pressure now to about 3.5E+6 in less than 2 day within a distance of 10 cm from the fracture boundary, and to 1 m at about 55 day, respectively

The simulation results show the importance of membrane efficiency value of the clay experiencing osmosis on the pressure increase observed in clay pores. In the subsurface, compacted clays having porosity less than 10% with NaCl concentration about 55,000 ppm can have high membrane efficiency which can be more than 95% membrane efficiency for montmorillonite, chlorite, and illite and about 90% membrane efficiency for kaolinite, theoretically (Marine and Fritz 1981). It can be concluded that clay-swelling pressure in subsurface in the condition as used in the simulation above can be high, thus we should aware of the possibility of significant formation damage happened due to clay-swelling pressure.

4 Theoretical Modeling and Numerical Simulation of Two-phase Flow in Shale Gas with Clay-swelling Effect

In this part we describe a mathematical formulation and a new generation of simulator developed to mimic the two-phase (aqueous and gas) flow in shale gas reservoir with three distinct porosities (organic, slit-shaped-inorganic and clay pores) applying the conceptual petrophysical model shown in Fig. 1. An earlier version of the mathematical model has been presented in Eveline et al. (2016). The simulator is an expansion of TAMU-FTsim, which is a variant of the TOUGH+ simulator (Moridis 2014; Moridis and Freeman 2014).

The developed simulator includes two phases, water and gas, with three components, H_2OH2O, CH_4CH4 and salt distributed in three porosities (organic, slit-shaped-inorganic and clay pores). The organic pores contain gas phase, which consists of CH_4CH4 component only, as free-gas and adsorbed-gas. The inorganic slit-shaped pores contain water and gas phases

consisting of three components, H_2O, CH_4H2O, $CH4$ and salt. The clay pores on the other hand, contain water phase consisting of three components, H_2O, CH_4H2O, $CH4$ and salt. Flow and transport between the discretized simulation elements are through the inorganic slit-shaped pores only. Note that, although they do not contribute to the storage of hydrocarbons, the clay pores experience pressure and chemical potential gradients as the driving forces for molecular transport as described in Sect. 2.

4.1 Mathematical Model and Numerical Solution

Mathematical Model

Mass balance equations to be solved in this part are written in the form of partial differential equation as in Eq. (5) discussed in Sect. 3. The mass balance equations for component H_2O,CH_4H2O,$CH4$ and salt are as follows:

$$\partial\partial t\{\phi_I(x^{H_2OA}\rho_A S_A+x^{H_2OG}\rho_G S_G)\}+\nabla.\{\mathbf{F}^{H_2OA}||_{adv}+\mathbf{F}^{H_2OG}||_{adv}+\mathbf{F}^{H_2OA}||_{dif}+\mathbf{F}^{H_2OG}||_{dif}\}+w^{H_2OA,IC}=q^{H_2O}\partial\partial t\{\phi I(xAH2O\rho ASA+xGH2O\rho GSG)\}+\nabla.\{FAH2O|adv+FGH2O|adv+FAH2O|dif+FGH2O|dif\}+wA,ICH2O=qH2O \quad (14)$$

$$\partial\partial t\{\phi_I(x^{CH_4A}\rho_A S_A+x^{CH_4G}\rho_G S_G)+\rho_G\phi_k+M^{CH_4}\varepsilon_{ks}(1-\phi_{tot})C_\mu\}+\nabla.\{\mathbf{F}^{CH_4A}||_{adv}+\mathbf{F}^{CH_4G}||_{adv}+\mathbf{F}^{CH_4A}||_{dif}+\mathbf{F}^{CH_4G}||_{dif}\}+w^{CH_4A,IC}=q^{CH_4}\partial\partial t\{\phi I(xACH4\rho ASA+xGCH4\rho GSG)+\rho G\phi k+MCH4\varepsilon ks(1-\phi tot)C\mu\}+\nabla.\{FACH4|adv+FGCH4|adv+FACH4|dif+FGCH4|dif\}+wA,ICCH4=qCH4 \quad (15)$$

$$\partial\partial t(x^{SaltA}\rho_A S_A\phi_I)+\nabla.\{\mathbf{F}^{SaltA}||_{adv}+\mathbf{F}^{SaltA}||_{dif}\}+w^{SaltA,IC}=q^{Salt}\partial\partial t(xASaltpASA\phi I)+\nabla.\{FASalt|adv+FASalt|dif\}+wA,ICSalt=qSalt \quad (16)$$

In the Eq. (14) to (16), ϕ_I,ϕ_k,$\phi_C\phi I$,ϕk,ϕC and $\phi_{tot}\phi tot$ are the inorganic slit-shaped, organic, clay and total porosity in shale matrix where the total porosity is summation of the other porosities. The advective mass fluxes are described by Darcy's law and the diffusive mass fluxes are typically described using Fick's law.

In the inorganic slit-shaped pores, two-phase flow is treated by the classical capillary pressure and relative permeability effects which vary as a function of phase saturation. Here, wettability of the inorganic pores is assumed to be strongly water-wet and initially, a small amount of irreducible water phase coexists with the gas-phase.

Flow and transport model of gas phase in the organic and inorganic slit-shaped pores follows the approach presented by Wasaki and Akkutlu (2015). This approach is similar to conventional treatment of the two-phase flow in porous media: each phase follows its own path obeying its own transport mechanisms, also assumes that pore pressure is in equilibrium within the specified bulk volume, and it is the same in organic and inorganic pores. Gas-phase flow and transport mechanism including advective and diffusive mechanisms. The diffusive mechanisms are surface diffusion of the sorbed-phase of the organic solid and molecular diffusion as follows:

$$\mathbf{F}_{CH_4G}||_{dif} = -\rho_G \phi_I S_G \tau_G D_{CH_4o,G} \nabla x_{CH_4G} - M_{CH_4} D_s \nabla C_\mu F_{GCH4}|_{dif} = -\rho_G \phi_I S_G \tau_G D_{o,GCH4} \nabla x_{GCH4} - M_{CH4} D_s \nabla C_\mu \quad (17)$$

There is mass-exchange between the slit-shaped pores and the clay pores driven by hydraulic pressure and chemical potential gradient as described in Eq. (18) to (20). The mass-exchange term follows the approach used to describe mass-exchange between organic and inorganic pores in shale gas matrix (Akkutlu and Fathi 2012). Here, the flow and transport exchange model is following the osmosis model developed in Sect. 3.

The mass-exchange can cause building up of pressure inside the clay pores (clay-swelling pressure). The increased pressure inside the clay pores (current clay-pore pressure minus initial clay-pore pressure) then is added into the original P_{conf}Pconf in Eq. (1). This additional pressure causes the effective stress $(P_{conf} - \alpha P)$(Pconf−αP) in Eq. (1) is increasing, thus reduce permeability of the slit-shaped pores.

Mass-exchange of H_2O, CH_4H2O,CH4 and salt between the slit-shaped pores and the clay pores are defined as follows:

$$w_{H_2OA,IC} = \ell_{IC}\{x_{H_2OA}\rho_A k_m \mu_A [P_{A,I} - P_{A,C}] - x_{H_2OA}\lambda(\rho_A)^2 [x_{SaltA,I} - x_{SaltA,C}] + \rho_A \phi_C \tau_A D_{H_2Oo,A}[x_{H_2OA,I} - x_{H_2OA,C}]\} w_{A,ICH2O} = \ell_{IC}\{x_{AH2O}\rho_A k_m \mu_A [P_{A,I} - P_{A,C}] - x_{AH2O}\lambda(\rho_A)^2 [x_{A,ISalt} - x_{A,CSalt}] + \rho_A \phi_C \tau_A D_{o,AH2O}[x_{A,IH2O} - x_{A,CH2O}]\} \quad (18)$$

$$w_{CH_4A,IC} = \ell_{IC}\{x_{CH_4A}\rho_A k_m \mu_A [P_{A,I} - P_{A,C}] - x_{CH_4A}\lambda(\rho_A)^2 [x_{SaltA,I} - x_{SaltA,C}] + \rho_A \phi_C \tau_A D_{CH_4o,A}[x_{CH_4A,I} - x_{CH_4A,C}]\} w_{A,ICCH4} = \ell_{IC}\{x_{ACH4}\rho_A k_m \mu_A [P_{A,I} - P_{A,C}] - x_{ACH4}\lambda(\rho_A)^2 [x_{A,ISalt} - x_{A,CSalt}] + \rho_A \phi_C \tau_A D_{o,ACH4}[x_{A,ICH4} - x_{A,CCH4}]\} \quad (19)$$

$$w_{SaltA,IC} = \ell_{IC}\{(1-\sigma)\rho_A x_{SaltA}[k_m \mu_A (P_{A,I} - P_{A,C}) - \lambda \rho_A (x_{SaltA,I} - x_{SaltA,C})] + (1-\sigma)\rho_A \phi_C \tau_A D_{Salto,A}(x_{SaltA,I} - x_{SaltA,C})\} w_{A,ICSalt} = \ell_{IC}\{(1-\sigma)\rho_A x_{ASalt}[k_m \mu_A (P_{A,I} - P_{A,C}) - \lambda \rho_A (x_{A,ISalt} - x_{A,CSalt})] + (1-\sigma)\rho_A \phi_C \tau_A D_{o,ASalt}(x_{A,ISalt} - x_{A,CSalt})\} \quad (20)$$

Here, $\ell_{IC}\ell IC$ is the shape factor $(1/m_2);P_{A,I}(1/m2);PA,I$ is the inorganic pore pressure (Pa); $P_{A,C}PA,C$ is the clay-pore pressure (Pa); and $\lambda\lambda$ is as described in Eq. (10).

In Eq. (15), the third term in left-hand-side is the sorbed-gas accumulation of CH_4CH4 in kerogen solid. The sorbed-gas concentration in kerogen grain volume $(C_\mu)(C\mu)$ is described as follows (Wasaki and Akkutlu 2015):

$$C_\mu=V_{sL}\rho_{sc,gas}\rho_{grain}\varepsilon_{ks}M_{CH_4}PP+P_LC\mu=VsL\rho sc,gas\rho grain\varepsilon ksMCH4PP+PL \quad (21)$$

Numerical Solution

The simulator developed in this part includes three thermophysical state which are single aqueous phase and two-phases in matrix domain which has three pores, and two-phases in fracture domain with single pore. Primary variable is chosen to be able describing a system involving mass-exchange by osmosis mechanism between pores within the element. Other unknown variables are set by the use of constitutive, equilibrium restriction, and constraint equations. Here, we use Henry's equation to get the fraction of CH_4CH4 in the aqueous phase.

The primary variables for single aqueous phase in matrix domain are pressure, CH_4CH4 mol fraction in slit-shaped pore, salt mol fraction in slit-shaped pore, salt mol fraction in clay pore, pressure in clay pore, and temperature. The primary variables for two-phase in matrix domain are pressure, gas-phase saturation, salt mass fraction in aqueous phase in slit-shaped pore, salt mass fraction in clay pore, pressure in clay pore, and temperature. The primary variables for two-phase in fracture domain are pressure, gas-phase saturation, H_2OH2O mol fraction in aqueous phase, salt mol fraction in aqueous phase, H_2OH2O mol fraction in gas phase, and temperature.

The mass balance equations Eq. (14) to (16) are solved in the same manner as in the previous method which is described in Sect. 3.2. The mass balance equations are discretized in space using the integral finite difference method, and time is discretized as a first-order finite difference. All the unknown thermodynamic parameters in the flux and source/sink terms are evaluated at new time level. The mass balance equations become a set of residual equations in the form of Eq. (11).

We construct in the form Eq. (13), the Jacobian matrix equations, from the residual equations above where the Jacobian matrix $(\sum_i\partial R_{\kappa,k+1n}\partial X_i)\sum i\partial Rn\kappa,k+1\partial Xi)$ is got by differentiating the residual equations in terms of primary variables $(X_i)(Xi)$. Again, the dimension of the Jacobian matrix is $(n_{element}\times n_{equation})\times(n_{element}\times n_{equation})$ $(nelement\times nequation)\times(nelement\times nequation)$, and the unknowns are the $n_{element}\times n_{equation}nelement\times nequation$ primary variables. Solution of

the Jacobian matrix equations proceeds in an iterative manner until the residuals ($R_{\kappa,k+1n}$)$R_{n\kappa,k+1}$) are reduced below a preset convergence tolerance that describes an acceptable (and very low) mass and/or energy balance error.

4.2 Simulation of Two-phase Flow in Shale Gas with Clay-swelling Effect

Simulation of five shut-in cases is conducted to observe the effect of salt concentration, salt type, initial water saturation, and clay-membrane efficiency to permeability evolution, the details of shut-in cases are shown in Table 2. Also, we run production cases after shut-in to observe the impact of permeability impairment during shut-in to well production performance.

Table 2

Two-phase simulation, shut-in cases

Case	Initial Sw in slit-shaped pore	Salt type	Salt mass fraction in fracturing fluid	Salt mass fraction in aqueous phase in shale
Case 1	0.2	NaCl	0.0001	0.05
Case 2	0.2	NaCl	0.02	0.05
Case 3	0.2	NaCl	0.02	0.15
Case 4	0.2	KCl	0.02	0.15
Case 5	0.05	NaCl	0.0001	0.05

The specific problem to which the numerical simulation is applied assumes a quarter of a single vertical hydraulic fracture perpendicular to a horizontal well and the adjacent stimulated shale gas volume as shown in Fig. 1. The geometry of the problem in xyz directions is $5\times100\times105\times100\times10$ m which is divided into 500 gridblocks in the x-direction. We set the most left of the gridblocks as hydraulic fracture element. Here, we are interested to understand the imbibition and osmosis mechanisms and their impact to permeability alteration related to water in the hydraulic fracture that we simplify the geometry in 1D.

Different initial salt concentration in the aqueous phase between hydraulic fracture element and shale matrix elements is applied to imitate condition in the hydraulic fractures and the shale matrix. Constant pressure of 3000 psi

and water saturation of 100% are applied in the hydraulic fracture element, which is equal to the initial pressure in the shale matrix elements to simulate shut-in and continuous shale–water interaction after hydraulic fracturing operation. In all numerical simulation, the initial water saturation, pressure, and temperature are the same as shown in Table 3. At initial time, the water saturation in the slit-shaped pores is assumed to be at irreducible water saturation of 20% with maximum capillary pressure values, except for the fifth case which has initial water saturation in the state of sub-irreducible. For each case, clay pores contain equal salt concentration to the slit-shaped pores. Different clay-membrane efficiencies are applied for each simulation case: 0.01; 0.1; 0.25; 0.5; 0.75; and 1.00. Other properties such as permeability and porosity are given in Table 3.

4.3 Simulation Results and Discussion

Shale gas well production performance is a function of matrix permeability adjacent to hydraulic fractures such that damage in this zone will cause a decrease in the well production performance. In this part, we want to show the nature of clay-swelling-induced imbibition-driven permeability damage using the newly developed simulator.

4.3.1 Shut-in, Case 1

Although initially the pressure is uniform, there exists a water flux from hydraulic fracture element into the adjacent shale element due to spontaneous imbibition mechanism caused by high capillary pressure in the shale matrix. The computed pressure (Figs. 6, 7a) and water saturation (Fig. 6) are increasing with time and propagating from the gridblocks adjacent to hydraulic fracture element toward the outer boundary. The calculated pressure wave velocity during the first day is approximately 2 m/day, and average water invasion velocity is 0.6 m/day. Pressure velocity is faster than water invasion velocity. However, these velocities are decreasing, and after the pressure in hydraulic fracture element is equalized with saturation and capillary effect in the adjacent shale element pore, the flux deceases. After 30 days, water invades to approximately 11 cm into the matrix. Simulation results also show that the estimated pressure and water saturation values at different time in the slit-shaped pores mostly are independent of clay-membrane efficiency since they reach nearly the same values in the presence of different clay-membrane efficiency.

Table 3

Input parameters for two-phase flow simulation in shale

Parameter	Value	Unit	Parameter	Value	Unit
Initial slit-	3000	psi	Sorption properties		

Parameter	Value	Unit	Parameter	Value	Unit
shaped pore pressure					
Initial clay-pore pressure	3000	psi	Grain Density	2650	kg/m3kg/m3
Initial temperature	60	∘C∘C	Langmuir volume (V_{sL})(VsL)	5.66E−03	m3/kgm3/kg
Porosity			Langmuir pressure (P_L)(PL)	3.45E+06	Pa
ϕ_kϕk (organic)	2%		Total organic grain volume / total grain volume (ε_{ks})(εks)	0.02	
ϕ_IϕI (inorganic)	6%				
ϕ_CϕC (clay)	10%		Diffusion coefficients		
Initial water saturation			Surface diffusion coefficient	1.00E−09	m2/sm2/s
in ϕ_kϕk	0%		Diffusion coefficient of CH_4CH4 in aqueous phase	1.72E−09	m2/sm2/s
in ϕ_IϕI	20%		Diffusion coefficient of salt in aqueous phase	2.60E−13	m2/sm2/s
in ϕ_CϕC	100%		Diffusion coefficient of CH_4CH4 in gas phase	1.00E−09	m2/sm2/s
Gangi model parameters (slit-shaped pore)			Osmotic model parameters		
k_0k0	1.00E−0	md	Clay-membrane	1.00E+0	nD

Parameter	Value	Unit	Parameter	Value	Unit
	2		permeability (k_m) (km)	0	
m	0.5		Shape factor	1.00E−05	
P_1P1	26000	psi	Clay-membrane efficiency (σ)(σ)	varied	
P_{conf}Pconf	15000	psi	Salt type	varied	
αα	0.5				

Open image in new window

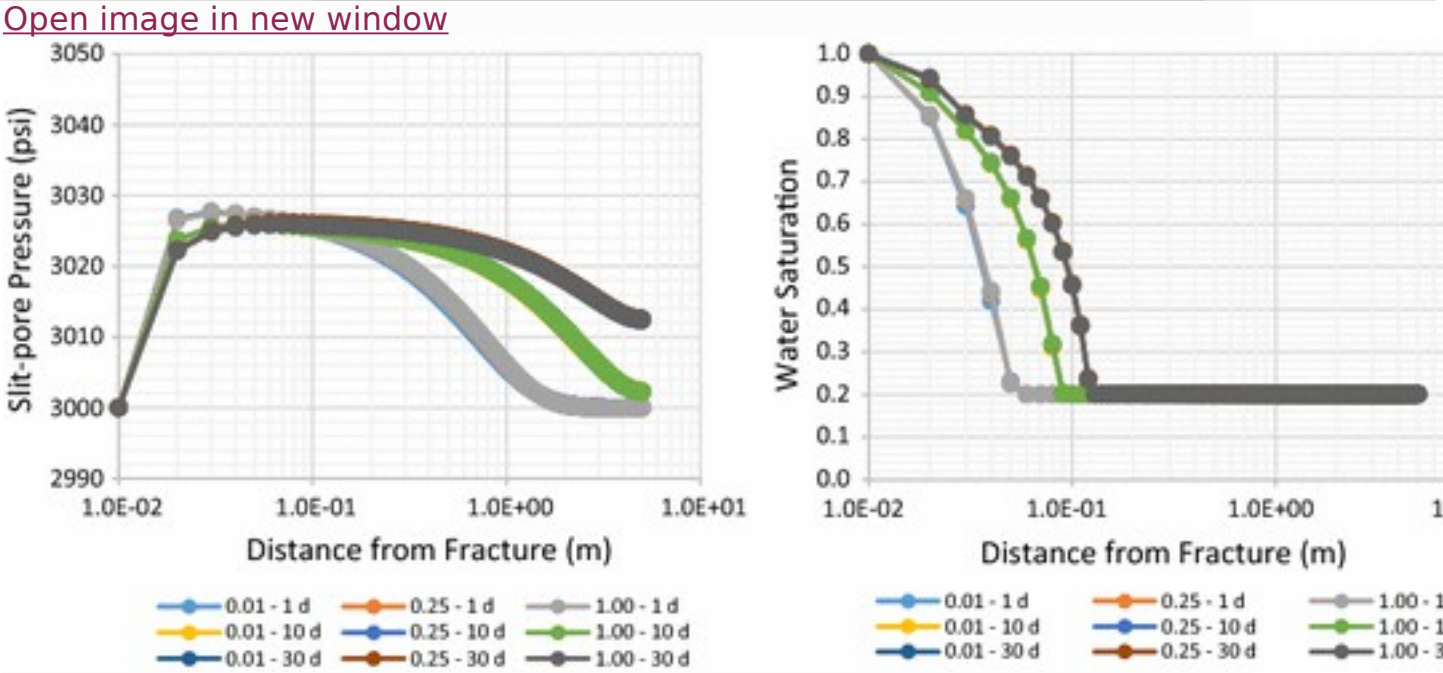

Fig. 6
Simulation results of Case 1. *Left* slit-shaped pore pressure; *Right* water saturation in slit-shaped pores at time 1, 10, and 30 days using clay-membrane efficiency of 0.01, 0.25, and 1.00

In clay pores, on the other hand, levels of pressure predicted are sensitive to the clay-membrane efficiency. Clay-pore pressure increases as the membrane efficiency is increased such that highest clay-pore pressure is reached in the case ideal membrane efficiency of 1.0. As shown in Fig. 7b, clay-pore pressure values is increasing with time and propagate from the gridblocks near hydraulic fracture element toward outer boundary and reach a distance about 11 cm from hydraulic fracture element. These increases

are corresponding to the fresh water movement in the slit-shaped pore toward the outer boundary as represent by water saturation increase in slit-shaped pores near hydraulic fracture (Fig. 6).

Figure 7c shows permeability reduction evolution in slit-shaped pores for different clay-membrane efficiency caused by pressure increase inside clay pores. At initial time, as pressure and fresh water in slit-shaped pores are still progressing toward outer boundary, permeability reduction near hydraulic fracture are small because clay-pore pressure is balanced with the slit-shaped pore pressure. There are fluid exchanges back and forth between the two pores due to hydraulic pressure differences and salt concentration differences (osmosis mechanism). At a certain time when no significant water can move further toward the outer boundary because pressure in the slit-shaped pores near hydraulic fracture elements has reached equalization with capillary and saturation effects, osmosis mechanism takes place more significant and pressure begin to build up high in clay pores. When clay-membrane efficiency is 0.01, clay-pore pressure can be 100 psi higher than slit-pore pressures and permeability reductions are about 3–4%. While assuming ideal membrane, clay-pore pressures can reach about 900 psi higher and this causes permeability reduction up to 24% in 30 days.

Here, the discussion is focus to the absolute permeability of the porous medium, not the effective permeability. The effective permeability to gas will be more reduced if the water saturation is higher which cause the relative permeability to gas is lower.

Open image in new window

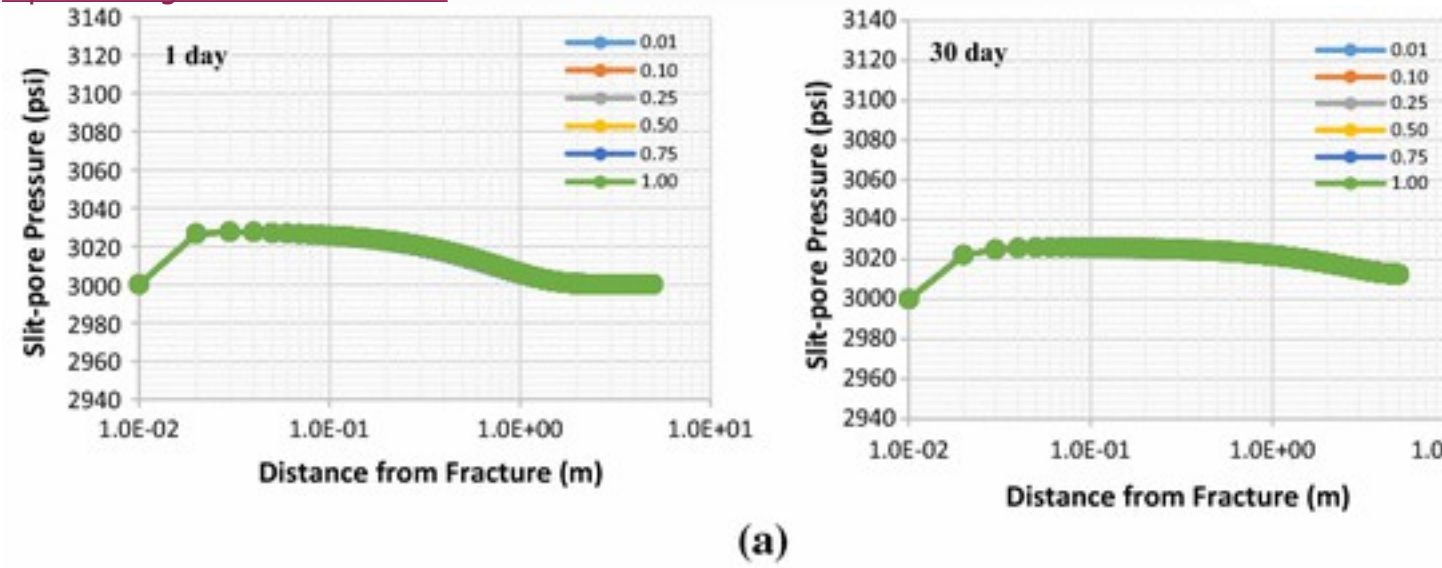

(a)

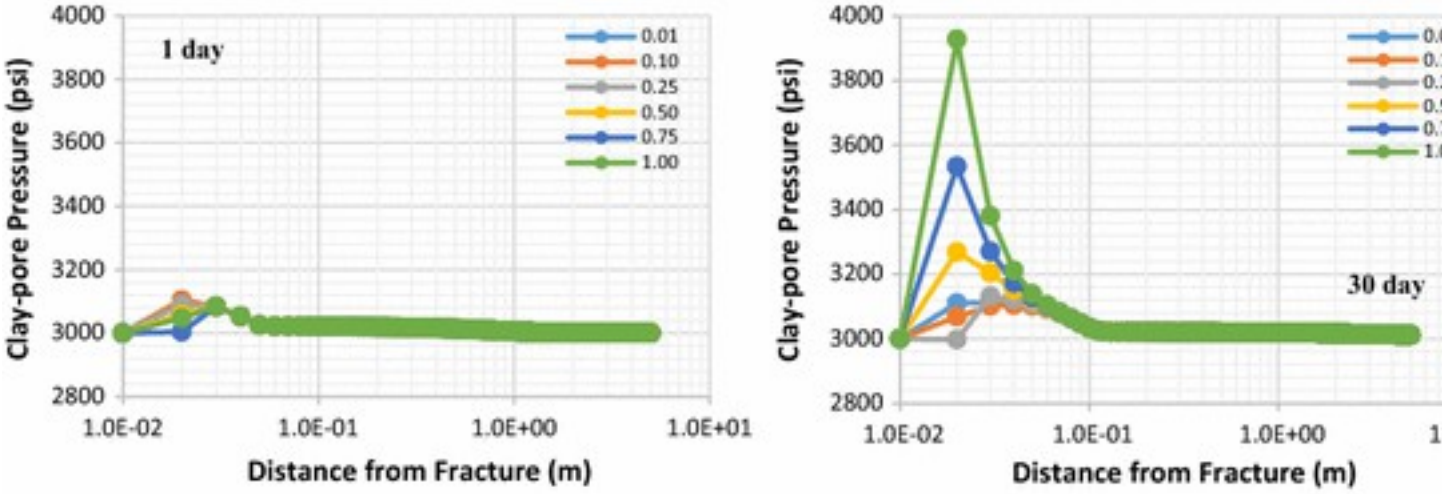

(b)

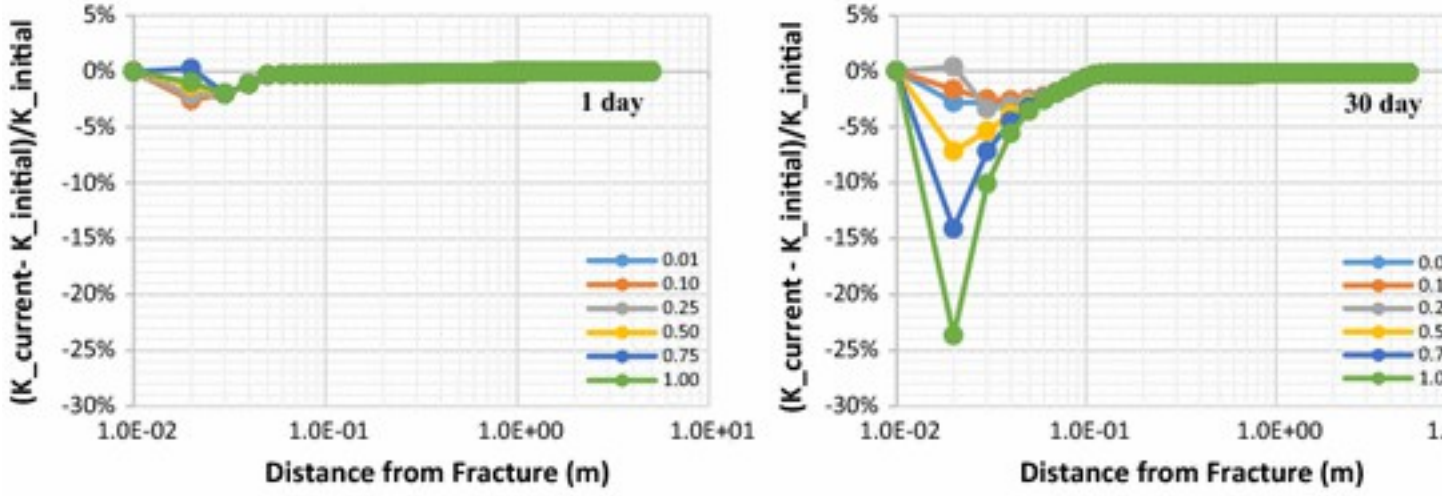

(c)

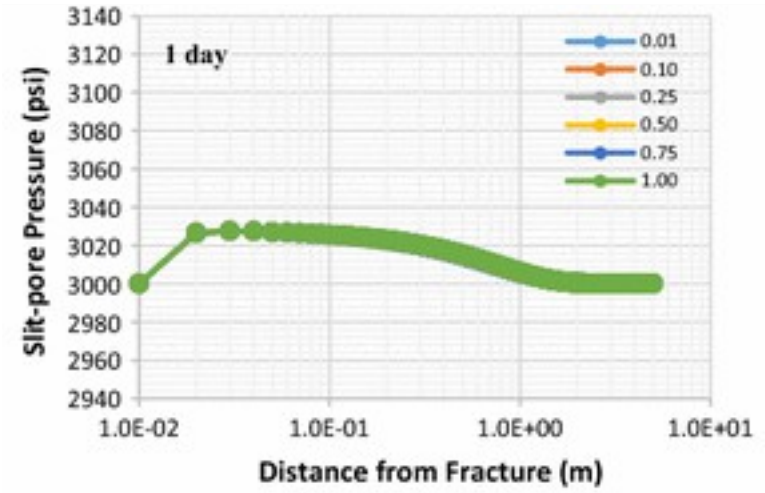
1 day
Slit-pore Pressure (psi)
Distance from Fracture (m)
0.01
0.10
0.25
0.50
0.75
1.00

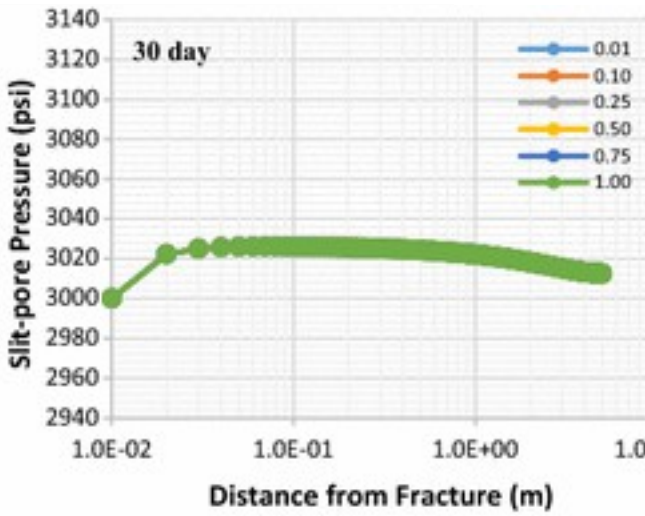
30 day
Slit-pore Pressure (psi)
Distance from Fracture (m)
0.01
0.10
0.25
0.50
0.75
1.00

(a)

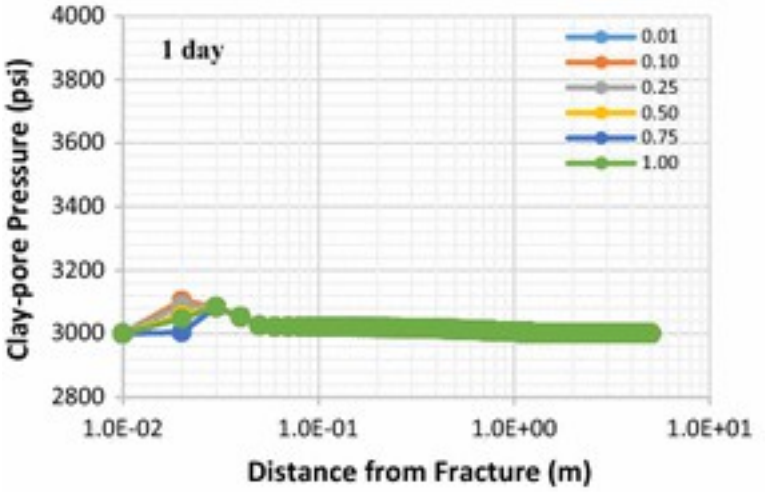
1 day
Clay-pore Pressure (psi)
Distance from Fracture (m)
0.01
0.10
0.25
0.50
0.75
1.00

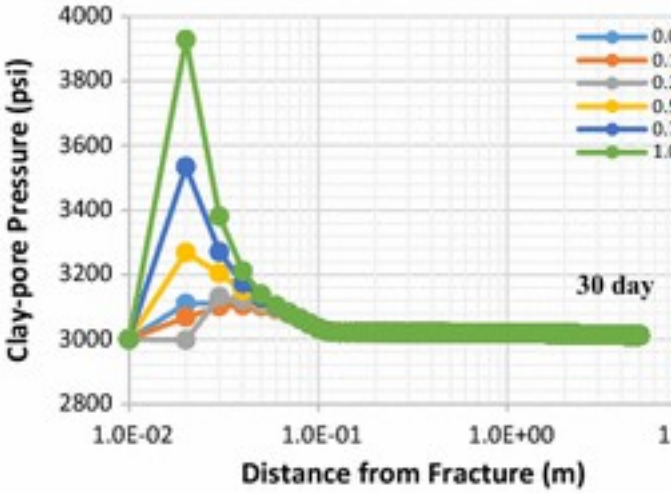
30 day
Clay-pore Pressure (psi)
Distance from Fracture (m)

(b)

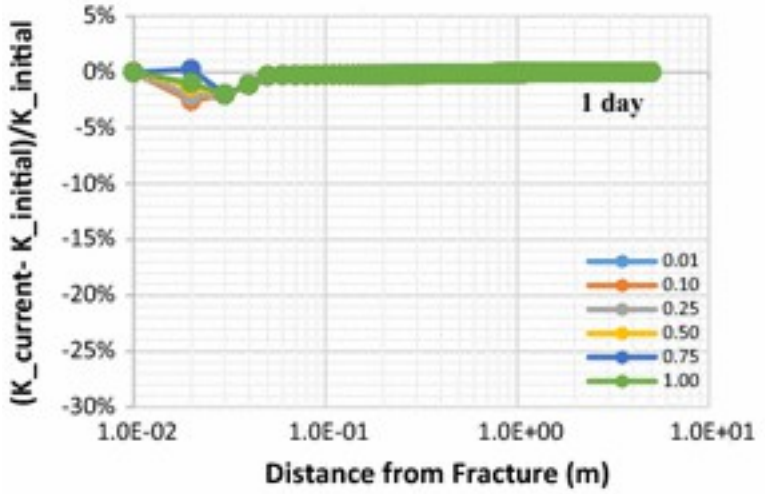
1 day
(K_current- K_initial)/K_initial
Distance from Fracture (m)
0.01
0.10
0.25
0.50
0.75
1.00

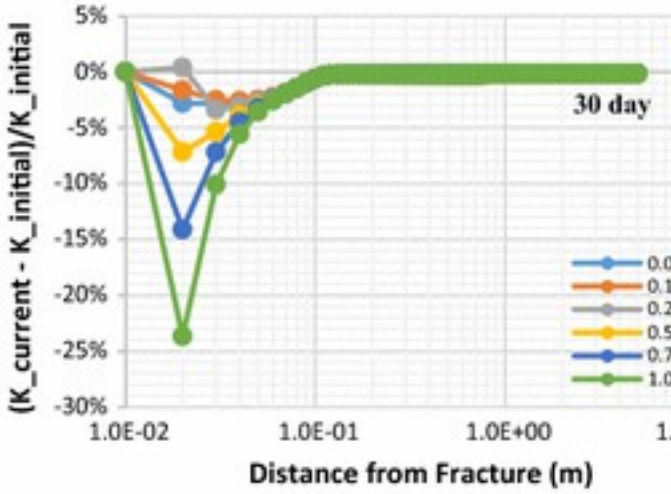
30 day
(K_current - K_initial)/K_initial
Distance from Fracture (m)

(c)

Fig. 7
Simulation results of Case 1: **a** slit-shaped pore pressure; **b** clay-pore pressure; **c**permeability reduction in slit-pore at time 1 and 30 days with varied clay-membrane efficiency of 0.01, 0.1, 0.25, 0.5, 0.75 and 1.00

4.3.2 Comparison of Shut-in Cases, 1 Through 5

Simulation results of case 1, 2, 3, and 4 (Fig. 8) show that permeability reduction occurs in all cases with different magnitude which is dependent on the salt concentration differences between hydraulic fracture and shale pores, the salt type, and the clay-membrane efficiency. Comparing case 1 and 2, which in both cases NaCl mass fraction in the aqueous phase inside shale pores being 5%, higher permeability reduction is occurred when hydraulic fracture is filled with nearly fresh water than when filled with NaCl mass fraction of 2%. Comparing case 2 and 3, which in both cases hydraulic fracture contains 2% NaCl, higher permeability reduction is occurred when salt concentration in the aqueous phase inside shale pores is higher. Comparing case 3 and 4, when different salts are dissolved in the aqueous phase, lower permeability reduction is occurred when KCl is the dissolved salt.

Open image in new window

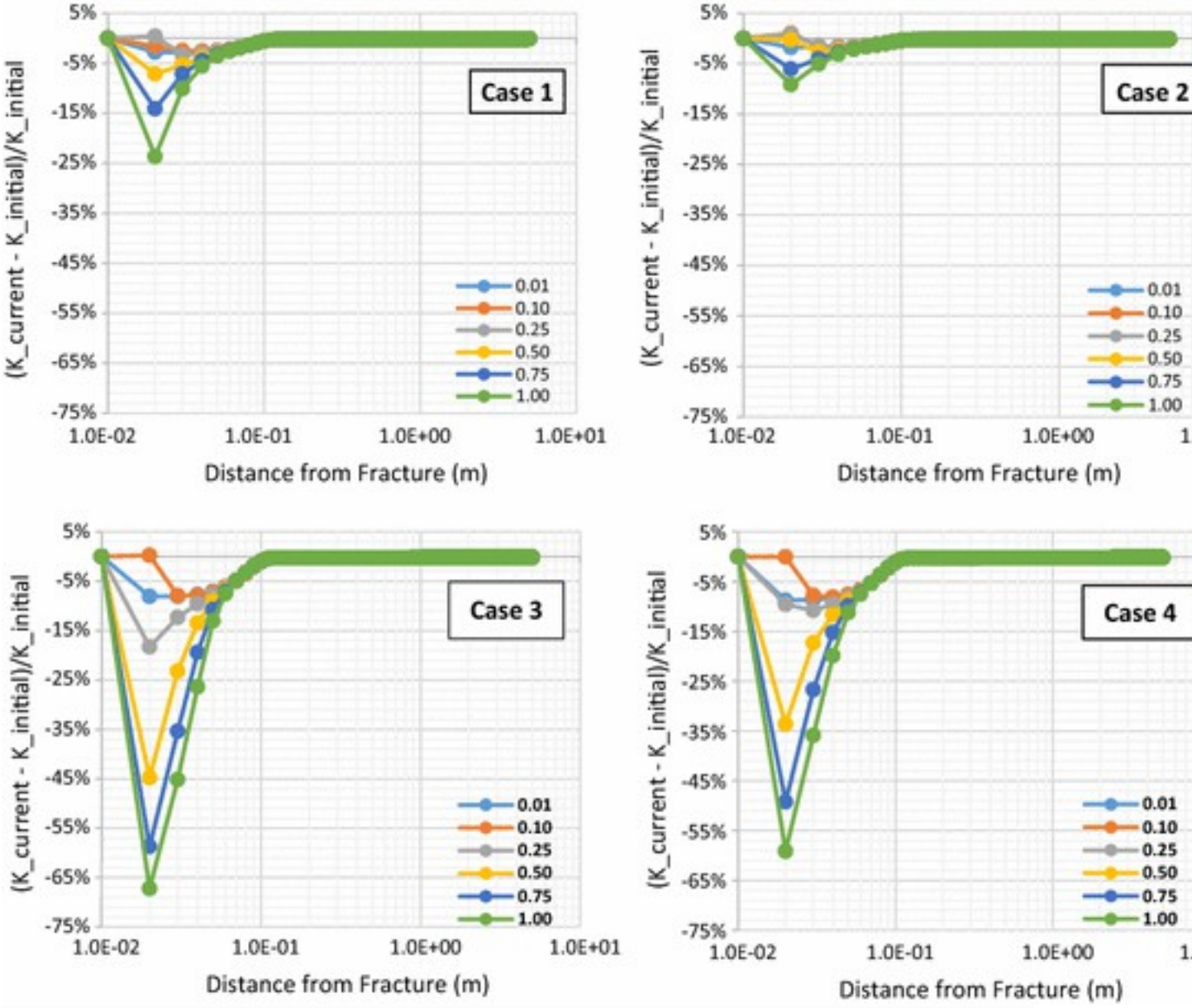

Fig. 8
Comparison of permeability reduction in slit-shaped pores of all simulation cases at time 30 days. *Different colors* are indicating different clay-membrane efficiency (0.01; 0.1; 0.25; 0.5; 0.75; and 1.0)

Figure 9 shows that, as time progresses, shale–water interaction continues and move slowly further toward outer boundary as a result of imbibition, causing expansion of the zone of clay pore increase and permeability reduction. This water imbibition is lowering salt concentration inside slit-shaped pores and resulting salt concentration difference between slit-shaped and clay pores. Theoretically, osmotic pressure increases until the salt concentration is equal between the two types of pores, if clay acts as an ideal membrane. Clays are leaky membrane, however, and that causes salt

dissolved in water in the clay pores filtrate through the clays, therefore the ideal osmotic pressure will not reach that high value experienced with the ideal case. This results show that the damage zone can expand further when clay-water keep interacting. This indicate that early clean-up is necessary to avoid expansion of clay–water interaction zone that can cause expansion of permeability damage zone, hence shale gas well production performance reduction.

Open image in new window

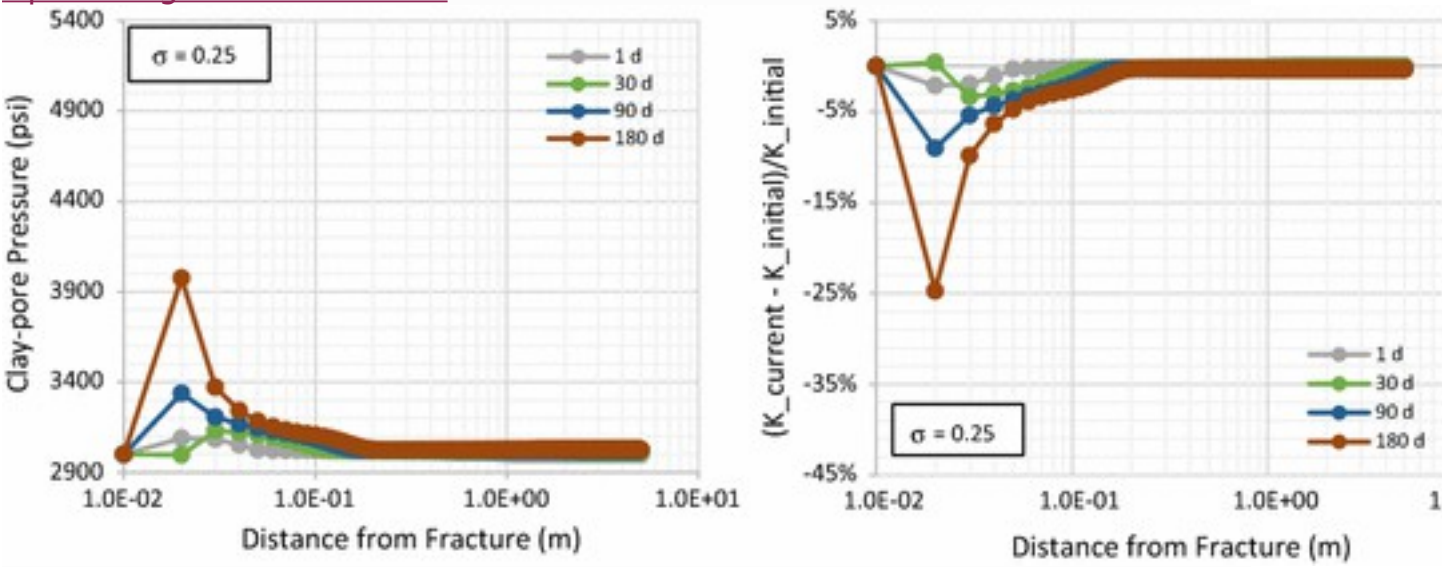

Fig. 9
Effect of duration (Case 1, membrane efficiency of 0.25): *Left* clay-pore pressure increases with time; *Right* permeability reduction increases with time, as shown with *different color*

Case 5 considers a shale formation with a sub-irreducible water saturation. Comparing case 1 and case 5 indicates that when shale matrix has a saturation below the irreducible water saturation, permeability reduction occurs more severe during the same duration of shale–water interaction. As shown in Fig. 10, on the left figure, water invasion zone for case 5 is smaller than case 1. This is because as water penetrates into the slit-shaped pores, water remains immobile at the leading edge of the of the saturation wave until saturation in the pores increases and becomes higher than the irreducible water saturation. This leads to elongated times of water–clay interaction between the slit-shaped pore containing fracturing water and high-salinity clay pore. Consequently, the formation experiences higher level of clay-pore pressure as shown in the right side of figure, Fig. 10, and eventually this lead to larger permeability reduction.

Other sets of simulation were conducted using the same parameters as case 5 except for the initial water saturation in the slit-shaped pores which were varied up to 40%. Fig. 11 shows permeability reduction at 30 day for varied initial water saturation using clay-membrane efficiency 1.0.

Open image in new window

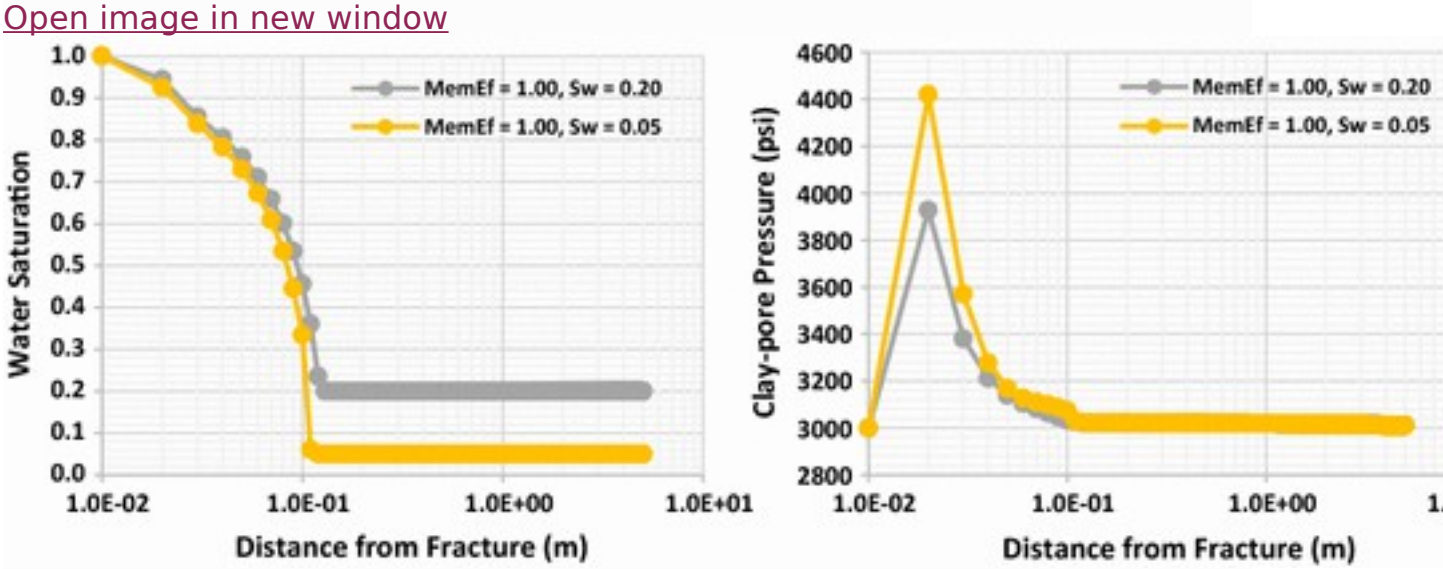

Fig. 10
Comparison between case 1 and case 5 (sub-irreducible water saturation) at 30 day, effect of initial water saturation. *Left* water saturation; *Right* clay-pore pressure

Open image in new window

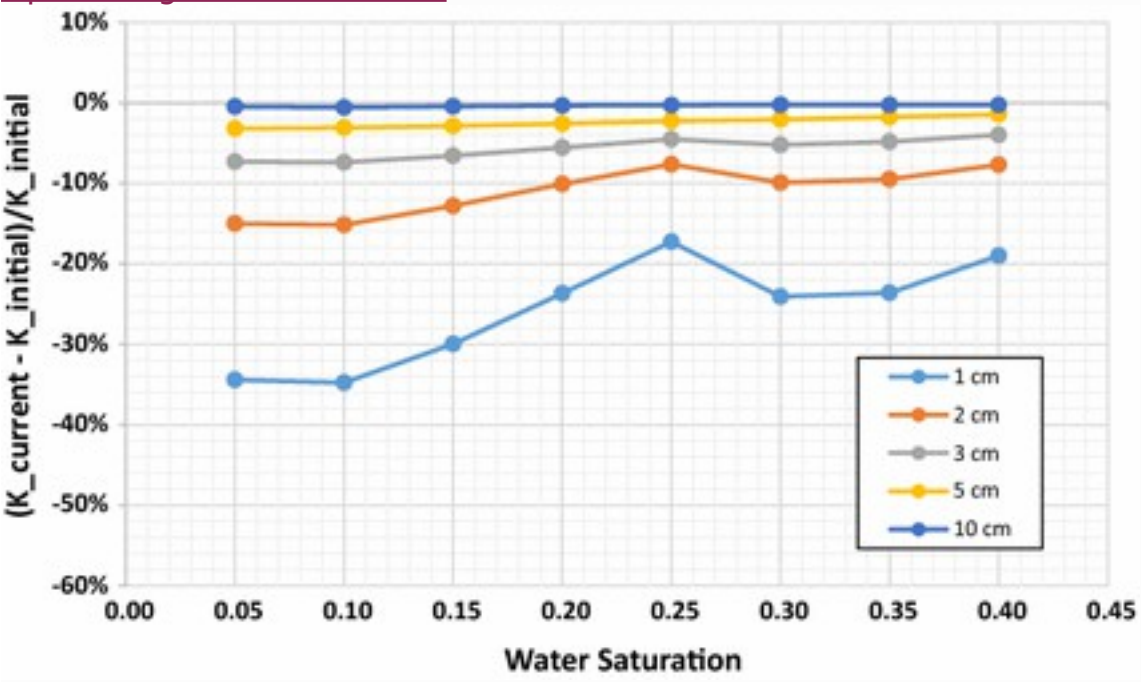

Fig. 11
Permeability reduction at 30 day for different initial water saturation in model shale at several distances from the hydraulic fracture, using clay-membrane efficiency 1.0

4.3.3 Production Cases

We run simulation cases of production after shut-in for 30 days to compare the impact of permeability impairment to production performance between

irreversible and reversible damage as shown in Fig. 12. In the irreversible damage case, we set the permeability damage occurred during shut-in as permanent and geomechanics effect to permeability is only through decreasing formation pore pressure due to production. On the other hand, in the reversible damage case, we do not consider the permeability damage occurred during shut-in as permanent and set the geomechanics effect to permeability fully, which is affected by clay-pore pressure as well as formation pore pressure. As expected, production performance when the damage is irreversible is lower than when the damage is reversible.
Open image in new window

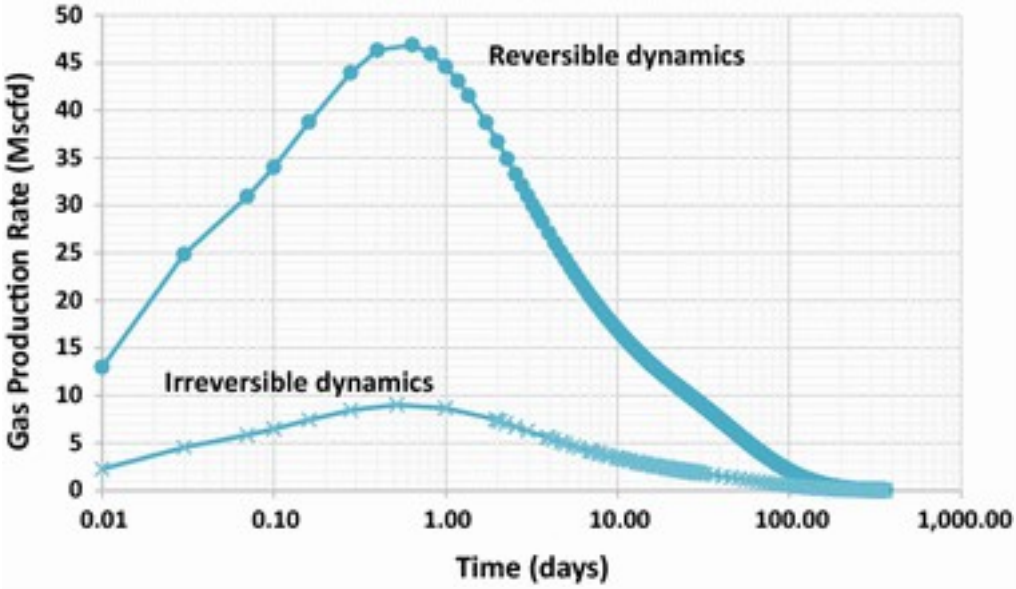

Fig. 12
Comparison of gas production rate between reversible and irreversible formation damage after shut-in 30 days, case 1, membrane efficiency of 0.25

5 Conclusion

A conceptual petrophysical model of shale matrix with an altered zone has been developed in order to understand imbibition and osmosis effect to permeability impairment related to hydraulic fracturing. In the model, the shale matrix contains organic, inorganic slit-shaped, and clay pores. Due to strong capillarity and water-wet characteristics of shale matrix, water imbibition from hydraulic fracture into slit-shaped pores in shale matrix occurs. This induces osmosis that water flows from slit-shaped pores to clay pores and as a result clay swelling happens.

A new simulator following the conceptual petrophysical model is developed. This simulator describes a system with three pores, two phases (gas and aqueous phases), and three components (H_2O,$CH_4$$H_2O$,$CH_4$ and salt) and includes imbibition and osmosis mechanisms and permeability alteration

due to clay swelling. In addition to this simulator, to understand osmosis effect in clays and validate mathematical model of osmosis in clays, we develop a simulator for a system of single pore, single aqueous phase, and two-components (H_2OH2O and salt) including osmosis. Simulation of single aqueous-phase transport in clays shows that high swelling pressures can occur in clays due to osmosis, and these are a function of salt type, salt concentration difference, and clay-membrane efficiency.

Simulation study of shut-in periods using the simulator with three pores, two phases, and three components indicates that due to clay content in shale matrix, shale–water interaction, and salinity difference between hydraulic fracture and the shale matrix, clay swelling can occur and it can cause a reduction in shale matrix permeability. More severe damage occurs if fresh water is used in the fracturing fluid. Even using 2% KCl in fracturing water still can significantly reduce permeability if the water in the clay/shale pores has high salinity. Continuing shale–water interaction can expand the damage zone further. Therefore, it is necessary to avoid prolonged imbibition of water into shale matrix, especially if we use fracturing fluids with salinity that can promote osmotic responses in the matrix. Simulation of systems with varied initial water saturation in slit-shaped pores shows that, when the shale matrix is at sub-irreducible water saturation levels, the reduction in permeability is more pronounced compared to those at the irreducible water saturation or higher. Simulation of production after shut-in shows that when permeability damage after shut-in is permanent or irreversible, lower well production performance is expected than when the permeability damage is reversible.

The new simulator can show effect of imbibition and osmosis to permeability changes in shale due to shale–water interaction following hydraulic fracturing operation. However, this new model is not yet validated and this show the need for further research which include laboratory measurement. In addition to that, it should be realized that this model only accommodate a specific case of formation damage due to shale–water interaction which are water blocking and clay swelling.

Notes

Acknowledgements

The authors thank to the Indonesian State Oil Company, PERTAMINA, for their support of this work.

References

1. Akkutlu, I.Y., Fathi, E.: Multiscale gas transport in shales with local kerogen heterogeneities. SPE J. **17**(04), 1002–1011 (2012). doi: 10.2118/146422-PACrossRefGoogle Scholar

2. Aksu, I., Bazilevskaya, E., Karpyn, Z.T.: Swelling of clay minerals in unconsolidated porous media and its impact on permeability. GeoResJ **7**, 1–13 (2015)CrossRefGoogle Scholar

3. Almulhim, A., Alharthy, N., Tutuncu, A.N., et al.: Impact of imbibition mechanism on flowback behavior: a numerical study. Presented at the Abu Dhabi International Petroleum Exhibition and Conference, 10–13 November 2014, Abu Dhabi, UAEGoogle Scholar

4. Asef, M., Farrokhrouz, M.: Shale Engineering: Mechanics and Mechanisms. CRC Press, Hoboken (2013)Google Scholar

5. Bader, S., Kooi, H.: Modelling of solute and water transport in semi-permeable clay membranes: comparison with experiments. Adv. Water Resour. **28**(3), 203–214 (2005)CrossRefGoogle Scholar

6. Bennion, D.B., Thomas, F.B.: Formation damage issues impacting the productivity of low permeability, low initial water saturation gas producing formations. J. Energy Resour. Technol. **127**(3), 240–247 (2005)CrossRefGoogle Scholar

7. Bennion, D.B., Bietz, R.F., Thomas, F.B., et al.: Reductions in the productivity of oil and low permeability gas reservoirs due to aqueous phase trapping. J. Can. Pet. Technol. (1994). doi: 10.2118/94-09-05Google Scholar

8. Bertoncello, A., Wallace, J., Blyton, C., et al.: Imbibition and water blockage in unconventional reservoirs: well-management implications during flowback and early production. SPE Reserv. Eval. Eng. **17**(04), 497–506 (2014)CrossRefGoogle Scholar

9. Bostrom, N., Chertov, M., Pagels, M., et al.: The time-dependent permeability damage caused by fracture fluid. Presented at the SPE International Symposium and Exhibition on Formation Damage Control, 26–28 February 2014, Lafayette, Louisiana, USA. doi: 10.2118/168140-MS

10. Chenevert, M.E.: Shale alteration by water adsorption. J. Pet. Technol. **22**(09), 1141–1148 (1970). doi: 10.2118/2401-PACrossRefGoogle Scholar

11. Cheng, Y.: Impact of water dynamics in fractures on the performance of hydraulically fractured wells in gas-shale reservoirs. J. Can. Pet.

Technol. **51**(02), 143–151 (2012). doi: 10.2118/127863-PACrossRefGoogle Scholar

12. Eveline, V.F., Akkutlu, I.Y., Moridis G.J.: Impact of hydraulic fracturing fluid damage on shale gas well production performance. Presented at the SPE Annual Technical Conference and Exhibition, 26–28 September, Dubai, UAE (2016). doi: 10.2118/181677-MS

13. Fakcharoenphol, P., Torcuk, M.A., Wallace, J., et al.: Managing shut-in time to enhance gas flow rate in hydraulic fractured shale reservoirs: a simulation study. Presented at the SPE Annual Technical Conference and Exhibition, 30 September–2 October, New Orleans, Louisiana, USA. doi: 10.2118/166098-MS

14. Fan, L., Thompson, J. W., Robinson, J.R.: Understanding gas production mechanism and effectiveness of well stimulation in the haynesville shale through reservoir simulation. Presented at the Canadian Unconventional Resources and International Petroleum Conference, Calgary, 19–21 October 2010. doi: 10.2118/136696-MS

15. Fritz, S.J., Marine, I.W.: Experimental support for a predictive osmotic model of clay membranes. Geochim. Cosmochim. Acta **47**(8), 1515–1522 (1983)CrossRefGoogle Scholar

16. Gangi, A.F.: Variation of Whole and Fractured Porous Rock Permeability with Confining Pressure, vol. 15. Elsevier, Amsterdam (1978)Google Scholar

17. Holditch, S.A.: Factors affecting water blocking and gas flow from hydraulically fractured gas wells. J. Pet. Technol. **31**(12), 1515–1524 (1979). doi: 10.2118/7561-PACrossRefGoogle Scholar

18. Kamath, J., Laroche, C.: Laboratory-based evaluation of gas well deliverability loss caused by water blocking. SPE J. **8**(01), 71–80 (2003). doi: 10.2118/83659-PACrossRefGoogle Scholar

19. Keijzer, T.J.S.: Chemical Osmosis in Natural Clayey Materials, vol. 196. Ph.D. Dissertation, Utrecht University (2000)Google Scholar

20. Marine, I.W., Fritz, S.J.: Osmotic model to explain anomalous hydraulic heads. Water Resour. Res. **17**(1), 73–82 (1981)CrossRefGoogle Scholar

21. Moridis, G.: User's Manual of the TOUGH+ Core Code v1. 5: A General-Purpose Simulator of Non-Isothermal Flow and Transport through Porous and Fractured Media. Report No. LBNL-6871E, Ernest Orlando Lawrence Berkeley National Laboratory, Berkeley, CA (US) (2014)Google Scholar

22. Moridis, G.J., Freeman, C.M.: The RealGas and RealGasH2O options of the TOUGH+ code for the simulation of coupled fluid and heat flow in tight/shale gas systems. Comput. Geosci. **65**, 56–71 (2014). doi: 10.1016/j.cageo.2013.09.010CrossRefGoogle Scholar

23. Pagels, M., Willberg, D., Edelman, E., et al.: Quantifying fracturing fluid damage on reservoir rock to optimize production. Presented at the Unconventional Resources Technology Conference, 12–14 August, Denver, Colorado, USA, 2013. doi: 10.1190/URTEC2013-180

24. Passey, Q., Bohacs, K., Esch, W., et al.: From oil-prone source rock to gas producing reservoir—geologic and petrophysical characterization of shale-gas reservoirs. Presented at the International Oil and Gas Conference and Exhibition in China, 8–10 June, Beijing, China, 2010. doi: 10.2118/131350-MS

25. Pruess, K., Oldenburg, C., Moridis, G.: TOUGH2 User's Guide Version 2. Lawrence Berkeley National Laboratory, Berkeley (1999)CrossRefGoogle Scholar

26. Sharma, M., Agrawal, S: Impact of liquid loading in hydraulic fractures on well productivity. Presented at the SPE Hydraulic Fracturing Technology Conference, 4–6 February, The Woodlands, Texas, USA, 2013Google Scholar

27. van Oort, E.: On the physical and chemical stability of shales. J. Pet. Sci. Eng. **38**(3–4), 213–235 (2003)CrossRefGoogle Scholar

28. van Oort, E., Hale, A.H., Mody, F.K., et al.: Transport in shales and the design of improved water-based shale drilling fluids. SPE Drill. Complet. **11**(03), 46–137 (1996). doi: 10.2118/28309-PAGoogle Scholar

29. Wasaki, A., Akkutlu, I.Y.: Permeability of organic-rich shale. SPE J. **20**(06), 1384–1396 (2015). doi: 10.2118/170830-PACrossRefGoogle Scholar

Copyright information

About this article

CrossMark

Cite this article as:

Eveline, V.F., Akkutlu, I.Y. & Moridis, G.J. Transp Porous Med (2017) 116: 727. https://doi.org/10.1007/s11242-016-0798-4

- **Received**03 July 2016

- **Accepted**16 November 2016
- **First Online**10 December 2016
- **DOI**https://doi.org/10.1007/s11242-016-0798-4
- **Publisher Name**Springer Netherlands
- **Print ISSN**0169-3913
- **Online ISSN**1573-1634
- About this journal
- Reprints and Permissions

Personalised recommendations

Actions

Download PDF

Cite article

- How to cite?
- .RISPapersReference ManagerRefWorksZotero
- .ENWEndNote
- .BIBBibTeXJabRefMendeley

Share article

Table of contents

- Article
- Abstract
- List of Symbols
- Greek Letters
- 1 Introduction
- 2 Petrophysical Model of Shale
- 3 Aqueous-phase Transport in Clay Including Osmosis
- 4 Theoretical Modeling and Numerical Simulation of Two-phase Flow in Shale Gas with Clay-swelling Effect
- 5 Conclusion
- Notes
- References
- Copyright information
- About this article

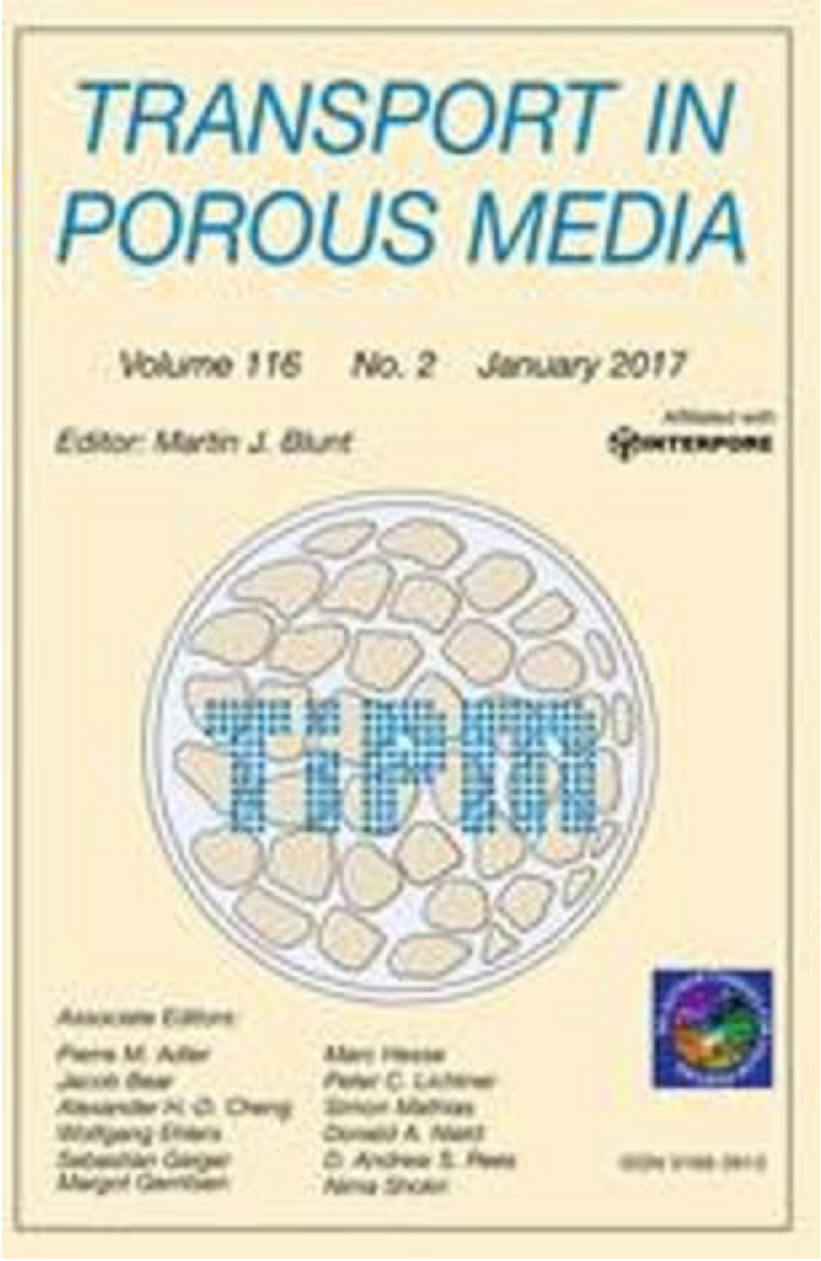

Transport in Porous Media
Transport in Porous Media
January 2017, Volume 116, Issue 2, pp 727–752| Cite as

Numerical Simulation of Hydraulic Fracturing Water Effects on Shale Gas Permeability Alteration

- Authors
- Authors and affiliations

- Vena. F. Eveline
- I. Yucel Akkutlu
- George J. Moridis
-
  - o
-
  - o
-
  - o

1. 1.
2. 2.

Article
First Online: 10 December 2016

Abstract

Hydraulic fracturing has been recognized as the necessary well completion technique to achieve economic production from shale gas formation. However, following the fracturing, fluid–wall interactions can form a damaged zone nearby the fracture characterized by strong capillarity and osmosis effects. Here, we present a new reservoir multi-phase flow model which includes these mechanisms to predict formation damage in the aftermath of the fracturing during shut-in and production periods. In the model, the shale matrix is treated as a multi-scale porosity medium including interconnected organic, inorganic slit-shaped, and clay porosity fields. Prior to the fracturing, the matrix holds gas in the organic and the inorganic slit-shaped pores, water with dissolved salt in the inorganic slit-shaped pores and the clay pores. During and after fracturing, imbibition causes water invasion into the matrix, and then, the injected water–clay interaction may lead to clay-swelling pressure development due to osmosis. The swelling pressure gives additional stress to slit-shaped pores and cause permeability reduction in the inorganic matrix. We develop a simulator describing a system of three pores, two phases (aqueous and gaseous phases), and three components (H_2O,CH_4H2O,CH4, and salt), including osmosis and clay-swelling effect on the permeability. The simulation of aqueous-phase transport through clay shows that high swelling pressure can occur in clays as function of salt type, salt concentration difference, and clay-membrane efficiency. The new model is used to demonstrate the damage zone characteristics. The simulation of two-phase flow through the shale formation shows that, although fracturing is a rapid process, fluid–wall interactions continue to occur after the fracturing due to imbibition mechanism, which allows water to penetrate into the inorganic pore network and displace the gas in-place near the fracture. This water invasion leads to

osmosis effect in the formation, which cause clay swelling and the subsequent permeability reduction. Continuing shale–water interactions during the production period can expand the damage zone further.

Keywords

Numerical simulation Osmosis Formation damage Clay swelling Hydraulic fracturing

List of Symbols

A_{nm}Anm
: Surface are between element n and m (m^2m2)

C_{μ}Cμ
: Sorbed-gas concentration in kerogen grain volume (mol/m^3mol/m3)

$D_{H_2O_{o,A}}$;$D_{CH_{4o,A}}$;$D_{Salt_{o,A}}$Do,AH2O;Do,ACH4;Do,ASalt
: Free-diffusion coefficient of H_2OH2O, CH_4CH4 and salt in the aqueous phase (m^2/sm2/s)

$\mathbf{F}_{H_2OA}$;$\mathbf{F}_{SaltA}$FAH2O;FASalt
: Total mass flux of H_2OH2O and salt in aqueous-phase flow (kg/sm^2kg/sm2)

$\mathbf{F}_{H_2OA|||_{adv}}$;$\mathbf{F}_{H_2OG|||_{adv}}$FAH2O|adv;FGH2O|adv
: Advective mass flux of H_2OH2O in aqueous- and gas-phase flow (kg/sm^2kg/sm2)

$\mathbf{F}_{CH_4A|||_{adv}}$;$\mathbf{F}_{CH_4G|||_{adv}}$FACH4|adv;FGCH4|adv
: Advective mass flux of CH_4CH4 in aqueous- and gas-phase flow (kg/sm^2kg/sm2)

$\mathbf{F}_{SaltA|||_{adv}}$FASalt|adv
: Advective mass flux of salt in aqueous-phase flow (kg/sm^2kg/sm2)

$\mathbf{F}_{H_2OA|||_{dif}}$;$\mathbf{F}_{H_2OG|||_{dif}}$FAH2O|dif;FGH2O|dif
: Diffusion mass flux of H_2OH2O in aqueous- and gas-phase flow (kg/sm^2kg/sm2)

$\mathbf{F}_{CH_4A|||_{dif}}$;$\mathbf{F}_{CH_4G|||_{dif}}$FACH4|dif;FGCH4|dif
: Diffusion mass flux of CH_4CH4 in aqueous- and gas-phase flow (kg/sm^2kg/sm2)

$\mathbf{F}_{SaltA|||_{dif}}$FASalt|dif
: Diffusion mass flux of salt in aqueous-phase flow (kg/sm^2kg/sm2)

k_IkI
: Slit-shaped pore permeability (m^2m2)

$k_m$km
: Permeability of porous medium acting as semi-permeable membrane (m^2m2)

k_0k0
: Slit-shaped pore permeability at zero effective stress (m^2m2)

ℓ_{IC}ℓIC
: Shape factor ($1/m^2$1/m2)

m
: Coefficient in Gangi's permeability model (-)

M_κMκ
: Mass accumulation of component κκ

M_sMs
: Salt molar mass (kg/mol)

M_{CH_4}MCH4
: Molecular weight of CH_4CH4 (kg/mol)

P
: Slit-shaped pore pressure (Psi; Pa)

P_A;P_GPA;PG
: Aqueous- and gas-phase pressure (Psi; Pa)

$P_{A,I}$PA,I
: Inorganic slit-shaped pore pressure (Psi; Pa)

$P_{A,C}$PA,C
: Clay-pore pressure (Psi; Pa)

P_{conf}Pconf
: Confining pressure (Psi; Pa)

P_1P1
: Effective stress when the slit-shaped pores are close completely (Psi; Pa)

P_LPL
: Langmuir pressure (Psi; Pa)

q_κqκ
: Source/sink of component κκ (kg/sm^3kg/sm3)

q_{H_2O};q_{Salt};q_{CH_4}qH2O;qSalt;qCH4
: Source/sink of component H_2OH2O, salt and CH_4CH4 (kg/sm^3kg/sm3)

R
: Gas constant, equal to 8.3145 (J/mol K) or 0.082 (atm l/mol K)

$R_{\kappa,k+1n}$Rnκ,k+1
: Residuals of component *K* at time k+1, in element n

S_A;S_GSA;SG
: Aqueous- and gas-phase saturation

t
: Time

T

Temperature (∘C; K∘C; K)

$\bar{V}_{-}\bar{V}_{-}$

Partial molar volume of solvent (liters per mol)

$x_s x_S$

Salt mass fraction

$x_{H_2OA}; x_{SaltA}; x_{CH_4A} x_{AH2O}; x_{ASalt}; x_{ACH4}$

Mass fraction of component $H_2O H2O$, salt and $CH_4 CH4$ in aqueous-phase flow

$x_{H_2OG}; x_{SaltG}; x_{CH_4G} x_{GH2O}; x_{GSalt}; x_{GCH4}$

Mass fraction of component $H_2O H2O$, salt and $CH_4 CH4$ in gas-phase flow

$x_{SaltA,I}; x_{H_2OA,I} x_{A,ISalt}; x_{A,IH2O}$

Salt and $H_2O H2O$ mass fraction in inorganic pore

$x_{SaltA,C}; x_{H_2OA,C} x_{A,CSalt}; x_{A,CH2O}$

Salt and $H_2O H2O$ mass fraction in clay pore

$V_n Vn$

Volume of element n ($m^2 m2$)

$V_{sL} VsL$

Langmuir volume, sorbed-gas volume per total grain mass ($m^3/kg m3/kg$)

$w_{H_2OA,IC}; w_{CH_4A,IC}; w_{SaltA,IC} w_{A,ICH2O}; w_{A,ICCH4}; w_{A,ICSalt}$

Mass-exchange of $H_2O H2O$, $CH_4 CH4$ and salt between slit-shaped and clay-pore mass ($kgm^{-3}s^{-1} kgm-3s-1$)

Greek Letters

$\alpha \alpha$

Effective stress coefficient (-)

$\varepsilon_{ks} \varepsilon ks$

Total organic content, organic grain volume per total grain volume (-)

$\kappa \kappa$

Component

μ_A and $\mu_G \mu A$ and μG

Viscosity of aqueous- and gas-phase (Pa s)

$\pi \pi$

Osmotic pressure (Pa)

$\rho_A; \rho_G \rho A; \rho G$

Aqueous- and gas-phase density ($kg/m^3 kg/m3$)

$\rho_f \rho f$

Fluid density ($kg/m^3 kg/m3$)

ρ_{grain}ρgrain
: Grain density (kg/m3kg/m3)

$\rho_{sc,gas}$ρsc,gas
: Gas density in standard condition (kg/m3kg/m3)

σσ
: Clay-membrane efficiency (-)

$\tau_A;\tau_G$τA;τG
: Tortuosity of the aqueous- and gas-phase (-)

v
: Dissociation coefficient (-)

ϕϕ
: Porosity of porous medium (fraction)

ϕ_CϕC
: Clay porosity (fraction)

ϕ_IϕI
: Inorganic slit-shaped pore porosity (fraction)

ϕ_kϕk
: Organic (kerogen) porosity (fraction)

1 Introduction

1.1 Background

Due to tight nature of shale formations, shale gas wells require stimulation, such as hydraulic fracturing, in order to produce economically. One of the fracturing methods frequently applied to shale is slickwater fracturing. During the treatment, a water-based fluid is injected in large volumes in order to overcome the parting pressure of the formation and fracture and to transport proppants into the created fractures effectively. Field experience has shown that not all of the injected water flows back when the production stage begins, however. For example, the recovery of the flowback water varied between 10–30% of the injected volume during the first few months of production in Haynesville shale wells (Fan et al. 2010). A large portion of the injected water is left behind in the created fracture system (Fan et al. 2010; Sharma and Agrawal 2013). In addition, it is argued that the recovery of the flowback water is low because a portion of the injected water could invade into the formation and left behind during the production. Experimental works have shown imbibition of water into the shale matrix (Pagels et al. 2013; Bertoncello et al. 2014; Bostrom et al. 2014).

Water invasion into the formation could take place during the fracturing and, perhaps to an even larger extent, after the fracturing, during the well shut-in and production stages. The invading water is expected to damage the

formation due to two major effects: water-blocking effect and clay-swelling effect.

1.1.1 Water-Blocking Effect

Water that fills the fractures will imbibe into the shale matrix due to water-wet properties of the inorganic clayey matrix. Invading water locally displaces the gas in the matrix and creates a multi-phase flow environment near the fracture. Unfavorable saturation conditions during the production can influence the gas flow and, consequently, hinder the gas well performance. This phenomenon, known as water-blocking or phase-trapping, is one of the most severe damage mechanisms in low-permeability gas reservoirs with sub-irreducible water saturation (Bennion et al. 1994; Bennion and Thomas 2005).

Previously, simulation study in tight gas reservoirs showed water-blocking can significantly reduce gas production due to capillarity-driven permeability damage in the invaded zone (Holditch 1979). A recent experiment of water imbibition into shale showed that the imbibing-water remains trapped in the pore network and decreases permeability to gas (Bertoncello et al. 2014). A simulation and history-matching study by Bertoncello et al. (2014) showed that water invasion during fracturing was responsible for reduction in gas production. Other experimental works showed that permeability damage due to imbibition and water blockage could be a time-dependent process for some shales and could be a permanent damage for other shales. Transient behavior of water-blocking have been studied independently by researchers (Kamath and Laroche 2003; Bertoncello et al. 2014; Bostrom et al. 2014).

Bertoncello et al. (2014) studied water-blocking in shale gas reservoir due to water imbibition mechanism using simulation. In their description of the formation, two types of pores coexist in the shale reservoir: large pores in oil-wet organic matrix and small pores in water-wet inorganic matrix. Accordingly, during hydraulic fracturing, high-pressure water leaks off into the shale matrix, invading the large oil-wet pores first, displacing the oil and subsequently being trapped. The trapped water will naturally imbibe into the small, water-wet pores and decrease the water saturation along the fracture face and in the oil-wet pore network. They conducted a simulation-based history-matching study to observe the effect of water invasion. As a baseline case, a scenario was considered with no water invasion. Due to the absence of water invasion, the bottomhole pressure remained high even during early production when the production rate was the largest, which confirmed the water invasion during fracturing was responsible for the reduced gas production. In other cases including the water invasion effect indicated that immediate well cleanup following stimulation could improve well deliverability. When the well is flowed back immediately, invasion into the

matrix was limited; hence, more of the fracturing fluid was recovered at the surface. Other cases with different depth of water invasion were also considered and showed that deeper invasion will cause lower gas production rate especially in early production time. In the case when early cleanup is infeasible for operational reasons, significant water-blocking may occur. According to their analysis, remediation of this water-blocking can be done by shutting in the well long enough to allow imbibition of water from the large oil-wet pores to the small water-wet pores. This could decrease water saturation in the matrix near the fracture face and free the oil-wet pores. During the shut-in, water imbibition removes the water from the main flow paths into small pores and allows easier access for the free gas flow. More water imbibes into small matrix pores, the less water recovery these wells experience.

Other simulation works studied imbibition by rapid suck-in of the fracturing water into the water-wet pores in the shale matrix and dissipation of the water saturation beyond the zone of primary invasion. This process cleans up injected water in fractures and cause enhancement in gas production rate after the shut-in period (Cheng 2012; Fakcharoenphol et al. 2013; Almulhim et al., 2014).

1.1.2 Clay-Swelling Effect

Invading water interactions with clays in the shale formation lead to development of swelling-related in situ stress development. Swelling in clay minerals and in shale has been observed for decades. Chenevert (1970) conducted water adsorption experiments using shale samples containing clay minerals (illite, kaolinite, montmorillonite, and chlorite). When the samples were exposed to fresh water, volumetric expansion of the samples was observed indicating that the samples swelled. Shale samples rich in montmorillonite showed larger expansion than the other shale samples. The observed expansion was anisotropic such that the expansion in the direction perpendicular to the shale bedding planes were larger than those in the direction parallel to the bedding plane. When shale samples were confined, large hydrational stresses were developed within the samples as a function of the duration of adsorption.

Formation damage occurs when the reservoir rock contains highly reactive minerals such as clays known to be sensitive to fresh water. Shale is a sedimentary rock rich in clays. Experimental works involving shale–water interactions have previously showed permeability impairment when shale is brought in contact with water (Chenevert 1970; Bostrom et al. 2014). Severe formation damage takes place due to clay swelling when the clay content of the shale is high (Aksu et al. 2015).

Osmosis has been suggested as the possible transport mechanism for the swelling pressure development inside shale (Marine and Fritz 1981; Fritz and Marine 1983). The swelling of clays is due to an imbalance between the chemical potentials of the contacted fresh water and the water in clay pores.

1.2 Objectives and Approaches

Low water recovery after hydraulic fracturing operation in some shale gas wells indicates that water stays in subsurface, in the wellbore, in the fractures, and in the adjacent shale matrix. There will be continuing interaction between the injected water and the shale matrix that can induce damage over extended times.

In this paper, using theoretical modeling and numerical simulation, we are interested in understanding the mechanisms of imbibition and osmosis (and their interplay) developing in a multi-scale pore network representative of resource shale formations, quantifying their impact on permeability impairment due to continuing shale–water interaction in shale gas well hydraulic fractures. The motivation of this work is that if we have a better understanding of hydraulic fracturing fluid damage, we can conduct well stimulation operations in a manner that can avoid the damage and, hence, lead to a significantly improved well performance.

We thus present a new modeling approach to numerically measure the impact of hydraulic fracturing fluid in shale formations in the presence of both imbibition and osmosis effects. During the application of the model, it is assumed that water cannot be removed from the fractures completely; hence, water–shale interaction occurs at the fracture surfaces continuously. This is different from previous work, for example, experimental works that observed the time dependence of permeability due to water imbibition in shale samples by Bostrom et al. (2014). In their experimental work, after water imbibition period, which shows reduction in permeability, water was removed and permeability was continuously monitored during a certain period in the absence of water. In addition, we considered in our simulations elongated shut-in times to study large-time behavior of the water invasion and the formation damage. Finally, due to number of page limitation, the flow-back stage simulation and analysis are left out and will be discussed in a subsequent manuscript in near future.

In the first part of this paper, a new theoretical shale petrophysical model is proposed with three distinct (multi-scale) porosity fields in the matrix. We show the hydraulic connectivity among the porosity fields and consider modeling imbibition and osmosis in this multi-scale pore structure. Osmosis occurs in shale due to clays acting as a semi-permeable membrane and leads to clay swelling and reduction in shale permeability. In the second

part, the adapted osmosis model will be introduced and discussed. A significant level of improvement in theoretical description of osmosis has been experienced during the last decade based on non-equilibrium thermodynamic arguments. Then, a mathematical model and its numerical solution of aqueous-phase transport in clay including osmosis will be presented and the model will be validated using a previously conducted laboratory experiment. Next, results of a set of forward simulations will be presented to investigate single aqueous-phase transport in clay assuming a block of clay transected by a fracture filled with relatively dilute water. In the third part, mathematical formulation and numerical solution of two-phase flow in shale gas with clay-swelling effect will be presented. Then, a set of numerical simulations are conducted to show the impact of salt type, salt concentration difference, clay-membrane efficiency, and initial water saturation to permeability alteration in the shale formation near the hydraulic fracture. These simulations are performed considering initial and boundary condition representative of the post-hydraulic fracturing operation when the aqueous-phase fills the created hydraulic fracture and when there is continuing water–matrix interactions at the fracture wall. Finally, we discuss impact of hydraulic fracturing fluid damage to shale gas well performance.

2 Petrophysical Model of Shale

Shale is a sedimentary rock that is composed of extremely fine-grained particles, typically less than 4 microns in diameter, but may contain variable amounts of silt-sized particles, up to 62.5 microns with wide variation of composition including clay, quartz, feldspar, carbonates, and organic matter (Passey et al. 2010). In this paper, we will focus our discussion to clay minerals in shale, specifically imbibition and osmosis processes observed and to the associated permeability damage. Shale may contain varied types and amount of clay minerals. Common clay minerals found in shale are kaolinite, smectite (typically montmorillonite), illite, and chlorite.

Clay in general is a layered silicate mineral. It has basic silicate structure unit consisting of silica tetrahedron and alumina octahedron which are combined in different proportions (typically, 1:1 or 2:1) to form sheet structures that have large amount of unbalanced electric charges. The varieties of clay minerals are made by different combination of basic sheet structures with different forms of bonding between the combined sheets (Asef and Farrokhrouz 2013).

Four different types of water can be found in shale associated with the clays: intercrystalline water, osmotic water, bound water, and free water, where porosity is defined as sum of free water, osmotic water, and to a lesser extent intercrystalline water (Asef and Farrokhrouz 2013). Intercrystalline

water is present in association with cations to neutralize negative charges in clay particle; osmotic water is an adsorbed surface layer associated with negative clay charges; bound water is structurally hydrogen and hydroxyl groups within clay molecule itself; and free water is in the pore space between clay grains. Here, our focus is mostly on the osmotic water or interlayer water present between clay sheets which can cause swelling pressure.

Multi-scale, multi-porosity nature of shale matrix that is going to be adopted in this work is an extension of another petrophysical model that has recently been described by Wasaki and Akkutlu (2015). Accordingly, resource shale contains organic round pores and slit-shaped pores. Round-shaped organic pores are generated by thermal maturation and during conversion of kerogen into hydrocarbon fluids, while slit-shaped pores are a result of cracking caused by fluid pressures in excess of hydrostatic.

Unlike the Wasaki and Akkutlu (2015) approach, however, the shale matrix in this study holds additionally the so-called clay pores, see Fig. 1. Organic pores are pores inside organic materials. These pores may contain natural gas in adsorbed and free-states. Slit-shaped pores which have a geometry of a narrow channel or a micro-crack are pores that are located in the inorganic matrix. These pores have hydraulic connection to or transected the organic pores. The length dimension of these slit-shaped pores are varied and may range from one to tens micrometer. These pores could also be considered as the micro- and nano-scale cracks developed parallel to the bedding planes. The slit-shaped pores mostly has water-wet wettability and may contain water and gas. Clay pores, on the other hand, are the voids in between interlayer clay sheets.

Swelling pressure or hydration pressure can be described as a lumped physico-chemical forces acting primarily in the clay fabric which includes the van der Waals attraction, the electrostatic Born repulsion, and short-range repulsive–attractive forces generated from hydration/solvation of clay surfaces and the ions inside the interlayer clay pores (van Oort 2003). In a shale system containing clays and other silt-sized minerals, besides the physico-chemical forces described before, other forces can be categorized as the mechanical forces which include *in situ* vertical and horizontal stresses, pore pressure, and stress acting at intergranular contact points.

As described in detail in the next section, osmosis is the possible mechanism to generate swelling pressure inside clay pores. Here, we will discuss mechanism of formation damage in altered zone which is due to reduction in slit-shaped pore permeability caused by clay-swelling pressure. Altered zone is the shale matrix zone adjacent to hydraulic fracture which

experience changes in reservoir properties due to hydraulic fracturing water imbibed into shale matrix.

The slit-shaped pores permeability is stress dependent and described by Gangi's permeability model (Gangi 1978; Wasaki and Akkutlu 2015) as follows:

$$k_I = k_0\{1-(P_{conf}-\alpha P P_1)^m\}^3 k_I = k_0\{1-(P_{conf}-\alpha P P_1)^m\}^3 \quad (1)$$

Here, $k_I k_I$ is the slit-shaped pore permeability $(m^2); k_0 (m^2); k_0$ is the permeability at zero effective stress $(m^2); P_{conf} (m^2); P_{conf}$ is the confining pressure (Pa); *P* is the slit-shaped pore pressure; $\alpha\alpha$ is the effective stress coefficient; $P_1 P_1$ is the effective stress when the slit-shaped pores are close completely (i.e., when $k_I = 0); and m k_I = 0); and m$ is a coefficient related with the surface roughness of the slit-shaped pores.

In Eq. (1), permeability is function of effective stress $(P_{conf}-\alpha P)$ $(P_{conf}-\alpha P)$ that increasing effective stress will cause reduction in permeability value. Swelling pressure inside clay pores give additional stress to slit-shaped pores, which account for increasing confining pressure, thus reduce slit-shaped pore permeability.

Open image in new window

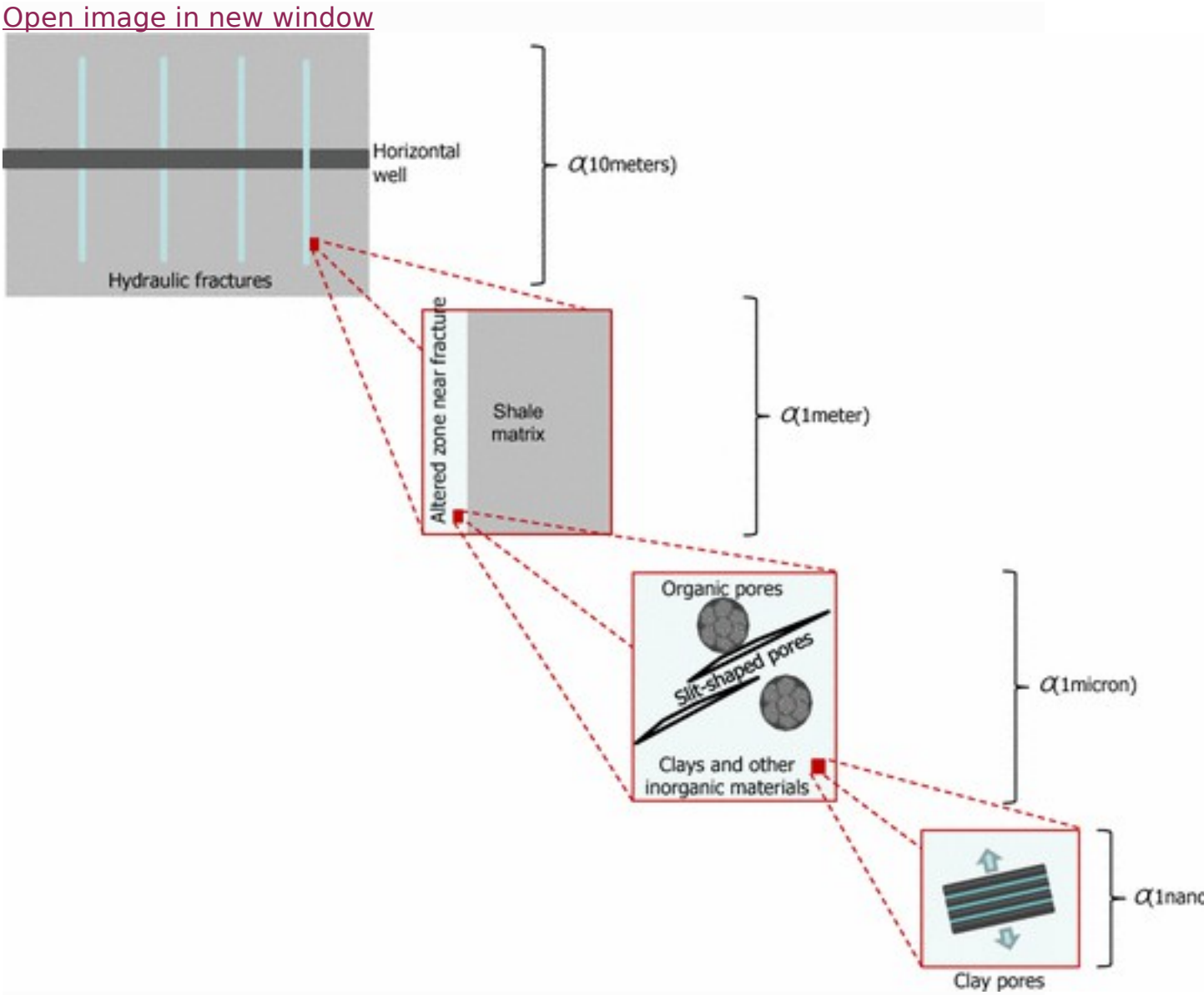

Fig. 1
Conceptual petrophysical model of shale matrix with altered zone due to hydraulic fracturing. *Blue arrows* represent the swelling-related stress caused by water invasion into clay interlayer pores (Eveline et al. 2016)

Open image in new window

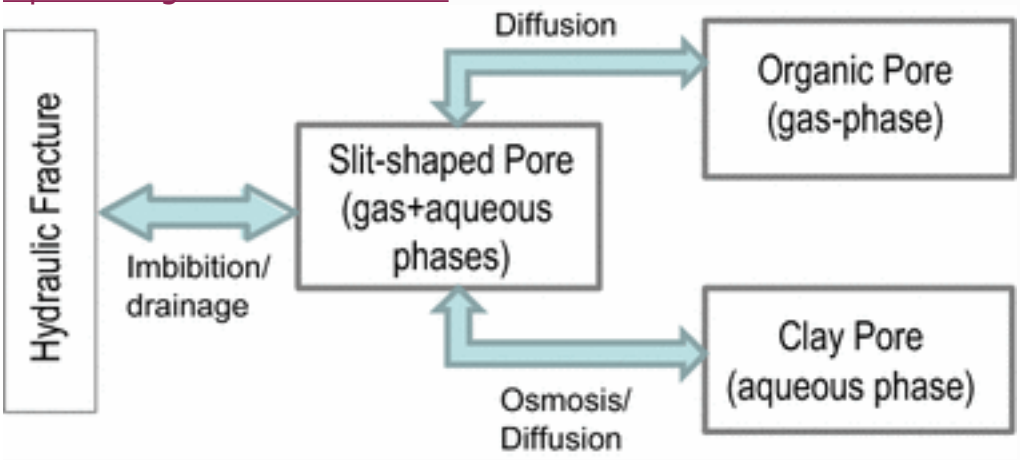

Fig. 2
Flow path between hydraulic fractures, slit-shaped pore, organic pore and clay pore

Figure 1 shows the proposed multiscale of pore structure within shale matrix and interaction paths between water and shale matrix due to hydraulic fracturing operation. Shale matrix contains three types of pores with different scales, as mentioned before, are organic, slit-shaped, and clay pores. Figure 2 shows the connection between hydraulic fracture and these pores. After hydraulic fracturing operation, there are hydraulic fracturing fluid containing water remained in the created hydraulic fractures. This water will interact with shale matrix and create an altered zone where permeability impairment may occur due to this interaction. This permeability impairment known also as formation damage can be caused by several mechanisms and one of them is caused by build up of pressure inside clay pores which dynamically change with time. This build-up of pressure inside clay pores which caused by osmotic mechanism can give additional stress and can reduce slit-shaped pore permeability which is stress-dependent characteristically.

3 Aqueous-phase Transport in Clay Including Osmosis

Before we continue developing a model that describe shale matrix as in the conceptual petrophysical model in Sect. 2, first here, we will discuss the development of mathematical model and simulator involving flow and transport of single aqueous phase in single clay pore which include osmosis as a transport mechanism through clay pore. The purpose of this step is to validate the osmosis model in clay before using it in modeling shale with three pores.

3.1 Osmosis Model

Osmosis could be considered as a molecular diffusion in the presence of a membrane. More specifically, it is a transport mechanism which occurs when a semi-permeable membrane separates two aqueous solutions of different chemical potential due to different salt concentration. Clay minerals can act as semi-permeable membrane because of the negative charges on clay particle surfaces (Marine and Fritz 1981). The negative charges attract cations in solution to adsorb onto clay surface and form a diffuse layer adjacent to the adsorb layer to create double layer. This double layer tends to prevent passage of charged ions through the semi-permeable membrane and only allow uncharged molecules such as water to pass. When the clay membrane is facing aqueous solution having different salt concentration from solution inside the clay, osmosis will occur such that uncharged water molecules flow from the lower salinity solution into the clay. If the more saline solution is contained within a confined clay membrane such as the clays in the subsurface formations, the water being transported into the confined clay will further increase the hydrostatic pressure inside the clay. The osmotic transport will continue until water activity in both solutions eventually becomes equal.

At equilibrium, for an ideal membrane, the increase in the hydrostatic pressure $(\Delta p)(\Delta p)$ is equal to osmotic pressure $(\pi)(\pi)$, which is defined as follows (Marine and Fritz (1981))

$$\pi = RTV^{-} \ln \text{activity of low salinity water} \text{activity of high-salinity water} \pi = RTV^{-} \ln \text{activity of low salinity water} \text{activity of high-salinity water} \quad (2)$$

Here, the activity of water is a unitless number, in which magnitude is dependent on salt concentration, pressure, and temperature. Water from the low-salinity solution will flow through membrane to the high-salinity solution side, to increase the activity of that solution by increasing hydrostatic pressure of that side. Activity of the water on the high-salinity side increases with the increase in hydrostatic pressure. The flow will continue until the activity of both solutions becomes equal.

Flux of mass and energy across a membrane can be driven by pressure, temperature, chemical, and electrical potential gradients (Marine and Fritz 1981; van Oort et al. 1996; Bader and Kooi 2005). In this paper, theoretical description of osmosis follows chemical osmosis model developed by Bader and Kooi (2005) which assumes the two driving forces of the mass flux are the hydraulic pressure and the chemical potential gradients. The model has been derived for an aqueous phase with single solute species. The osmotic pressure is approximated as follows:

$$\pi = vRT\rho^{f} M^{s} \nabla x^{s} \pi = vRT\rho^{f} M^{s} \nabla x^{s} \quad (3)$$

Here, $x_s$xs is the salt mass fraction; M_sMs is the salt molar mass (kg/mol) (kg/mol), and *v* is dissociation coefficient for the salt dissociating into *v* ions, which, for example, $v=2$v=2 for $MgSO_4$MgSO4, NaCl and KCl. Salt concentration is the main factor affecting osmotic pressure. However, for different salt types, equal salt concentration is not resulting equal osmotic pressure because different salt types have different molar mass and dissociation coefficient. For salts with equal dissociation coefficient, here $v=2$v=2 for example, the salts which have higher molar mass such as $MgSO_4$MgSO4than salts such as NaCl and KCl yield lower osmotic pressure.

Open image in new window

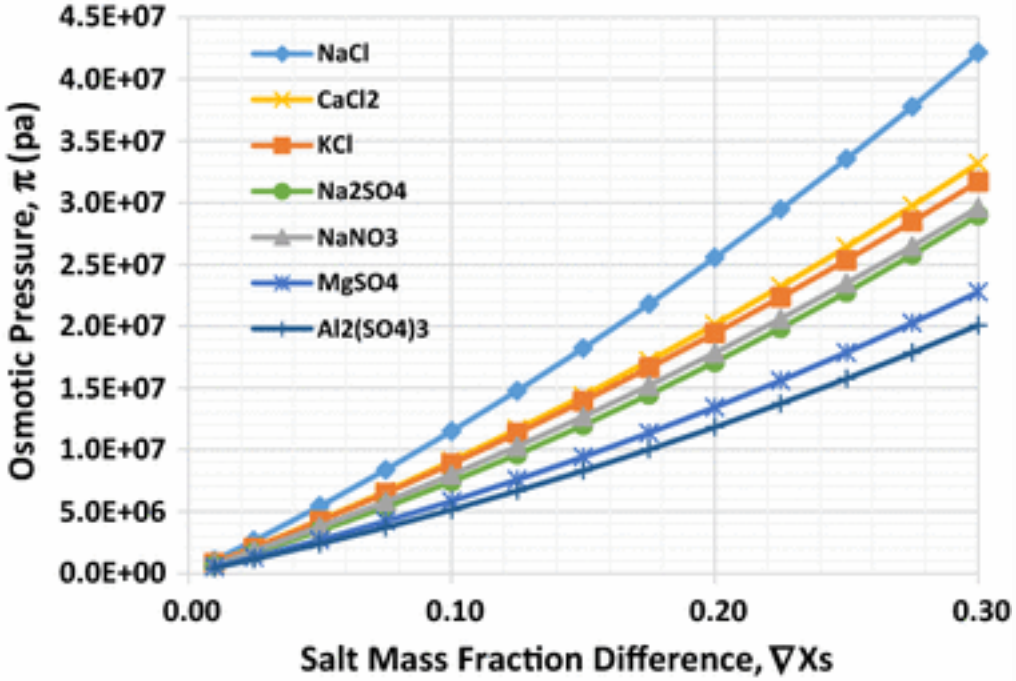

Fig. 3

Osmotic pressure for different salts and varying salt concentration difference are given at an initial pressure of 1.0E+7 Pa and temperature of $100\circ C$100∘C

Consider a container holding two aqueous solutions with different salt concentration separated by a semi-permeable membrane initially has pressure of 1.0E+7 Pa and temperature of $100\circ C$100∘C. The associated pressure increase (osmotic pressure) in the side of the semi-permeable membrane containing higher salt concentration can be calculated using Eq. (3). Then, the estimated changes in pressure due to osmosis are shown in Fig. 3 for different types of salts and different salt concentration values.

3.2 Mathematical Model and Numerical Solution

In this part, we describe a mathematical formulation and simulator which is developed to predict single aqueous-phase transport in clay involving

osmosis. Recently, a similar model has been presented in Eveline et al. (2016). The simulator is an expansion of TAMU-FTsim, which is a variant of the TOUGH+simulator (Moridis 2014; Moridis and Freeman 2014).

This particular simulator describes a system of single pore and two phases/two components. The two phases are aqueous phase and gas phase, and the two components are H_2OH2O and salt. Component H_2OH2O exists in both phases, while component salt is dissolved in the aqueous phase which is described as salt mass fraction of the aqueous phase. In the mathematical model below, only the aqueous phase is described, as we intend to simulate only single aqueous phase through clay.

Mathematical Model

The mass balance equations solved can be written in the following general form (Pruess et al. 1999):

$$ddt\int_{V_n} M_\kappa dV_n = \int_{\Gamma_n} \mathbf{F}_{\kappa\kappa}\cdot\mathbf{n}d\Gamma_n + \int_{V_n} q_\kappa dV_n ddt\int_{V_n} M_\kappa dV_n = \int_{\Gamma_n} F_{\kappa\kappa}\cdot n d\Gamma_n + \int_{V_n} q_\kappa dV_n \quad (4)$$

By applying Gauss' divergence theorem, Eq. (4) can be converted into the following partial differential equation (Pruess et al. 1999):

$$dM_\kappa dt = -div\mathbf{F}_{\kappa\kappa} + q_\kappa dM_\kappa dt = -divF_{\kappa\kappa} + q_\kappa \quad (5)$$

In the Eqs. (4) and (5), V_nVn is a volume element n; $M_\kappa n$; M_κ is mass accumulation of component $\kappa\kappa$; $\mathbf{F}_\kappa F_\kappa$is flux of component $\kappa\kappa$; and $q_\kappa q_\kappa$ is the source/sink of component $\kappa\kappa$.
In the form of Eq. (5), the H_2OH2O and salt mass balance equation in single aqueous-phase flow are as follows:

$$\partial\partial t(x^{H_2OA}\rho_A\phi) + \nabla.\mathbf{F}^{H_2OA} = q^{H_2O}\partial\partial t(xAH2O\rho A\phi) + \nabla.FAH2O = qH2O \quad (6)$$

$$\partial\partial t(x^{SaltA}\rho_A\phi) + \nabla.\mathbf{F}^{SaltA} = q^{Salt}\partial\partial t(xASalt\rho A\phi) + \nabla.FASalt = qSalt \quad (7)$$

The total mass flux equation of H_2OH2O and salt is defined below that the total mass flux of each component is a summation of advective and diffusive mass flux including osmosis which here defined following a mathematical model in Bader and Kooi, 2005.

$$\mathbf{F}^{H_2OA} = x^{H_2OA}\rho_A\{-k_m\mu_A\nabla(P_A) + \lambda\rho_A\nabla(x^{SaltA})\} FAH2O = xAH2O\rho A\{-km\mu A\nabla(PA) + \lambda\rho A\nabla(xASalt)\} \quad (8)$$

$$\mathbf{F}^{SaltA} = (1-\sigma)\rho_A x^{SaltA}\{-k_m\mu_A\nabla(P_A) + \lambda\rho_A\nabla(x^{SaltA})\} - (1-\sigma)\rho_A\phi\tau_A D^{Salto,A}\nabla(x^{SaltA}) FASalt = (1-\sigma)\rho A xASalt\{-km\mu A\nabla(PA) + \lambda\rho A\nabla(xASalt)\} - (1-\sigma)\rho A\phi\tau A Do,ASalt\nabla(xASalt)$$

(9)

where

$$\lambda=\sigma k^m \mu^A M^s v R T \lambda=\sigma k m \mu A M s v R T$$

(10)

Here, the transport of salt is a function of membrane efficiency (σ) (σ) where $\sigma=1\sigma=1$ for ideal membrane, $\sigma=0\sigma=0$ for non-reflective membrane, and $0<\sigma<10<\sigma<1$ for leaky/non-ideal membrane (Marine and Fritz 1981; van Oort et al. 1996; Bader and Kooi 2005).

Numerical Solution

The simulator developed in this part includes three thermophysical states which are single aqueous phase, single gas phase, and two-phases, aqueous and gas phases. However, as we intend to simulate only single aqueous phase through clay, here we focus to the thermophysical state of single aqueous phase.

In the thermophysical state of single aqueous phase, we choose primary variables that can uniquely described the system which involving osmosis. The primary variables are pressure, salt molar fraction and temperature. The salt fraction in the aqueous phase specifically will change the density of the aqueous phase.

The mass balance equations are discretized in space using the integral finite difference method, and time is discretized as a first-order finite difference. All the unknown thermodynamic parameters in the flux and source/sink terms are evaluated at the new time level or in fully implicit manner. The mass balance equations become residual equations, a set of coupled nonlinear algebraic equations as follows:

$$R_{\kappa,k+1n}=M_{\kappa,k+1n}-M_{\kappa,kn}-\Delta t V_n[\sum_m A_{nm}\mathbf{F}_{\kappa,k+1nm}+V_n q_{\kappa,k+1n}]=0 R n\kappa,k+1= Mn\kappa,k+1-Mn\kappa,k-\Delta t Vn[\sum mAnmFnm\kappa,k+1+Vnqn\kappa,k+1]=0$$

(11)

Here, k and k+1 are the current time and the new time level, respectively; $R_{\kappa,k+1n}Rn\kappa,k+1$ is the residuals of component $\kappa\kappa$ at time k+1, in element n; Δtn; Δt is the time step; V_nVn is element volume; $A_{nm}Anm$ is the flow surface between elements n and m. The unknowns are the $n_{element}\times n_{equation}nelement\times nequation$ independent primary variables $(X_i;i=1,\ldots,n_{element}\times n_{equation})(Xi;i=1,\ldots,nelement\times nequation)$ where $n_{element}nelement$ is the number of elements and $n_{equation}nequation$ is the number of equations for each element. The number of equations corresponds to the number of the primary variables.

Equation (11) is solved numerically using the Newton/Raphson iteration method. We introduce an iteration index *p* and expand the residuals in Eq. (11) at iteration step $p+1p+1$ in a Taylor series as follows:

$$R_{n\kappa,k+1}(X_{i,p+1}) = R_{n\kappa,k+1}(X_{i,p}) + \sum_i \partial R_{n\kappa,k+1}\partial X_i \Big|\Big|_p (X_{i,p+1} - X_{i,p}) + \cdots = 0 R_{n\kappa,k+1}(X_{i,p+1}) = R_{n\kappa,k+1}(X_{i,p}) + \sum_i \partial R_{n\kappa,k+1}\partial X_i \Big|_p (X_{i,p+1} - X_{i,p}) + \cdots = 0 \quad (12)$$

We get Jacobian matrix equations by retaining only the first derivative of Eq. (12) and rearranging terms to yield:

$$-\sum_i \partial R_{\kappa,k+1n}\partial X_i \Big|\Big|\Big|_p (X_{i,p+1} - X_{i,p}) = R_{n\kappa,k+1}(X_{i,p}) - \sum_i \partial R_{n\kappa,k+1}\partial X_i \Big| p(X_{i,p+1} - X_{i,p}) = R_{n\kappa,k+1}(X_{i,p}) \quad (13)$$

The Jacobian matrix, $\sum_i \partial R_{\kappa,k+1n}\partial X_i \sum_i \partial R_{n\kappa,k+1}\partial X_i$, is constructed by differentiating the set of residual equations in terms of primary variables $(X_i)(X_i)$. The dimension of the Jacobian matrix is $(n_{element} \times n_{equation}) \times (n_{element} \times n_{equation})$ $(nelement \times nequation) \times (nelement \times nequation)$. Solution of Eq. (13) proceeds in an iterative manner until the residuals $(R_{\kappa,k+1n})(R_{n\kappa,k+1})$ are reduced below a preset convergence tolerance that describes an acceptable (and very low) mass and/or energy balance error.

3.3 Validation of the Simulation Model using Osmosis Experiment

To validate the mathematical model and numerical solution of aqueous-phase flow through clay involving osmosis described in Sect. 3.2, we simulate previous osmosis experiment in clay sample (Keijzer 2000; Bader and Kooi 2005). The simulation parameters are shown in Table 1. We matched pressure increase due to osmosis (Fig. 4), as measured on a clay sample, thus providing evidence to validate the mathematical model of single aqueous-phase flow in clay including osmosis in the transport equations.

Figure 4 shows delta pressure (refer to the initial pressure) inside a clay sample in which ends are connected to two separate reservoirs with different salt concentration. The clay sample itself contains high salt concentration, equal to that in one of the reservoirs. Initially, pressure in the whole arrangement (clay and the two reservoirs) is equal. As the experiment is started, there is water influx from low salt reservoir into clay due to osmosis and pressure inside clay is increasing immediately. However, with time, pressure inside clay turn to decreasing behavior. This is because of two reason: First, as pressure in clay is increasing, there is reverse influx from clay into the low salt reservoir driven by pressure; second, the clay-membrane efficiency is not 100%; therefore, salt dissolved in the aqueous

phase can flow in and out which makes the initial high salt concentration in clay is even lower than initial value and lowering water influx due to osmosis.

Table 1

Parameters used in the chemical osmosis experiment (Keijzer 2000; Bader and Kooi 2005)

Parameter	Value	Unit
Rock and Fluid Properties		
Initial Pressure	5.00E+05	Pa
Initial Temperature	25	∘C∘C
Porosity	0.56	
Permeability	1.20E−09	m2m2
Salt diffusion coefficient	2.60E−13	m2/sm2/s
Membrane efficiency (σ)(σ)	0.0165	
Salt concentration in low salt reservoir	0.01	mol/L NaCl
Salt concentration in high salt reservoir	0.1	mol/L NaCl

Open image in new window

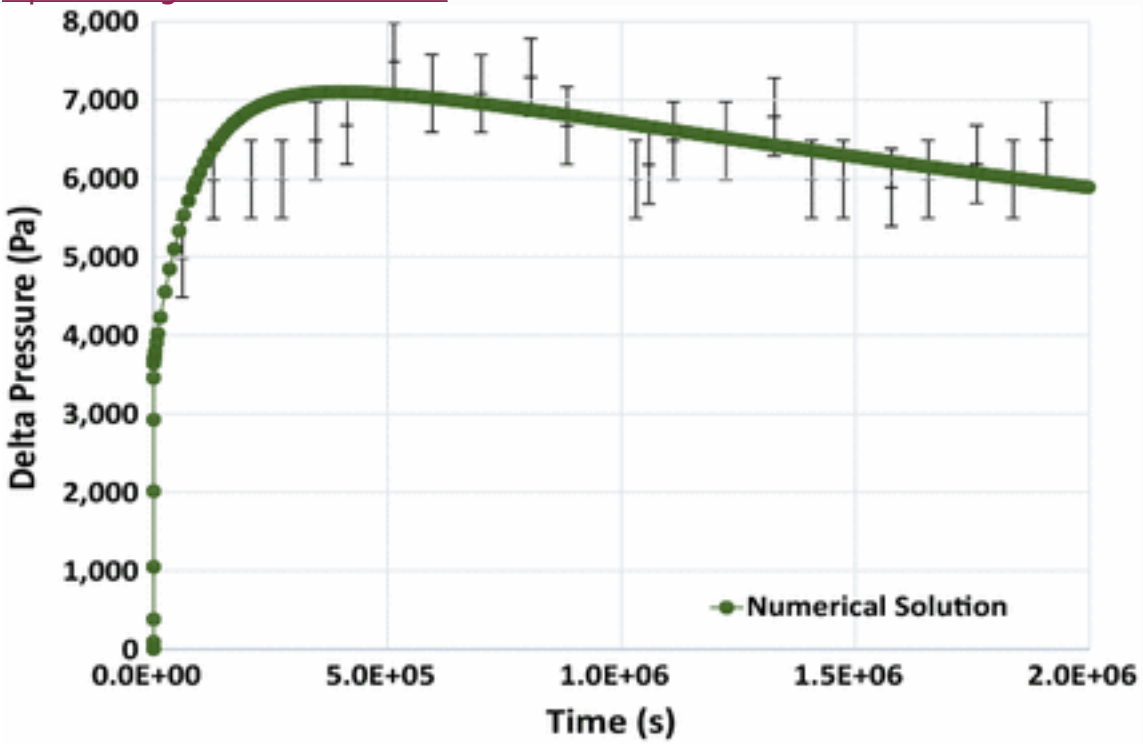

Fig. 4
Comparison between numerical simulation of single aqueous-phase flow in clay results and experimental data (Keijzer 2000; Bader and Kooi 2005) adopted from Eveline et al. (2016)

3.4 Simulation of Aqueous-phase Flow in Clay including Osmosis

Next, in order to understand behavior of the osmosis-related pressure increase (i.e., swelling pressure), we used the validated model in a series of forward simulations varying salt concentration differences. In these studies, we estimated the distribution of pressure across the clay. We also conducted simulations using different membrane efficiency. The simulations were one-dimensional (1D) of a system with dimensions of 5x100x10 m, which was divided into 500 equal-sized elements in the x-direction. The initial pressure was 2.07E+7 Pa and the temperature was 50◦C50◦C. The clay had an initial permeability of 218 nD and porosity of 10%. The first gridblock (corresponding to the fracture element) had a constant pressure of 2.07E+7 Pa, a temperature of 50◦C50◦C, and a NaCl salinity with a mass fraction of 0.01. Initially, the other elements of the system were fully saturated with H2OH2O with a NaCl mass fraction 0.05. Figure 5shows the simulation results after 90 days.

Open image in new window

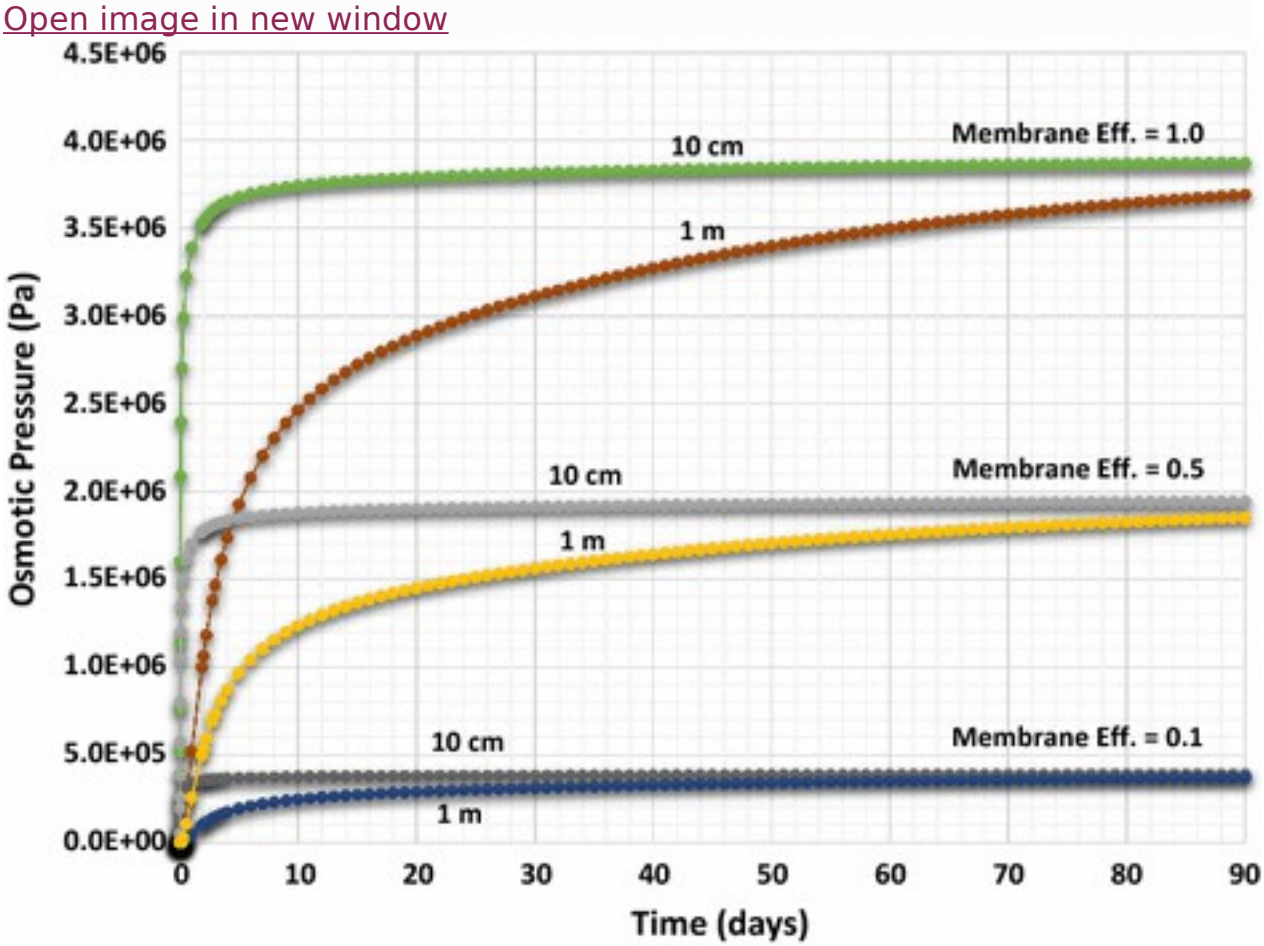

Fig. 5
Pressure evolution up to 90 days within a distance of 10 and 100 cm from a constant pressure element at the left boundary with varying membrane efficiency: 10, 50 and 100%

For a membrane efficiency of 10%, the results show that the salt concentration difference raised the pressure in the clay pores about 4.0E+5 Pa in less than two day within a distance of 10 cm from the fracture. At 55 day, the distance over which the pressure rose by 4.0E+5 Pa extended to 1 m, respectively. This pressure increase is due to the large contrast in salt concentration between the two adjacent elements. However, due to limited membrane efficiency, some of the salt ions can freely move across the element boundaries. Consequently, the observed pressure increase cannot reach the ideal osmotic pressure value and stays somewhat low. Initially, it is the chemical potential gradient that drives the water flux from the element with low salt concentration toward the adjacent element with high concentration. As the pressure increases, the hydraulic gradient begins to control the flux and drive water away from the fracture element.

In the case of membrane efficiency of 50%, the pressure increase predicted by the simulation is much higher. The existing contrast in salt concentration raises the pressure now to about 1.7E+6 Pa in less than 2 day within a distance of 10 cm from the fracture boundary, and to 1 m at about 55 day, respectively. As in to previous case, the limited membrane efficiency can cause some of the salt ions to move freely across the element boundaries, thus preventing the pressure increase to reach the value of the ideal osmotic pressure.

Using a membrane efficiency of 100% (ideal membrane), the pressure increase now reaches the ideal osmotic pressure value of about 3.8E+6 Pa which is comparable to the osmotic pressure calculated using Eq. (3). The salt concentration difference raises the pressure now to about 3.5E+6 in less than 2 day within a distance of 10 cm from the fracture boundary, and to 1 m at about 55 day, respectively

The simulation results show the importance of membrane efficiency value of the clay experiencing osmosis on the pressure increase observed in clay pores. In the subsurface, compacted clays having porosity less than 10% with NaCl concentration about 55,000 ppm can have high membrane efficiency which can be more than 95% membrane efficiency for montmorillonite, chlorite, and illite and about 90% membrane efficiency for kaolinite, theoretically (Marine and Fritz 1981). It can be concluded that clay-swelling pressure in subsurface in the condition as used in the simulation above can be high, thus we should aware of the possibility of significant formation damage happened due to clay-swelling pressure.

4 Theoretical Modeling and Numerical Simulation of Two-phase Flow in Shale Gas with Clay-swelling Effect

In this part we describe a mathematical formulation and a new generation of simulator developed to mimic the two-phase (aqueous and gas) flow in shale gas reservoir with three distinct porosities (organic, slit-shaped-inorganic and clay pores) applying the conceptual petrophysical model shown in Fig. 1. An earlier version of the mathematical model has been presented in Eveline et al. (2016). The simulator is an expansion of TAMU-FTsim, which is a variant of the TOUGH+ simulator (Moridis 2014; Moridis and Freeman 2014).

The developed simulator includes two phases, water and gas, with three components, H_2OH2O, CH_4CH4 and salt distributed in three porosities (organic, slit-shaped-inorganic and clay pores). The organic pores contain gas phase, which consists of CH_4CH4 component only, as free-gas and adsorbed-gas. The inorganic slit-shaped pores contain water and gas phases

consisting of three components, H_2O, CH_4H2O, $CH4$ and salt. The clay pores on the other hand, contain water phase consisting of three components, H_2O, CH_4H2O, $CH4$ and salt. Flow and transport between the discretized simulation elements are through the inorganic slit-shaped pores only. Note that, although they do not contribute to the storage of hydrocarbons, the clay pores experience pressure and chemical potential gradients as the driving forces for molecular transport as described in Sect. 2.

4.1 Mathematical Model and Numerical Solution

Mathematical Model

Mass balance equations to be solved in this part are written in the form of partial differential equation as in Eq. (5) discussed in Sect. 3. The mass balance equations for component H_2O,CH_4H2O,$CH4$ and salt are as follows:

$$\partial\partial t\{\phi_I(x^{H_2OA}\rho_A S_A+x^{H_2OG}\rho_G S_G)\}+\nabla.\{\mathbf{F}^{H_2OA}||_{adv}+\mathbf{F}^{H_2OG}||_{adv}+\mathbf{F}^{H_2OA}||_{dif}+\mathbf{F}^{H_2OG}||_{dif}\}+w^{H_2OA,IC}=q^{H_2O}\partial\partial t\{\phi I(xAH2O\rho ASA+xGH2O\rho GSG)\}+\nabla.\{FAH2O|adv+FGH2O|adv+FAH2O|dif+FGH2O|dif\}+wA,ICH2O=qH2O \quad (14)$$

$$\partial\partial t\{\phi_I(x^{CH_4A}\rho_A S_A+x^{CH_4G}\rho_G S_G)+\rho_G\phi_k+M^{CH_4}\varepsilon_{ks}(1-\phi_{tot})C_\mu\}+\nabla.\{\mathbf{F}^{CH_4A}||_{adv}+\mathbf{F}^{CH_4G}||_{adv}+\mathbf{F}^{CH_4A}||_{dif}+\mathbf{F}^{CH_4G}||_{dif}\}+w^{CH_4A,IC}=q^{CH_4}\partial\partial t\{\phi I(xACH4\rho ASA+xGCH4\rho GSG)+\rho G\phi k+MCH4\varepsilon ks(1-\phi tot)C\mu\}+\nabla.\{FACH4|adv+FGCH4|adv+FACH4|dif+FGCH4|dif\}+wA,ICCH4=qCH4 \quad (15)$$

$$\partial\partial t(x^{SaltA}\rho_A S_A\phi_I)+\nabla.\{\mathbf{F}^{SaltA}||_{adv}+\mathbf{F}^{SaltA}||_{dif}\}+w^{SaltA,IC}=q^{Salt}\partial\partial t(xASaltpASA\phi I)+\nabla.\{FASalt|adv+FASalt|dif\}+wA,ICSalt=qSalt \quad (16)$$

In the Eq. (14) to (16), ϕ_I,ϕ_k,$\phi_C\phi I$,ϕk,ϕC and $\phi_{tot}\phi tot$ are the inorganic slit-shaped, organic, clay and total porosity in shale matrix where the total porosity is summation of the other porosities. The advective mass fluxes are described by Darcy's law and the diffusive mass fluxes are typically described using Fick's law.

In the inorganic slit-shaped pores, two-phase flow is treated by the classical capillary pressure and relative permeability effects which vary as a function of phase saturation. Here, wettability of the inorganic pores is assumed to be strongly water-wet and initially, a small amount of irreducible water phase coexists with the gas-phase.

Flow and transport model of gas phase in the organic and inorganic slit-shaped pores follows the approach presented by Wasaki and Akkutlu (2015). This approach is similar to conventional treatment of the two-phase flow in porous media: each phase follows its own path obeying its own transport mechanisms, also assumes that pore pressure is in equilibrium within the specified bulk volume, and it is the same in organic and inorganic pores. Gas-phase flow and transport mechanism including advective and diffusive mechanisms. The diffusive mechanisms are surface diffusion of the sorbed-phase of the organic solid and molecular diffusion as follows:

$$\mathbf{F}_{CH_4G}||_{dif} = -\rho_G \phi_I S_G \tau_G D_{CH_4o,G} \nabla x_{CH_4G} - M_{CH_4} D_s \nabla C_\mu F_{GCH4}|_{dif} = -\rho_G \phi_I S_G \tau_G D_{o,GCH4} \nabla x_{GCH4} - M_{CH4} D_s \nabla C_\mu \quad (17)$$

There is mass-exchange between the slit-shaped pores and the clay pores driven by hydraulic pressure and chemical potential gradient as described in Eq. (18) to (20). The mass-exchange term follows the approach used to describe mass-exchange between organic and inorganic pores in shale gas matrix (Akkutlu and Fathi 2012). Here, the flow and transport exchange model is following the osmosis model developed in Sect. 3.

The mass-exchange can cause building up of pressure inside the clay pores (clay-swelling pressure). The increased pressure inside the clay pores (current clay-pore pressure minus initial clay-pore pressure) then is added into the original P_{conf}Pconf in Eq. (1). This additional pressure causes the effective stress $(P_{conf} - \alpha P)$(Pconf−αP) in Eq. (1) is increasing, thus reduce permeability of the slit-shaped pores.

Mass-exchange of H_2O, CH_4H2O,CH4 and salt between the slit-shaped pores and the clay pores are defined as follows:

$$w_{H_2OA,IC} = \ell_{IC}\{x_{H_2OA}\rho_A k_m \mu_A [P_{A,I} - P_{A,C}] - x_{H_2OA}\lambda(\rho_A)^2 [x_{SaltA,I} - x_{SaltA,C}] + \rho_A \phi_C \tau_A D_{H_2Oo,A}[x_{H_2OA,I} - x_{H_2OA,C}]\} w_{A,ICH2O} = \ell_{IC}\{x_{AH2O}\rho_A k_m \mu_A [P_{A,I} - P_{A,C}] - x_{AH2O}\lambda(\rho_A)^2 [x_{A,ISalt} - x_{A,CSalt}] + \rho_A \phi_C \tau_A D_{o,AH2O}[x_{A,IH2O} - x_{A,CH2O}]\} \quad (18)$$

$$w_{CH_4A,IC} = \ell_{IC}\{x_{CH_4A}\rho_A k_m \mu_A [P_{A,I} - P_{A,C}] - x_{CH_4A}\lambda(\rho_A)^2 [x_{SaltA,I} - x_{SaltA,C}] + \rho_A \phi_C \tau_A D_{CH_4o,A}[x_{CH_4A,I} - x_{CH_4A,C}]\} w_{A,ICCH4} = \ell_{IC}\{x_{ACH4}\rho_A k_m \mu_A [P_{A,I} - P_{A,C}] - x_{ACH4}\lambda(\rho_A)^2 [x_{A,ISalt} - x_{A,CSalt}] + \rho_A \phi_C \tau_A D_{o,ACH4}[x_{A,ICH4} - x_{A,CCH4}]\} \quad (19)$$

$$w_{SaltA,IC} = \ell_{IC}\{(1-\sigma)\rho_A x_{SaltA}[k_m \mu_A (P_{A,I} - P_{A,C}) - \lambda \rho_A (x_{SaltA,I} - x_{SaltA,C})] + (1-\sigma)\rho_A \phi_C \tau_A D_{Salto,A}(x_{SaltA,I} - x_{SaltA,C})\} w_{A,ICSalt} = \ell_{IC}\{(1-\sigma)\rho_A x_{ASalt}[k_m \mu_A (P_{A,I} - P_{A,C}) - \lambda \rho_A (x_{A,ISalt} - x_{A,CSalt})] + (1-\sigma)\rho_A \phi_C \tau_A D_{o,ASalt}(x_{A,ISalt} - x_{A,CSalt})\} \quad (20)$$

Here, $\ell_{IC}\ell IC$ is the shape factor $(1/m_2);P_{A,I}(1/m2);PA,I$ is the inorganic pore pressure (Pa); $P_{A,C}PA,C$ is the clay-pore pressure (Pa); and $\lambda\lambda$ is as described in Eq. (10).

In Eq. (15), the third term in left-hand-side is the sorbed-gas accumulation of CH_4CH4 in kerogen solid. The sorbed-gas concentration in kerogen grain volume $(C_\mu)(C\mu)$ is described as follows (Wasaki and Akkutlu 2015):

$$C_\mu=V_{sL}\rho_{sc,gas}\rho_{grain}\varepsilon_{ks}M_{CH_4}PP+P_LC\mu=VsL\rho sc,gas\rho grain\varepsilon ksMCH4PP+PL \quad (21)$$

Numerical Solution

The simulator developed in this part includes three thermophysical state which are single aqueous phase and two-phases in matrix domain which has three pores, and two-phases in fracture domain with single pore. Primary variable is chosen to be able describing a system involving mass-exchange by osmosis mechanism between pores within the element. Other unknown variables are set by the use of constitutive, equilibrium restriction, and constraint equations. Here, we use Henry's equation to get the fraction of CH_4CH4 in the aqueous phase.

The primary variables for single aqueous phase in matrix domain are pressure, CH_4CH4 mol fraction in slit-shaped pore, salt mol fraction in slit-shaped pore, salt mol fraction in clay pore, pressure in clay pore, and temperature. The primary variables for two-phase in matrix domain are pressure, gas-phase saturation, salt mass fraction in aqueous phase in slit-shaped pore, salt mass fraction in clay pore, pressure in clay pore, and temperature. The primary variables for two-phase in fracture domain are pressure, gas-phase saturation, H_2OH2O mol fraction in aqueous phase, salt mol fraction in aqueous phase, H_2OH2O mol fraction in gas phase, and temperature.

The mass balance equations Eq. (14) to (16) are solved in the same manner as in the previous method which is described in Sect. 3.2. The mass balance equations are discretized in space using the integral finite difference method, and time is discretized as a first-order finite difference. All the unknown thermodynamic parameters in the flux and source/sink terms are evaluated at new time level. The mass balance equations become a set of residual equations in the form of Eq. (11).

We construct in the form Eq. (13), the Jacobian matrix equations, from the residual equations above where the Jacobian matrix $(\sum_i\partial R_{\kappa,k+1n}\partial X_i)\sum i\partial Rn\kappa,k+1\partial Xi)$ is got by differentiating the residual equations in terms of primary variables $(X_i)(Xi)$. Again, the dimension of the Jacobian matrix is $(n_{element}\times n_{equation})\times(n_{element}\times n_{equation})$ $(nelement\times nequation)\times(nelement\times nequation)$, and the unknowns are the $n_{element}\times n_{equation}nelement\times nequation$ primary variables. Solution of

the Jacobian matrix equations proceeds in an iterative manner until the residuals ($R_{\kappa,k+1n}$)$R_{n\kappa,k+1}$) are reduced below a preset convergence tolerance that describes an acceptable (and very low) mass and/or energy balance error.

4.2 Simulation of Two-phase Flow in Shale Gas with Clay-swelling Effect

Simulation of five shut-in cases is conducted to observe the effect of salt concentration, salt type, initial water saturation, and clay-membrane efficiency to permeability evolution, the details of shut-in cases are shown in Table 2. Also, we run production cases after shut-in to observe the impact of permeability impairment during shut-in to well production performance.

Table 2

Two-phase simulation, shut-in cases

Case	Initial Sw in slit-shaped pore	Salt type	Salt mass fraction in fracturing fluid	Salt mass fraction in aqueous phase in shale
Case 1	0.2	NaCl	0.0001	0.05
Case 2	0.2	NaCl	0.02	0.05
Case 3	0.2	NaCl	0.02	0.15
Case 4	0.2	KCl	0.02	0.15
Case 5	0.05	NaCl	0.0001	0.05

The specific problem to which the numerical simulation is applied assumes a quarter of a single vertical hydraulic fracture perpendicular to a horizontal well and the adjacent stimulated shale gas volume as shown in Fig. 1. The geometry of the problem in xyz directions is $5\times100\times105\times100\times10$ m which is divided into 500 gridblocks in the x-direction. We set the most left of the gridblocks as hydraulic fracture element. Here, we are interested to understand the imbibition and osmosis mechanisms and their impact to permeability alteration related to water in the hydraulic fracture that we simplify the geometry in 1D.

Different initial salt concentration in the aqueous phase between hydraulic fracture element and shale matrix elements is applied to imitate condition in the hydraulic fractures and the shale matrix. Constant pressure of 3000 psi

and water saturation of 100% are applied in the hydraulic fracture element, which is equal to the initial pressure in the shale matrix elements to simulate shut-in and continuous shale–water interaction after hydraulic fracturing operation. In all numerical simulation, the initial water saturation, pressure, and temperature are the same as shown in Table 3. At initial time, the water saturation in the slit-shaped pores is assumed to be at irreducible water saturation of 20% with maximum capillary pressure values, except for the fifth case which has initial water saturation in the state of sub-irreducible. For each case, clay pores contain equal salt concentration to the slit-shaped pores. Different clay-membrane efficiencies are applied for each simulation case: 0.01; 0.1; 0.25; 0.5; 0.75; and 1.00. Other properties such as permeability and porosity are given in Table 3.

4.3 Simulation Results and Discussion

Shale gas well production performance is a function of matrix permeability adjacent to hydraulic fractures such that damage in this zone will cause a decrease in the well production performance. In this part, we want to show the nature of clay-swelling-induced imbibition-driven permeability damage using the newly developed simulator.

4.3.1 Shut-in, Case 1

Although initially the pressure is uniform, there exists a water flux from hydraulic fracture element into the adjacent shale element due to spontaneous imbibition mechanism caused by high capillary pressure in the shale matrix. The computed pressure (Figs. 6, 7a) and water saturation (Fig. 6) are increasing with time and propagating from the gridblocks adjacent to hydraulic fracture element toward the outer boundary. The calculated pressure wave velocity during the first day is approximately 2 m/day, and average water invasion velocity is 0.6 m/day. Pressure velocity is faster than water invasion velocity. However, these velocities are decreasing, and after the pressure in hydraulic fracture element is equalized with saturation and capillary effect in the adjacent shale element pore, the flux deceases. After 30 days, water invades to approximately 11 cm into the matrix. Simulation results also show that the estimated pressure and water saturation values at different time in the slit-shaped pores mostly are independent of clay-membrane efficiency since they reach nearly the same values in the presence of different clay-membrane efficiency.

Table 3

Input parameters for two-phase flow simulation in shale

Parameter	Value	Unit	Parameter	Value	Unit
Initial slit-	3000	psi	Sorption properties		

Parameter	Value	Unit	Parameter	Value	Unit
shaped pore pressure					
Initial clay-pore pressure	3000	psi	Grain Density	2650	kg/m3kg/m3
Initial temperature	60	∘C∘C	Langmuir volume (V_{sL})(VsL)	5.66E−03	m3/kgm3/kg
Porosity			Langmuir pressure (P_L)(PL)	3.45E+06	Pa
ϕ_kϕk (organic)	2%		Total organic grain volume / total grain volume (ε_{ks})(εks)	0.02	
ϕ_IϕI (inorganic)	6%				
ϕ_CϕC (clay)	10%		Diffusion coefficients		
Initial water saturation			Surface diffusion coefficient	1.00E−09	m2/sm2/s
in ϕ_kϕk	0%		Diffusion coefficient of CH_4CH4 in aqueous phase	1.72E−09	m2/sm2/s
in ϕ_IϕI	20%		Diffusion coefficient of salt in aqueous phase	2.60E−13	m2/sm2/s
in ϕ_CϕC	100%		Diffusion coefficient of CH_4CH4 in gas phase	1.00E−09	m2/sm2/s
Gangi model parameters (slit-shaped pore)			Osmotic model parameters		
k_0k0	1.00E−0	md	Clay-membrane	1.00E+0	nD

Parameter	Value	Unit	Parameter	Value	Unit
	2		permeability (k_m) (km)	0	
m	0.5		Shape factor	1.00E−05	
P_1P1	26000	psi	Clay-membrane efficiency (σ)(σ)	varied	
P_{conf}Pconf	15000	psi	Salt type	varied	
αα	0.5				

Open image in new window

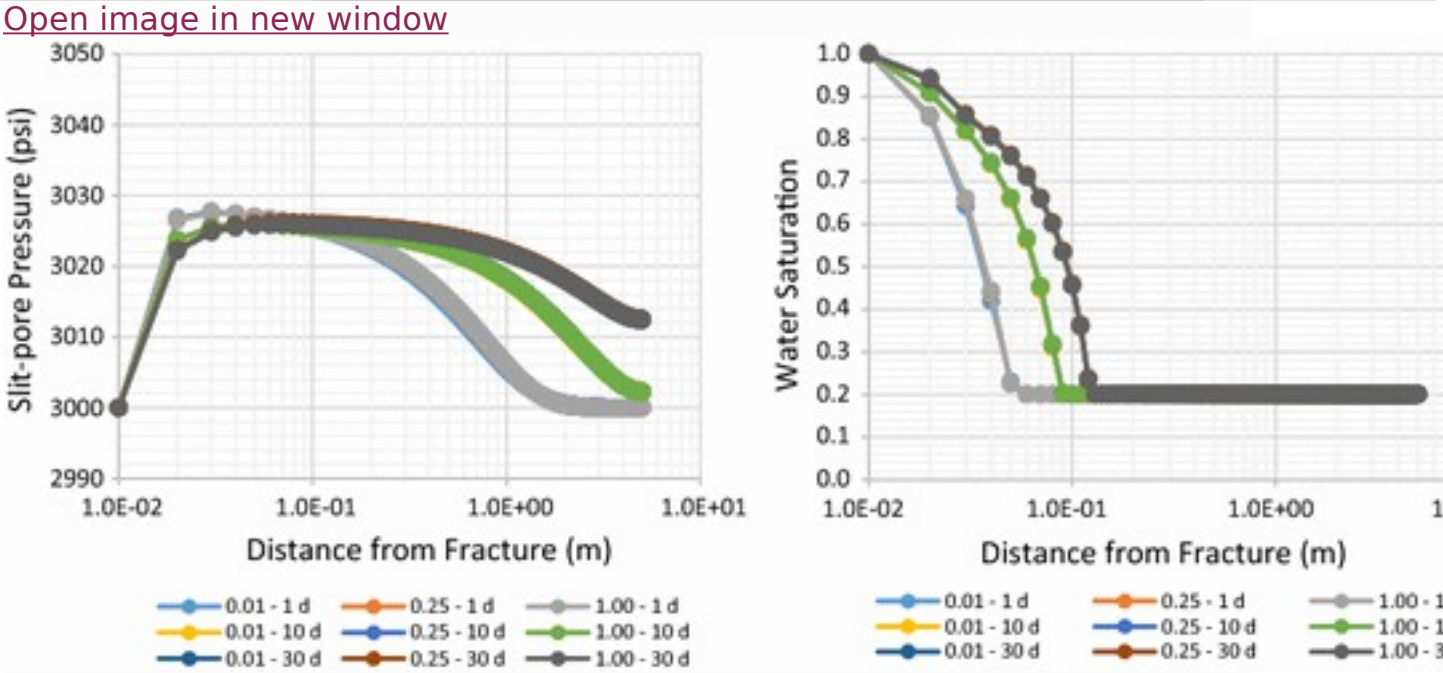

Fig. 6
Simulation results of Case 1. *Left* slit-shaped pore pressure; *Right* water saturation in slit-shaped pores at time 1, 10, and 30 days using clay-membrane efficiency of 0.01, 0.25, and 1.00

In clay pores, on the other hand, levels of pressure predicted are sensitive to the clay-membrane efficiency. Clay-pore pressure increases as the membrane efficiency is increased such that highest clay-pore pressure is reached in the case ideal membrane efficiency of 1.0. As shown in Fig. 7b, clay-pore pressure values is increasing with time and propagate from the gridblocks near hydraulic fracture element toward outer boundary and reach a distance about 11 cm from hydraulic fracture element. These increases

are corresponding to the fresh water movement in the slit-shaped pore toward the outer boundary as represent by water saturation increase in slit-shaped pores near hydraulic fracture (Fig. 6).

Figure 7c shows permeability reduction evolution in slit-shaped pores for different clay-membrane efficiency caused by pressure increase inside clay pores. At initial time, as pressure and fresh water in slit-shaped pores are still progressing toward outer boundary, permeability reduction near hydraulic fracture are small because clay-pore pressure is balanced with the slit-shaped pore pressure. There are fluid exchanges back and forth between the two pores due to hydraulic pressure differences and salt concentration differences (osmosis mechanism). At a certain time when no significant water can move further toward the outer boundary because pressure in the slit-shaped pores near hydraulic fracture elements has reached equalization with capillary and saturation effects, osmosis mechanism takes place more significant and pressure begin to build up high in clay pores. When clay-membrane efficiency is 0.01, clay-pore pressure can be 100 psi higher than slit-pore pressures and permeability reductions are about 3–4%. While assuming ideal membrane, clay-pore pressures can reach about 900 psi higher and this causes permeability reduction up to 24% in 30 days.

Here, the discussion is focus to the absolute permeability of the porous medium, not the effective permeability. The effective permeability to gas will be more reduced if the water saturation is higher which cause the relative permeability to gas is lower.

Open image in new window

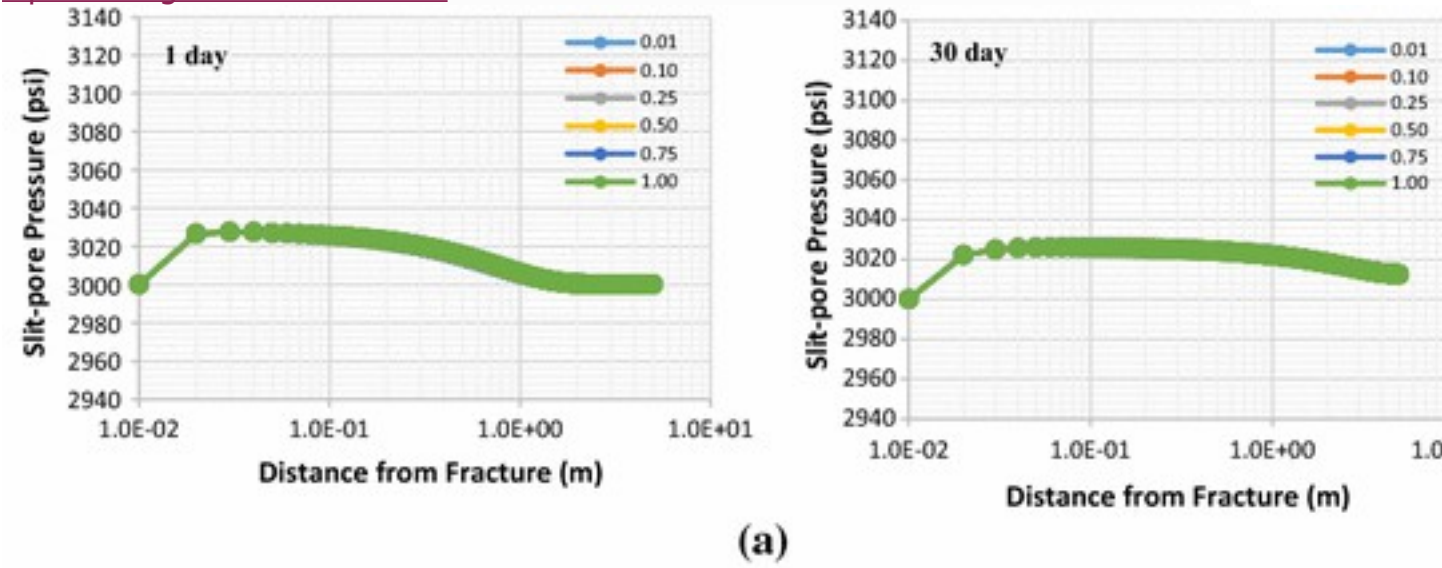

(a)

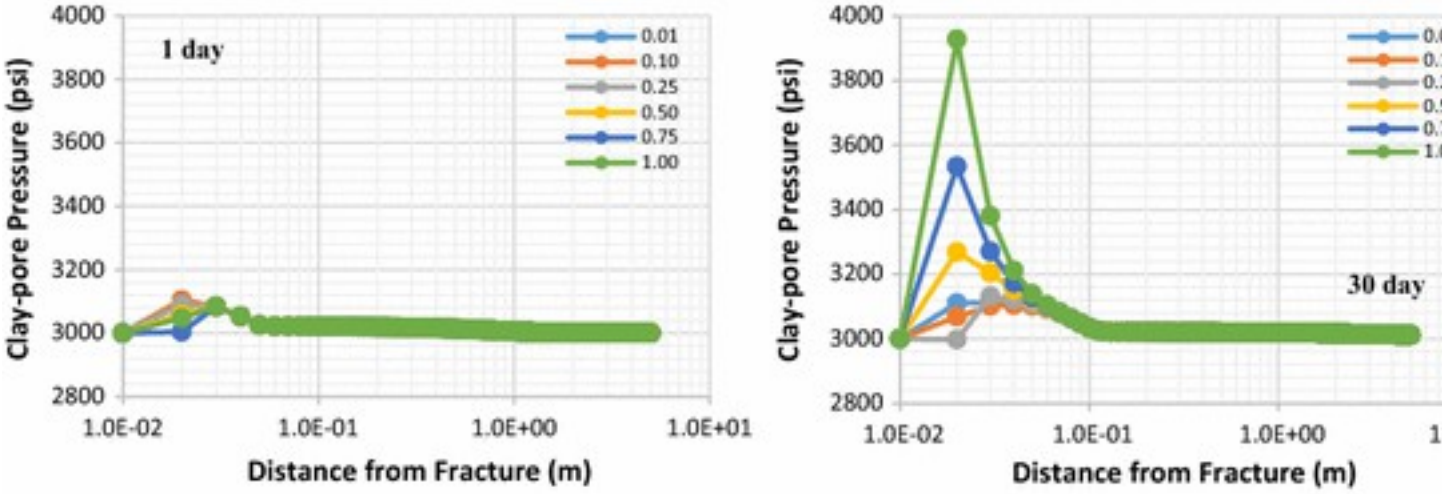

(b)

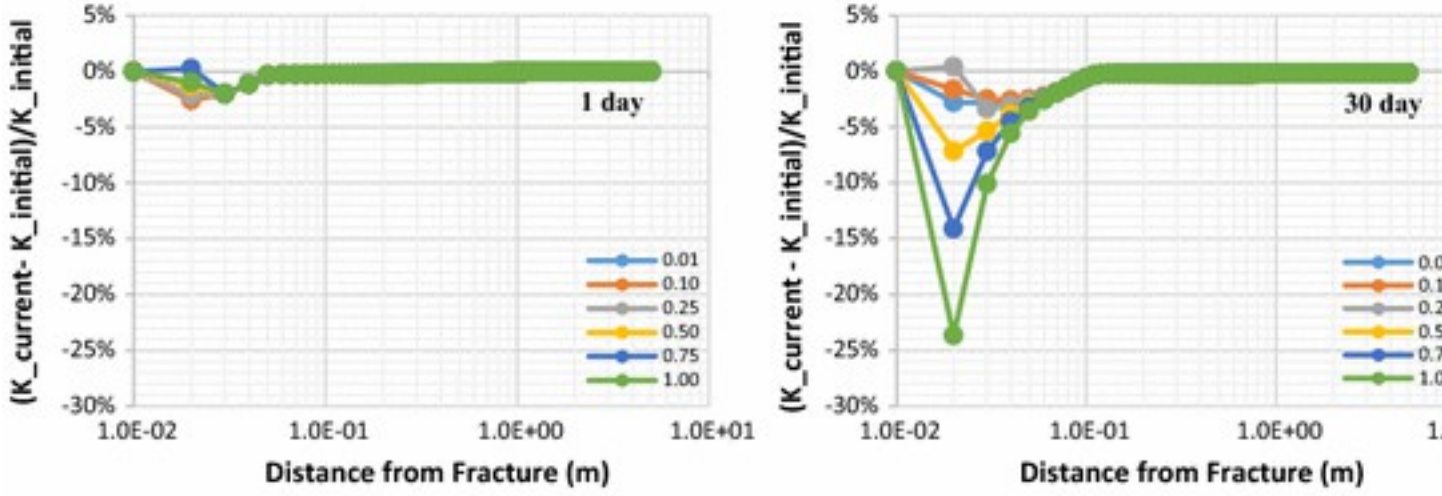

(c)

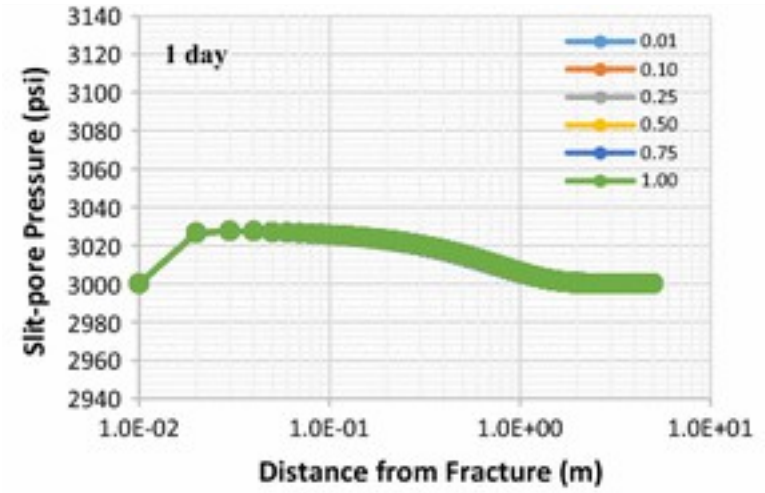
1 day
Slit-pore Pressure (psi)
Distance from Fracture (m)
0.01
0.10
0.25
0.50
0.75
1.00

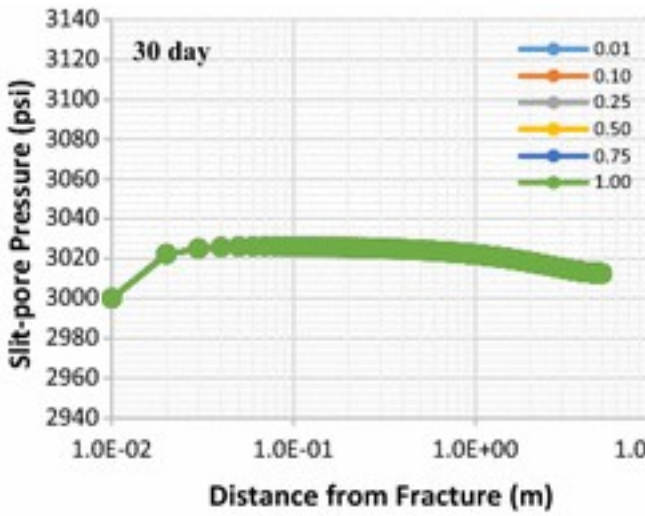
30 day
Slit-pore Pressure (psi)
Distance from Fracture (m)
0.01
0.10
0.25
0.50
0.75
1.00

(a)

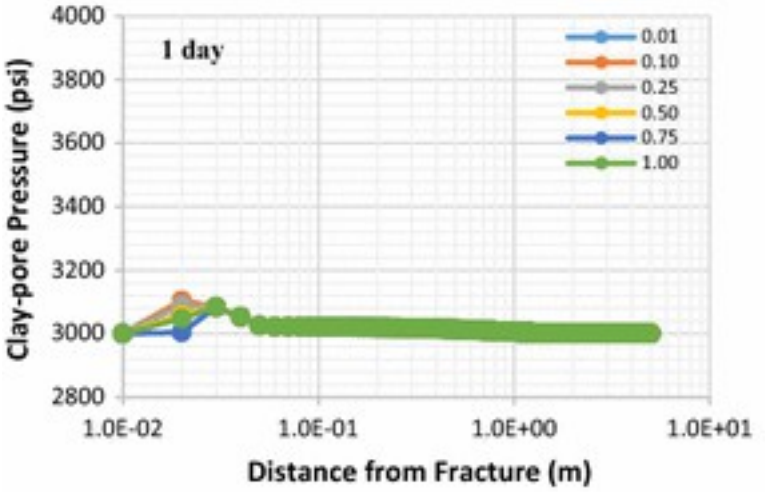
1 day
Clay-pore Pressure (psi)
Distance from Fracture (m)
0.01
0.10
0.25
0.50
0.75
1.00

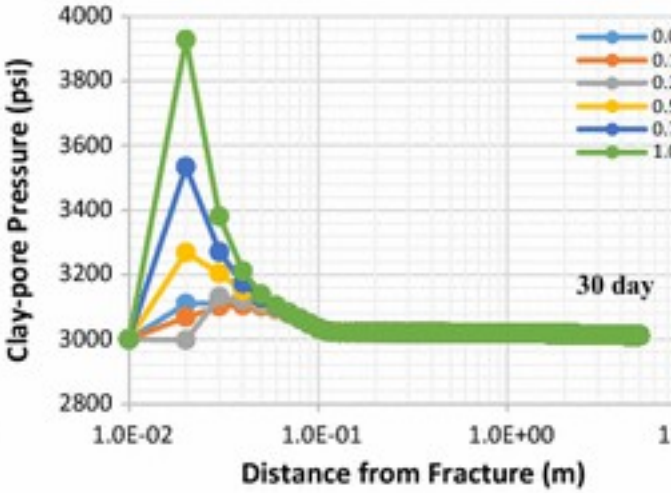
30 day
Clay-pore Pressure (psi)
Distance from Fracture (m)

(b)

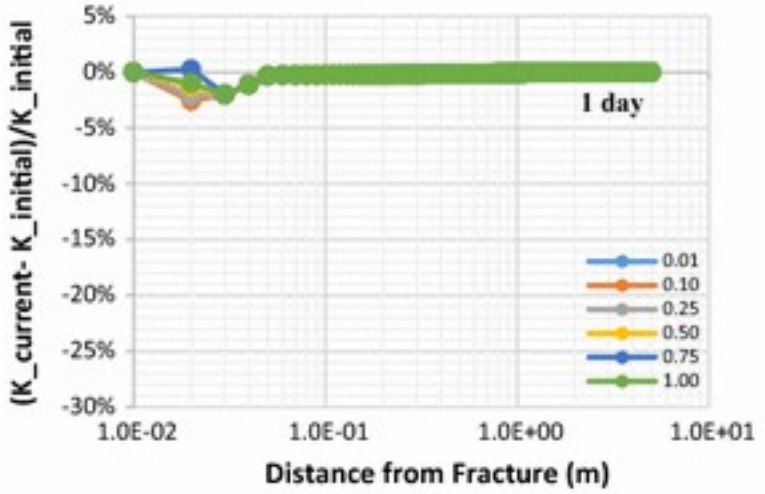
1 day
(K_current- K_initial)/K_initial
Distance from Fracture (m)
0.01
0.10
0.25
0.50
0.75
1.00

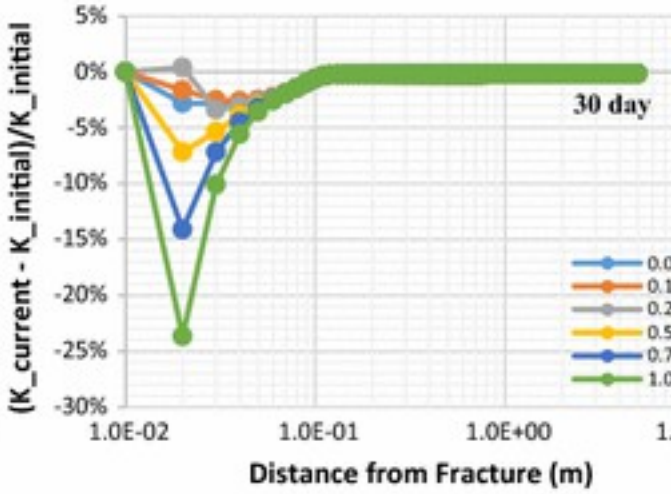
30 day
(K_current - K_initial)/K_initial
Distance from Fracture (m)

(c)

Fig. 7
Simulation results of Case 1: **a** slit-shaped pore pressure; **b** clay-pore pressure; **c**permeability reduction in slit-pore at time 1 and 30 days with varied clay-membrane efficiency of 0.01, 0.1, 0.25, 0.5, 0.75 and 1.00

4.3.2 Comparison of Shut-in Cases, 1 Through 5

Simulation results of case 1, 2, 3, and 4 (Fig. 8) show that permeability reduction occurs in all cases with different magnitude which is dependent on the salt concentration differences between hydraulic fracture and shale pores, the salt type, and the clay-membrane efficiency. Comparing case 1 and 2, which in both cases NaCl mass fraction in the aqueous phase inside shale pores being 5%, higher permeability reduction is occurred when hydraulic fracture is filled with nearly fresh water than when filled with NaCl mass fraction of 2%. Comparing case 2 and 3, which in both cases hydraulic fracture contains 2% NaCl, higher permeability reduction is occurred when salt concentration in the aqueous phase inside shale pores is higher. Comparing case 3 and 4, when different salts are dissolved in the aqueous phase, lower permeability reduction is occurred when KCl is the dissolved salt.

Open image in new window

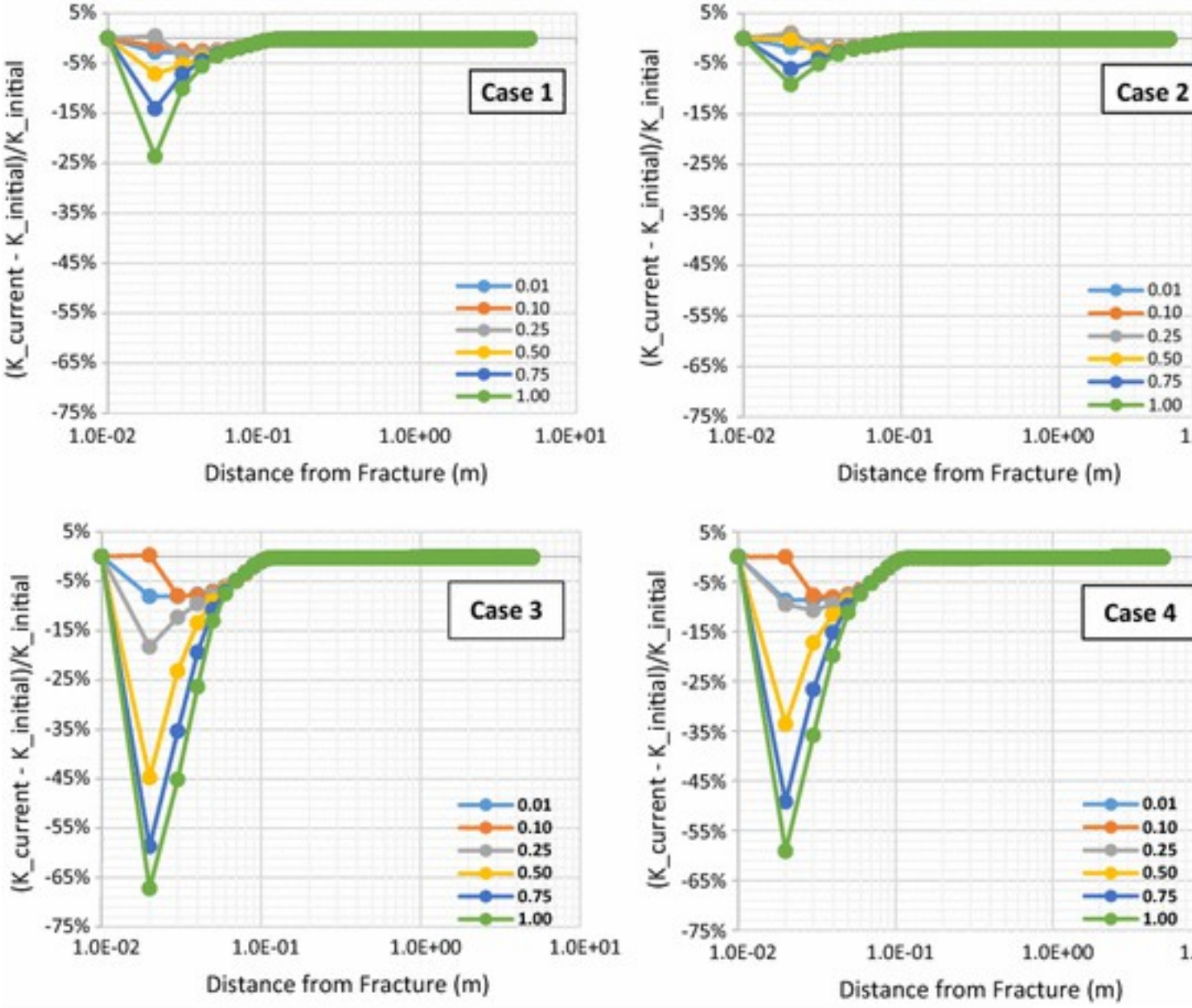

Fig. 8
Comparison of permeability reduction in slit-shaped pores of all simulation cases at time 30 days. *Different colors* are indicating different clay-membrane efficiency (0.01; 0.1; 0.25; 0.5; 0.75; and 1.0)

Figure 9 shows that, as time progresses, shale–water interaction continues and move slowly further toward outer boundary as a result of imbibition, causing expansion of the zone of clay pore increase and permeability reduction. This water imbibition is lowering salt concentration inside slit-shaped pores and resulting salt concentration difference between slit-shaped and clay pores. Theoretically, osmotic pressure increases until the salt concentration is equal between the two types of pores, if clay acts as an ideal membrane. Clays are leaky membrane, however, and that causes salt

dissolved in water in the clay pores filtrate through the clays, therefore the ideal osmotic pressure will not reach that high value experienced with the ideal case. This results show that the damage zone can expand further when clay-water keep interacting. This indicate that early clean-up is necessary to avoid expansion of clay–water interaction zone that can cause expansion of permeability damage zone, hence shale gas well production performance reduction.

Open image in new window

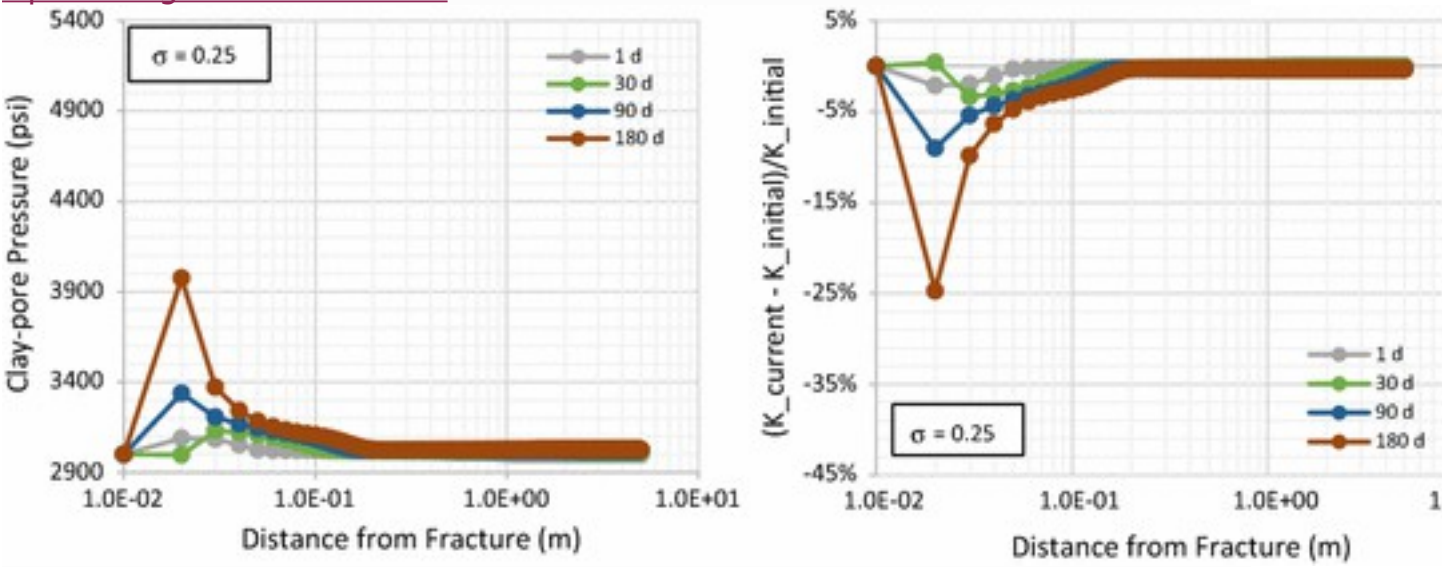

Fig. 9
Effect of duration (Case 1, membrane efficiency of 0.25): *Left* clay-pore pressure increases with time; *Right* permeability reduction increases with time, as shown with *different color*

Case 5 considers a shale formation with a sub-irreducible water saturation. Comparing case 1 and case 5 indicates that when shale matrix has a saturation below the irreducible water saturation, permeability reduction occurs more severe during the same duration of shale–water interaction. As shown in Fig. 10, on the left figure, water invasion zone for case 5 is smaller than case 1. This is because as water penetrates into the slit-shaped pores, water remains immobile at the leading edge of the of the saturation wave until saturation in the pores increases and becomes higher than the irreducible water saturation. This leads to elongated times of water–clay interaction between the slit-shaped pore containing fracturing water and high-salinity clay pore. Consequently, the formation experiences higher level of clay-pore pressure as shown in the right side of figure, Fig. 10, and eventually this lead to larger permeability reduction.

Other sets of simulation were conducted using the same parameters as case 5 except for the initial water saturation in the slit-shaped pores which were varied up to 40%. Fig. 11 shows permeability reduction at 30 day for varied initial water saturation using clay-membrane efficiency 1.0.

Open image in new window

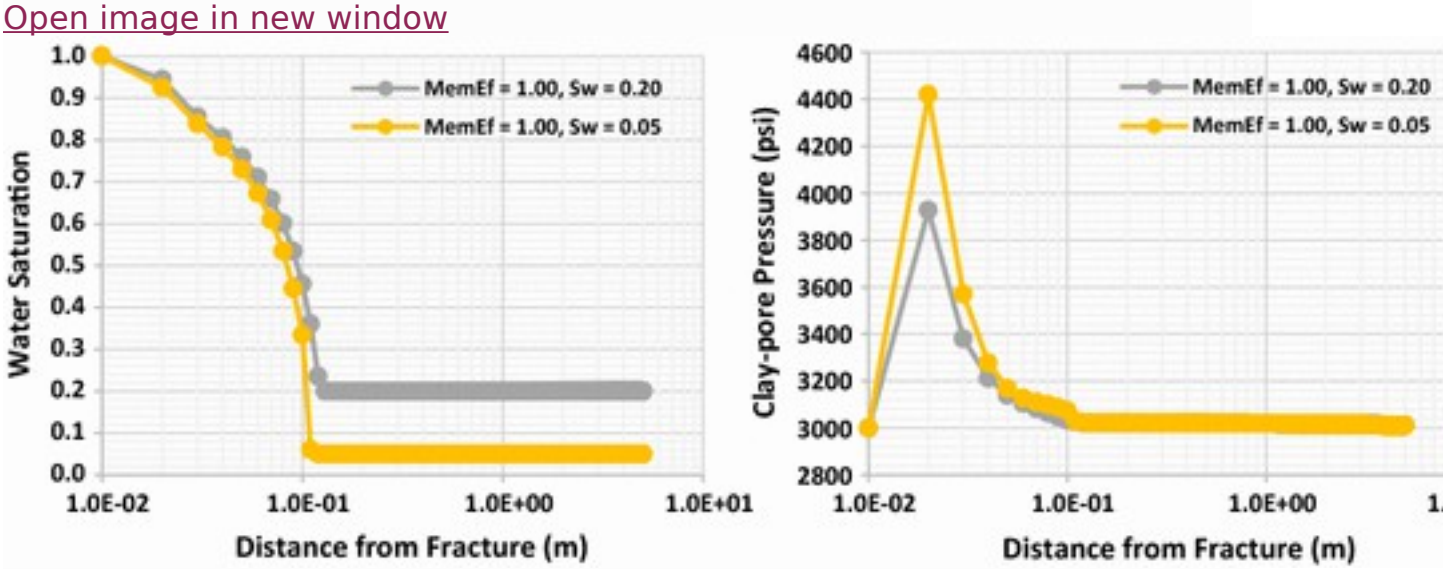

Fig. 10
Comparison between case 1 and case 5 (sub-irreducible water saturation) at 30 day, effect of initial water saturation. *Left* water saturation; *Right* clay-pore pressure

Open image in new window

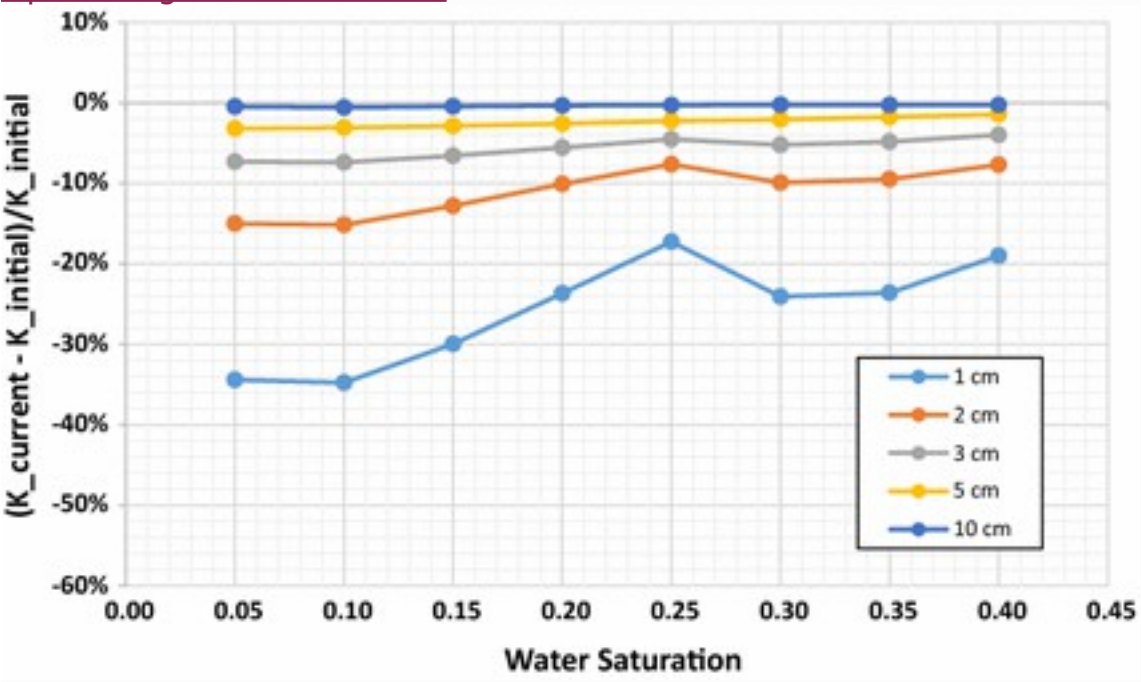

Fig. 11
Permeability reduction at 30 day for different initial water saturation in model shale at several distances from the hydraulic fracture, using clay-membrane efficiency 1.0

4.3.3 Production Cases

We run simulation cases of production after shut-in for 30 days to compare the impact of permeability impairment to production performance between

irreversible and reversible damage as shown in Fig. 12. In the irreversible damage case, we set the permeability damage occurred during shut-in as permanent and geomechanics effect to permeability is only through decreasing formation pore pressure due to production. On the other hand, in the reversible damage case, we do not consider the permeability damage occurred during shut-in as permanent and set the geomechanics effect to permeability fully, which is affected by clay-pore pressure as well as formation pore pressure. As expected, production performance when the damage is irreversible is lower than when the damage is reversible.
Open image in new window

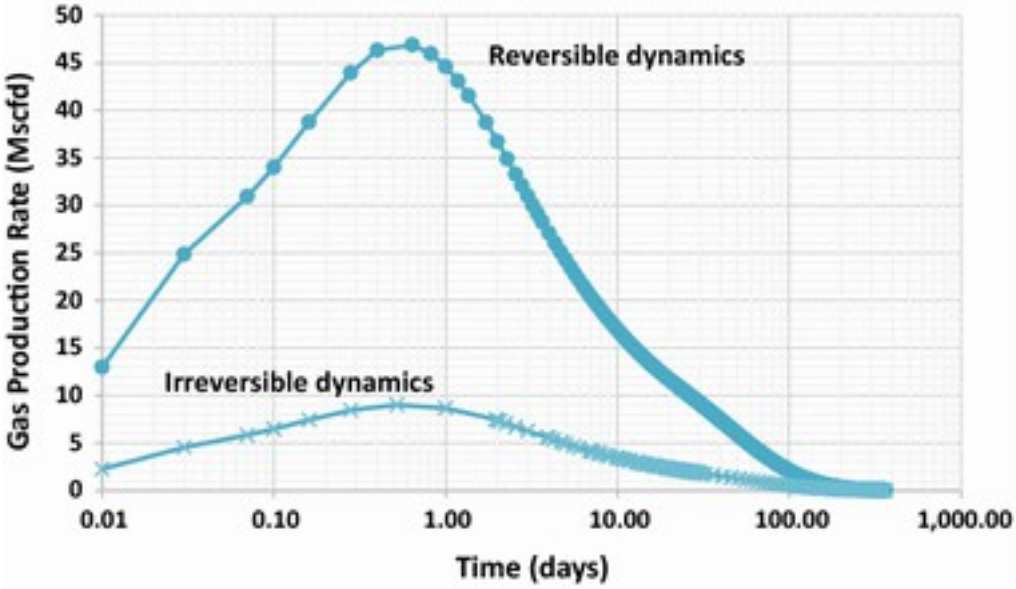

Fig. 12
Comparison of gas production rate between reversible and irreversible formation damage after shut-in 30 days, case 1, membrane efficiency of 0.25

5 Conclusion

A conceptual petrophysical model of shale matrix with an altered zone has been developed in order to understand imbibition and osmosis effect to permeability impairment related to hydraulic fracturing. In the model, the shale matrix contains organic, inorganic slit-shaped, and clay pores. Due to strong capillarity and water-wet characteristics of shale matrix, water imbibition from hydraulic fracture into slit-shaped pores in shale matrix occurs. This induces osmosis that water flows from slit-shaped pores to clay pores and as a result clay swelling happens.

A new simulator following the conceptual petrophysical model is developed. This simulator describes a system with three pores, two phases (gas and aqueous phases), and three components (H_2O,$CH_4$$H_2O$,$CH_4$ and salt) and includes imbibition and osmosis mechanisms and permeability alteration

due to clay swelling. In addition to this simulator, to understand osmosis effect in clays and validate mathematical model of osmosis in clays, we develop a simulator for a system of single pore, single aqueous phase, and two-components (H_2OH2O and salt) including osmosis. Simulation of single aqueous-phase transport in clays shows that high swelling pressures can occur in clays due to osmosis, and these are a function of salt type, salt concentration difference, and clay-membrane efficiency.

Simulation study of shut-in periods using the simulator with three pores, two phases, and three components indicates that due to clay content in shale matrix, shale–water interaction, and salinity difference between hydraulic fracture and the shale matrix, clay swelling can occur and it can cause a reduction in shale matrix permeability. More severe damage occurs if fresh water is used in the fracturing fluid. Even using 2% KCl in fracturing water still can significantly reduce permeability if the water in the clay/shale pores has high salinity. Continuing shale–water interaction can expand the damage zone further. Therefore, it is necessary to avoid prolonged imbibition of water into shale matrix, especially if we use fracturing fluids with salinity that can promote osmotic responses in the matrix. Simulation of systems with varied initial water saturation in slit-shaped pores shows that, when the shale matrix is at sub-irreducible water saturation levels, the reduction in permeability is more pronounced compared to those at the irreducible water saturation or higher. Simulation of production after shut-in shows that when permeability damage after shut-in is permanent or irreversible, lower well production performance is expected than when the permeability damage is reversible.

The new simulator can show effect of imbibition and osmosis to permeability changes in shale due to shale–water interaction following hydraulic fracturing operation. However, this new model is not yet validated and this show the need for further research which include laboratory measurement. In addition to that, it should be realized that this model only accommodate a specific case of formation damage due to shale–water interaction which are water blocking and clay swelling.

Notes

Acknowledgements

The authors thank to the Indonesian State Oil Company, PERTAMINA, for their support of this work.

References

1. Akkutlu, I.Y., Fathi, E.: Multiscale gas transport in shales with local kerogen heterogeneities. SPE J. **17**(04), 1002–1011 (2012). doi: 10.2118/146422-PACrossRefGoogle Scholar

2. Aksu, I., Bazilevskaya, E., Karpyn, Z.T.: Swelling of clay minerals in unconsolidated porous media and its impact on permeability. GeoResJ **7**, 1–13 (2015)CrossRefGoogle Scholar

3. Almulhim, A., Alharthy, N., Tutuncu, A.N., et al.: Impact of imbibition mechanism on flowback behavior: a numerical study. Presented at the Abu Dhabi International Petroleum Exhibition and Conference, 10–13 November 2014, Abu Dhabi, UAEGoogle Scholar

4. Asef, M., Farrokhrouz, M.: Shale Engineering: Mechanics and Mechanisms. CRC Press, Hoboken (2013)Google Scholar

5. Bader, S., Kooi, H.: Modelling of solute and water transport in semi-permeable clay membranes: comparison with experiments. Adv. Water Resour. **28**(3), 203–214 (2005)CrossRefGoogle Scholar

6. Bennion, D.B., Thomas, F.B.: Formation damage issues impacting the productivity of low permeability, low initial water saturation gas producing formations. J. Energy Resour. Technol. **127**(3), 240–247 (2005)CrossRefGoogle Scholar

7. Bennion, D.B., Bietz, R.F., Thomas, F.B., et al.: Reductions in the productivity of oil and low permeability gas reservoirs due to aqueous phase trapping. J. Can. Pet. Technol. (1994). doi: 10.2118/94-09-05Google Scholar

8. Bertoncello, A., Wallace, J., Blyton, C., et al.: Imbibition and water blockage in unconventional reservoirs: well-management implications during flowback and early production. SPE Reserv. Eval. Eng. **17**(04), 497–506 (2014)CrossRefGoogle Scholar

9. Bostrom, N., Chertov, M., Pagels, M., et al.: The time-dependent permeability damage caused by fracture fluid. Presented at the SPE International Symposium and Exhibition on Formation Damage Control, 26–28 February 2014, Lafayette, Louisiana, USA. doi: 10.2118/168140-MS

10. Chenevert, M.E.: Shale alteration by water adsorption. J. Pet. Technol. **22**(09), 1141–1148 (1970). doi: 10.2118/2401-PACrossRefGoogle Scholar

11. Cheng, Y.: Impact of water dynamics in fractures on the performance of hydraulically fractured wells in gas-shale reservoirs. J. Can. Pet.

Technol. **51**(02), 143–151 (2012). doi: 10.2118/127863-PACrossRefGoogle Scholar

12. Eveline, V.F., Akkutlu, I.Y., Moridis G.J.: Impact of hydraulic fracturing fluid damage on shale gas well production performance. Presented at the SPE Annual Technical Conference and Exhibition, 26–28 September, Dubai, UAE (2016). doi: 10.2118/181677-MS

13. Fakcharoenphol, P., Torcuk, M.A., Wallace, J., et al.: Managing shut-in time to enhance gas flow rate in hydraulic fractured shale reservoirs: a simulation study. Presented at the SPE Annual Technical Conference and Exhibition, 30 September–2 October, New Orleans, Louisiana, USA. doi: 10.2118/166098-MS

14. Fan, L., Thompson, J. W., Robinson, J.R.: Understanding gas production mechanism and effectiveness of well stimulation in the haynesville shale through reservoir simulation. Presented at the Canadian Unconventional Resources and International Petroleum Conference, Calgary, 19–21 October 2010. doi: 10.2118/136696-MS

15. Fritz, S.J., Marine, I.W.: Experimental support for a predictive osmotic model of clay membranes. Geochim. Cosmochim. Acta **47**(8), 1515–1522 (1983)CrossRefGoogle Scholar

16. Gangi, A.F.: Variation of Whole and Fractured Porous Rock Permeability with Confining Pressure, vol. 15. Elsevier, Amsterdam (1978)Google Scholar

17. Holditch, S.A.: Factors affecting water blocking and gas flow from hydraulically fractured gas wells. J. Pet. Technol. **31**(12), 1515–1524 (1979). doi: 10.2118/7561-PACrossRefGoogle Scholar

18. Kamath, J., Laroche, C.: Laboratory-based evaluation of gas well deliverability loss caused by water blocking. SPE J. **8**(01), 71–80 (2003). doi: 10.2118/83659-PACrossRefGoogle Scholar

19. Keijzer, T.J.S.: Chemical Osmosis in Natural Clayey Materials, vol. 196. Ph.D. Dissertation, Utrecht University (2000)Google Scholar

20. Marine, I.W., Fritz, S.J.: Osmotic model to explain anomalous hydraulic heads. Water Resour. Res. **17**(1), 73–82 (1981)CrossRefGoogle Scholar

21. Moridis, G.: User's Manual of the TOUGH+ Core Code v1. 5: A General-Purpose Simulator of Non-Isothermal Flow and Transport through Porous and Fractured Media. Report No. LBNL-6871E, Ernest Orlando Lawrence Berkeley National Laboratory, Berkeley, CA (US) (2014)Google Scholar

22. Moridis, G.J., Freeman, C.M.: The RealGas and RealGasH2O options of the TOUGH+ code for the simulation of coupled fluid and heat flow in tight/shale gas systems. Comput. Geosci. **65**, 56–71 (2014). doi: 10.1016/j.cageo.2013.09.010CrossRefGoogle Scholar

23. Pagels, M., Willberg, D., Edelman, E., et al.: Quantifying fracturing fluid damage on reservoir rock to optimize production. Presented at the Unconventional Resources Technology Conference, 12–14 August, Denver, Colorado, USA, 2013. doi: 10.1190/URTEC2013-180

24. Passey, Q., Bohacs, K., Esch, W., et al.: From oil-prone source rock to gas producing reservoir—geologic and petrophysical characterization of shale-gas reservoirs. Presented at the International Oil and Gas Conference and Exhibition in China, 8–10 June, Beijing, China, 2010. doi: 10.2118/131350-MS

25. Pruess, K., Oldenburg, C., Moridis, G.: TOUGH2 User's Guide Version 2. Lawrence Berkeley National Laboratory, Berkeley (1999)CrossRefGoogle Scholar

26. Sharma, M., Agrawal, S: Impact of liquid loading in hydraulic fractures on well productivity. Presented at the SPE Hydraulic Fracturing Technology Conference, 4–6 February, The Woodlands, Texas, USA, 2013Google Scholar

27. van Oort, E.: On the physical and chemical stability of shales. J. Pet. Sci. Eng. **38**(3–4), 213–235 (2003)CrossRefGoogle Scholar

28. van Oort, E., Hale, A.H., Mody, F.K., et al.: Transport in shales and the design of improved water-based shale drilling fluids. SPE Drill. Complet. **11**(03), 46–137 (1996). doi: 10.2118/28309-PAGoogle Scholar

29. Wasaki, A., Akkutlu, I.Y.: Permeability of organic-rich shale. SPE J. **20**(06), 1384–1396 (2015). doi: 10.2118/170830-PACrossRefGoogle Scholar